# DIGITAL DEPOSITION OF YTTRIA PATTERNS ON TITANIUM SHEETS

by

GABRIEL FERNANDEZ

B.S., Mechanical Engineering
National University of Mexico (UNAM), 1995

Submitted to the Department of Mechanical Engineering
in Partial Fulfillment of the
Requirements for the Degree of

MASTER OF SCIENCE

at the

Massachusetts Institute of Technology

June 1997



Signature of Author _____
Department of Mechanical Engineering
May 28, 1997

Certified by _____
Emanuel M. Sachs
Professor of Mechanical Engineering
Thesis Supervisor

Accepted by _____
Ain A. Sonin
Chairman, Graduate Committee

# Digital Deposition of Yttria Patterns on Titanium Sheets

by

Gabriel Fernandez Ares de Parga

Submitted to the Department of Mechanical Engineering
on May 28, 1997, in partial fulfillment of the
requirements for the Degree of Master of Science

Abstract

The ability to apply Yttria patterns on titanium sheets is required on a secondary manufacturing operation. The freedom to create 2 dimensional patterns as well as 3 dimensional ones by using Three Dimensional Printing allows for the application of Yttria patterns onto these sheets without the use of any type of screens. Two methods for creating these patterns were identified and studied.

The first approach consists of selectively printing binder on top of spread layer of powder. A second layer of powder is spread while the binder is still wet. The binder will then dry fixing the Yttria powder to the sheet on the selected positions. Sheets were printed using different particle sizes. Results show that patterns can be applied with good edge definition and uniform thickness using powder ranging from -53μm down to -20μm. The sheets were tested successfully in the secondary operation.

And alternative approach consists of mixing the binder and the ceramic powder to create a slurry. The slurry will then be selectively printed onto the sheet using Three Dimensional Printing. A formulation for a –20 μm Yttria powder slurry was developed using Poly Acrylic Acid as dispersant and Polyethylene Glycol as binder. Slurries with 20 volume fraction and less were dispersed and jetted through a 102 μm nozzle. These slurries adhered well to the titanium sheet as they were printed. The formulation was tested successfully in the secondary operation.

Following the High-Risk Approach patterns without deflection were printed. For a 102 μm nozzle the best flow rate was determined, as well as the optimal line spacing. The best procedure to print a certain area was to print a first round of lines, dry them and then print lines in between the first set. The average roughness of the layer printed was 14 μm.

In order to allow future printing of slurries with a nozzle size of 102 μm and deflection, the design of a print head to accommodate these slurries was also investigated

Thesis Supervisor: Dr. Emanuel Sachs
Title: Professor of Mechanical Engineering

## Dedication

**To my wife**
**who is the most important part of my life.**

**To my family**
**for all their love and support**

## Acknowledgements

I would like to thank the Boeing Company who made this project possible. Special thanks to Mr. John Fischer for all his help and support.

I would like to acknowledge all the support of the staff and students in the 3D printing project:

Ely Sachs, thanks for all important things you have taught me. I will never forget the opportunity you gave me.

Javier Baños, thanks for your help but above that thanks for your friendship.

Jeannie Yoo, thanks for everything, including my tennis lessons.

Dave Brancazio, Jim Serdy and Mike Rynerson thanks for all the help and good ideas that I received from you.

Jason Grau, for your help and friendship

Thank you, P.J. Baker, Laura Zaganjori, Michael Caradonna, Xiaorong Xu, Thomas Becker and Honglin Guo.

I would also like to acknowledge the support from other people outside the 3D printing group.

Luis Parra, Luis Ramirez and Gustavo Buhacoff thanks all for your support.

Fred Cote, for the endless help in the machine shop.

Gerry Wentworth and Kevin Baron, thanks.

# Contents

## List of Figures

## List of Tables.

# Chapter 1 Introduction

## 1.1 Motivation

In some industry applications the necessity of developing a better and more reliable manufacturing processes is essential. Better products fabricated in lesser amounts of time are daily required. Some current manufacturing processes does not fulfill the total expectations; therefore the development of a new technique or the adaptation of another has to be achieved. In the case of the Aerospace industry, all the parts must have very high standards of quality making the control of the manufacturing processes a key issue. In the particular case of the fabrication of "Yttria Patterns on Titanium Sheets", the actual manufacturing procedure is not good enough to meet the high quality standards the application requires. Screen-printing and other methods does not seem to work in appropriate ways; therefore the search for a new fabrication technique is necessary.

The ability to apply yttria patterns on titanium sheets is required in a proprietary Boeing process. The freedom to create 2 dimensional patterns as well as 3 dimensional ones by the use of the 3-D Printing process allows for the fabrication of these sheets without the use of any type of screens. It is possible to adapt the 3D-Printing technology to this process by simply printing one layer of material on top of the titanium sheet. Because there are no analog methods used for this application the process has been described as *Digital Deposition of Yttria Patterns on Titanium Sheets by 3D-Printing*. This process is potentially capable of much better edge definition and pattern registration than would ever be possible with screen-printing. In addition, the main virtue of the process is that it does not require any tools to print a pattern.

## 1.2 Goals

Printing specific patterns of ceramic powder and binder on the sheets can be made using the current 3D-Printing with some minor changes. Two approaches have been identified as potential construction methods. Both techniques have advantages and

disadvantages. The first approach, considered as the *Low Risk Approach*, consists of printing binder on top of a manually or automatically spread powder layer. In contrast, the second one combines the binder and the ceramic powder creating slurry. In general the binders used in 3D-Printing are not slurries. The challenge of this method lies in printing slurries with large particle sizes. These suspensions have to be jetted through nozzles that are bigger than the conventional ones. This approach will be considered as the *High Risk Approach.*

The overall goal of this project is to determine the feasibility of these processes. In parallel, it is an objective of this work is to determine which method is more reliable and robust enough to stand several hours of operation. The 3D-Printing process has unique features that make possible the use of different material systems. Some of the specific goals of this project are:

Low Risk:

- Demonstrate the actual printing process jetting normal binder on top of a chemically cleaned titanium sheet with powder.
- Determine the adequate printing sequence.
- Identify the key parameters of the printing process.
- Print several test pattern onto titanium sheets with powder.
- Optimize the process in order to achieve the best edge definition as well as layer thickness and surface finish.
- Test the performance of the printed sheets. (Boeing shall evaluate the performance.)

High Risk:

- Adapt the current printing machine in order to accommodate slurry-based fluids.
- Jet particles as big as 20 μm through nozzles smaller than 120 μm.

- Develop a slurry-based formula that will perform the intended purposes on the sheet after jetting including binding the powder to the sheet and burning off cleanly.
- Identify the key parameters of the process.
- Redesign, if necessary, part of the 3DP printhead in order to accommodate all the changes that come with the use of bigger nozzles and heavier fluids.
- Print several test patterns on sheets
- Test the performance of the printed sheets. (Boeing shall evaluate the performance.)

## 1.3 - THREE DIMENSIONAL PRINTING

Three Dimensional Printing (3DP) is a process for the rapid fabrication of three-dimensional parts directly from computer models [Sachs et al, 1992]. The process creates parts by a layered printing process. The information of each layer is obtained by applying a slicing algorithm to the computer model part. An individual two-dimensional layer is created by adding a layer of powder to the top of a piston cylinder containing a powder bed and the part being fabricated. The new powder layer is selectively joined where the part is to be formed by "ink-jet" printing the binder material. The piston, powder bed and part are lowered and a new layer of powder is spread out and selectively joined. The layering process is repeated until the part is completely printed. Unbound powder temporarily supports unconnected portions of the component, allowing overhangs, undercuts and internal volumes to be created. The unbound powder is removed upon process completion, leaving the finished part. The 3D Printing process sequence is shown in figure 1.2.1.

3D Printing was initially developed for the production of ceramic shells and cores to be later used for the casting of metal parts. In this embodiment of the process, a powder is spread into the powder piston and selectively bound using colloidal silica as a binder. After completion of printing, the parts is fired in a furnace to further bond the

silica to the alumina and strengthen the part sufficiently so that it can be used as a ceramic mold.

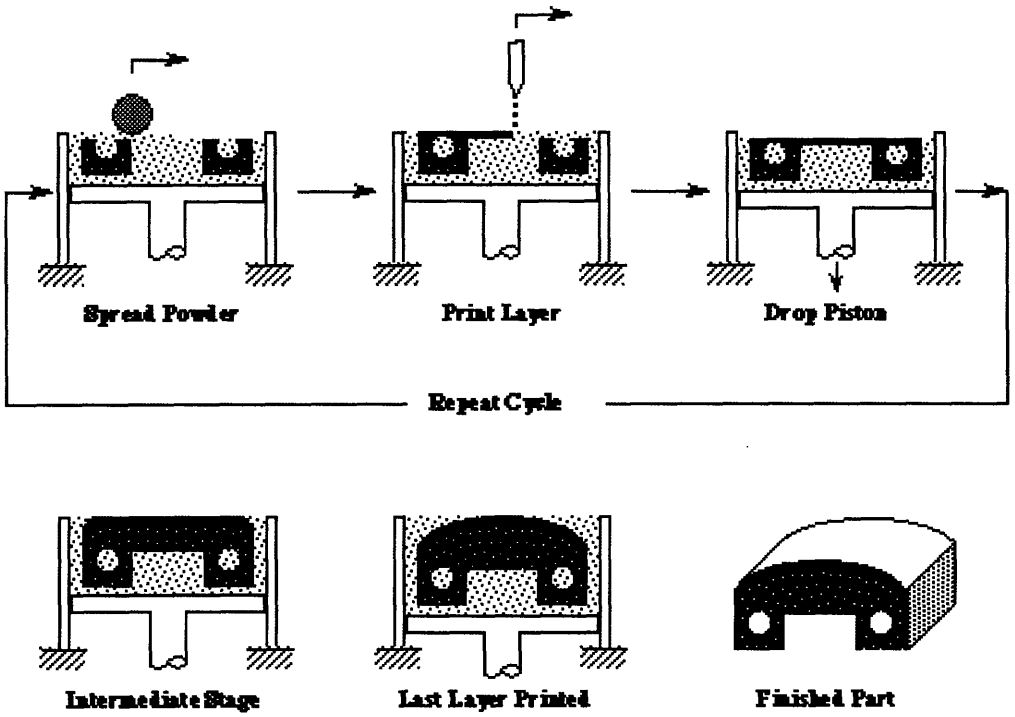


**Figure 1.3.1 the 3D-Printing Sequence**

In general the printing nozzle has a circular opening of 47-50 μm in diameter, but currently other diameters are being explored. The nozzle is stimulated by a piezoelectric transducer vibrating at a tuned frequency is used to break the stream into droplets. Commands to modulate the binder stream are derived from CAD data.

An important aspect of the 3D Printing process that had yet to be exploited was its inherent flexibility with respect to materials systems. Although developed around alumina powder and silica binder, there were no fundamental restrictions to the type of powder and binder, which could be used. Any material that could be attained in powdered form is usable in the process. Binder selection for a given powder would hinge on the type of post-processing which would be required. Also, the binder would have to be dispensable from an ink-jet style printhead compatible with the existing

machine, although currently Drop on Demand print heads can also be used to create a part. Figure 1.2.2 shows a drawing of a 3DP system.

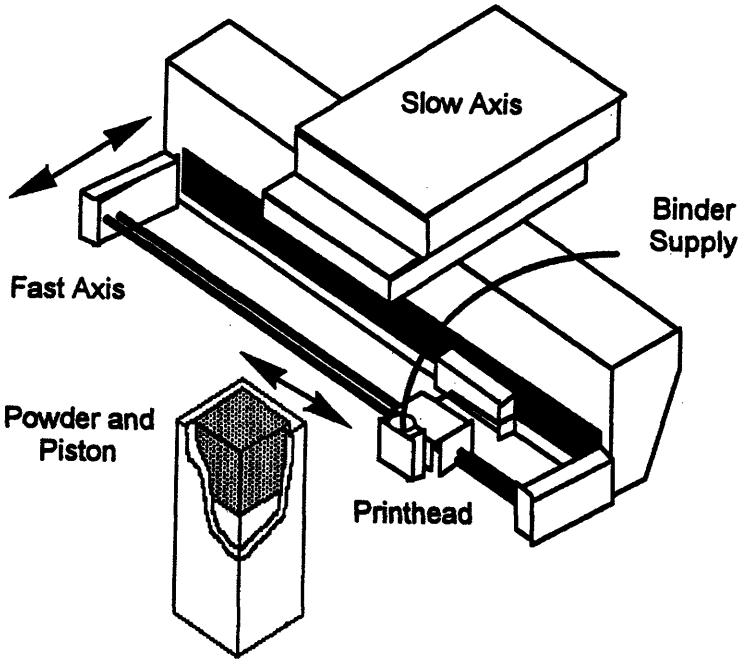


**Figure 1.3.2 A 3DP machine**

This research effort employs the 3D-Printing process to deposit a single layer of ceramic material. Eventually, the conception of printing several layers can also be used to achieve a desire thickness of the primer layer. In other words, if after printing the first layer of powder the thickness of such layer is not the specified one a succeeding layer can be printed using the same CAD information. The pattern can be created on a normal CAD program where the depth of the solid doesn't matter. The file would then be processed into a Stereolithography (STL) file and then sliced into a 3DP file which slices the part so it can be interpreted and rastered on top of the titanium sheet.

## 1.4 Ink-jet Printing

The 3D-Printing process uses Ink-jet printing technology where liquids that are jetted through small nozzles travel through the air in form of a continuous laminar flow cylinder [Heinzl et. al.]. The continuous part of the jet disintegrates spontaneously into a train of droplets. The transformation of the jet into droplets occurs because of a disturbance initiated at the nozzle. This disturbance can be controlled using a piezo attached to the nozzle. Rayleigh (1878) studied the problem for nonviscous liquid jets. Later, Weber (1931) treated the same problem including viscosity in the calculations and reached very similar results to that of Rayleigh. Bruce (1976) showed that results are accurate up to a viscosity of 10 cP.

As stated before, two approaches are going to be followed along the course of this work. The ink-jet printing technology is going to be used for both cases with some variations. In the case of the Low Risk Approach, normal nozzles, binder fluids and printing parameters will be used; while in the High Risk two configurations can be followed. The first one is just the jetting of the slurry through a larger orifice nozzle. The second one is the use of the compound jet. This method is an alternative way to generate a slurry jet [Heinzl et. al.]. Hermanrud and Hertz (1979) developed it. A high speed jet emerges from an orifice below the surface of a stationary fluid. After breaking through the surface, the primary jet is enclosed by a concentric layer of the stationary fluid, which has been dragged along by viscous forces between the jet and the fluid. Usually the submerged nozzle is very small in diameter and emerges under high pressure. This is considered the primary fluid while the one that rests in the pool is the secondary fluid. The compound jet breaks into a train of droplets in the same conventional way as the normal jet. We can see an illustration of the method in figure 1.4.1.

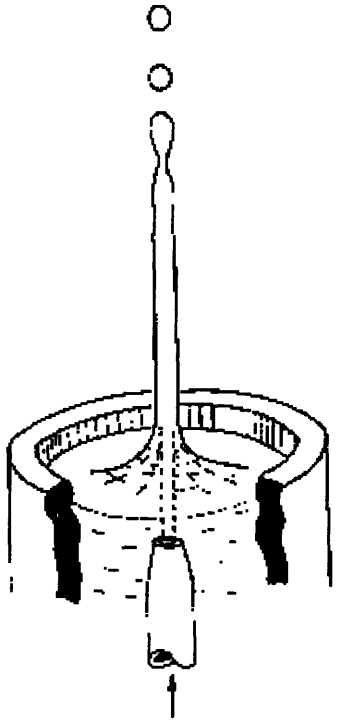

**Figure 1.4.1 The compound jet.**

For purpose of this research its clear that the normal printing mode is easier to implement. The compound jet would present a lot of problems because the sheets will have to be printed upwards. Anyway, the compound jet presents a lot of advantages in regards to fluid properties. As an example, the primary fluid could be water or binder while the secondary fluid could be the slurry. Problems such as clogging of the nozzle could be easily avoided by using a compound jet although a series of other problems may arise. In the event that the conventional printing would fail, then the possibility of using a compound jet will be explored.

## Chapter 2. Low-Risk Approach

### 2.1 Characterization of the materials received by Boeing.

**A. - Powder**: Yttrium oxide, a chemical compound better know as yttria was the material selected by Boeing to deposit on the chemically cleaned titanium sheets. The next table presents some of the most important characteristics of the ceramic powder.

| Chemical Formula | $Y_2O_3$ |
|---|---|
| Molecular Weight | 225.807 |
| Density | 5.01 gr./cc. |
| Melting Point | 2410 C |
| Appearance | White solid powder , no odor |

**Table 2.1.1 Bulk Properties of Yttria**

After receiving the powder, a particle distribution test was performed. It is important to know the exact particle distribution of the sample in order to classify and separate several size ranges for later printing experiments. It is also important to obtain a representative sample of the appropriate amount. In particle size analysis, we must recognize that sampling and handling may change the physical state of the sample. The technique used for separating the Yttria is called sieving. Sieving is the classification of particles in terms of their ability or inability to pass through an aperture of controlled size [Reed 1986]. The powder was introduced onto a stack of sieves with successfully finer apertures below, and the particles were agitated to induce translation until blocked by a smaller aperture. The finer sieved used was 20 μm., while the bigger one was 75 μm. The powder was dried before sieving, watching carefully not to contaminate it. The original sample contained a huge range of particle sizes; therefore different sizes were selected and separated for the several futures printing tests. The particle size distribution lies in a very wide range, it goes from particles below 20 μm up to particles bigger than 100 μm. The Low-Risk Approach is not really concerned with how small the particles have to be

because there is no jetting involved. Nevertheless, it is important to determine the exact size of the particles that are being used for future tests. Figure 2.1.1 presents the particle size distribution.

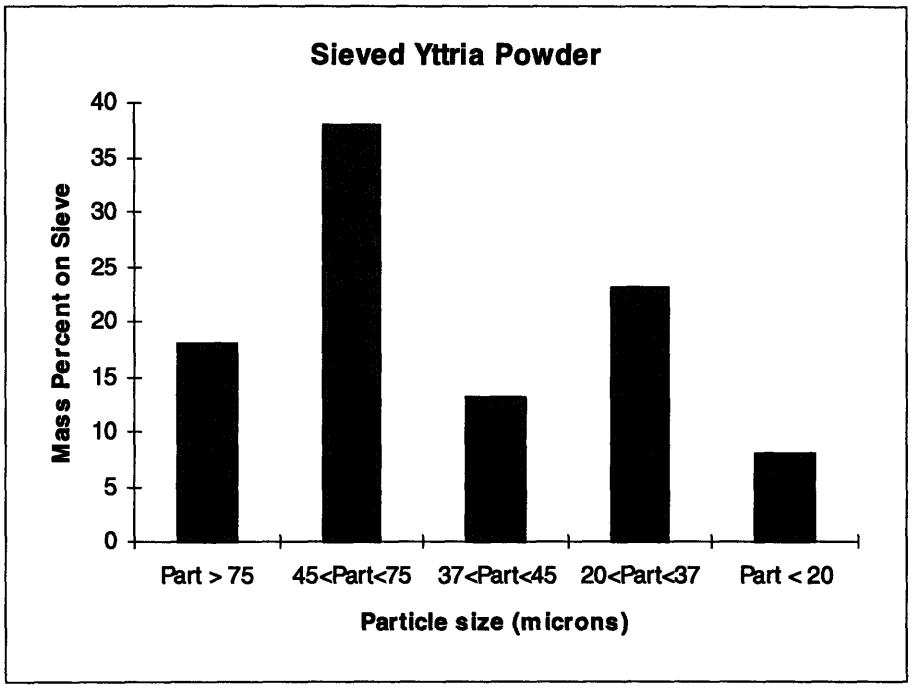


**Figure 2.1. 1 Distribution of powder particle size in the sample provided by Boeing**

In order to confirm the results obtained from sieving, the Stokes sedimentation method was followed. This technique is based on a simple balance of forces concept, and after several algebraic steps we find the following expression for the settling velocity of the particle [Reed 1986]:

$$Vs = \frac{g}{18} \frac{dp^2(\rho_p - \rho_f)}{\mu}$$

$\rho_p$ is the density of the particle
$\rho_f$ is the density of the fluid
$d_p$ is the diameter of the particle
$\mu$ is the viscosity of the fluid

The above formula works better for big particles. When smaller particle sizes are involved, Brownian motion plays a factor and disturbs the tests. The next table shows the

results obtained for the sedimentation technique using water as fluid, the experiments were made on a big graduated cylinder. In the cylinder, a distance of 80 mm was marked at the center of the cylinder. The container was then filled completely with water and sample of the specific powder was placed at the top of the cylinder. The particles traveled through the cylinder and across the known distance in a certain amount of time. The settling velocity was obtained by dividing the fixed distance by the time.

| Yttria Powder Sieved (μm) | Settling Time (cm/s) | Stokes Particle size diameter (μm) |
|---|---|---|
| > 75 | Vs=1.57 | dp=79 and bigger |
| > 45 and < 75 | Vs=0.79 | dp=60.4 |
| > 37 and < 45 | Vs=0.43 | dp=44 |
| > 20 and < 37 | Vs=0.31 | dp=37.7 |
| < 20 | Vs=0.24 | dp=31 |

**Table 2.1.2 Settling time for the particles in the powder sample provided by Boeing**

The results confirm that the sieved powder is the size it should be, with the exception of the smaller particles.

Another form of finding out the particle size of certain sample is to use Microscopy. Scanning Electron Microscope (SEM) was used to observe different samples of powder. This technique shows the nominal size and shape of the particles. Also pictures can be taken at very high magnifications to observe atypical particles as well as finer details of the shape and surface characteristics. In order to use the SEM, dry powder must be mounted on a stub. Then, the sample is gold coated in a vacuum atmosphere prior to the SEM session.

Polaroid photographs were taken. In these photos we can corroborate the difference in particle size. At the same time we can look at the shape and the appearance of the particles. The shape of the particles is very irregular and the surface is seen to be rough. Figures 2.1.2-2.1.4 show these photos.

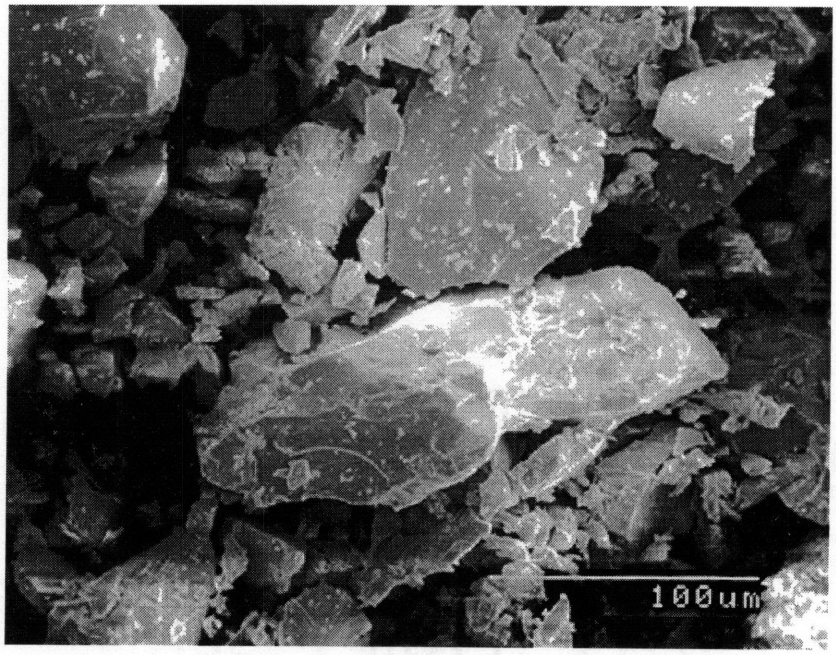


**Picture 2.1.2**

**Unprocessed Yttria powder from the sample provided by Boeing.**
**Particle size range lies between 10 to 130 µm.**

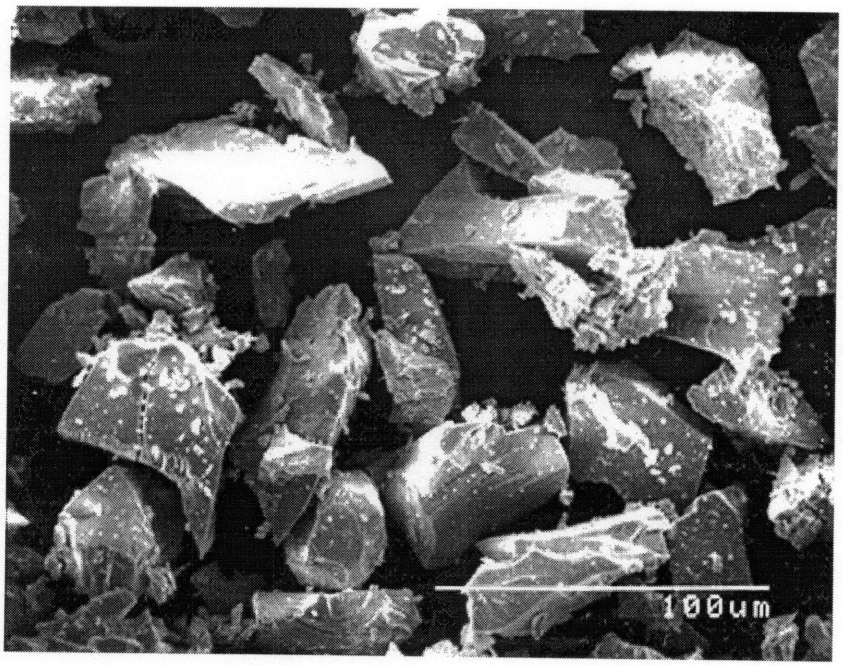


**Figure 2.1.3**
**Particles between 20 and 37 microns from the sample provided by Boeing**

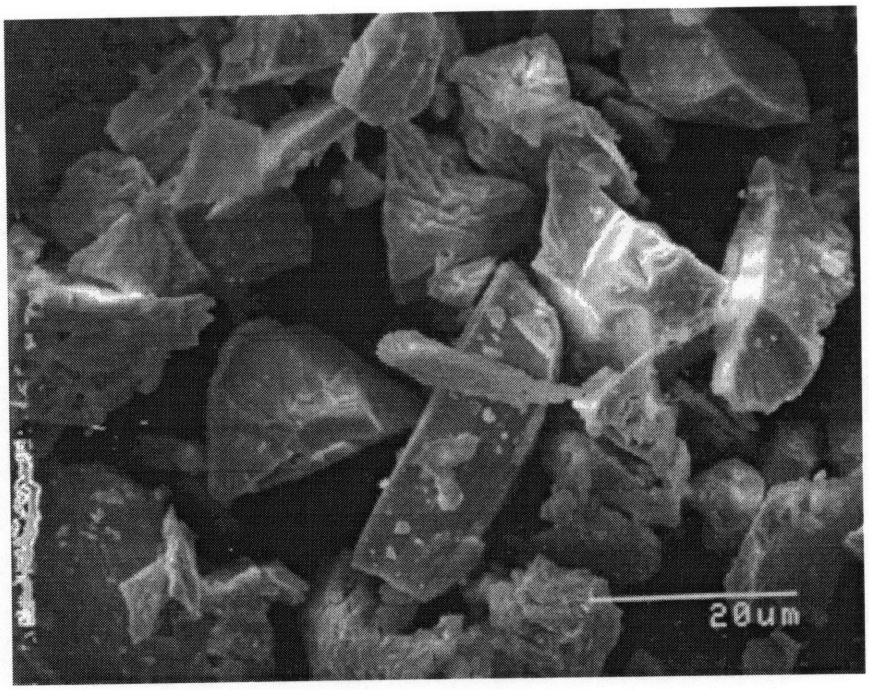


**Figure 2.1.4 Particles below 20 microns from the sample provided by Boeing.**

**B. - Titanium Sheets:** Several batches of titanium sheets were received along the course of this research. The sheets were cleaned prior to any printing or processing. The cleaning process was made according to the BAC-5753 specification. Etching is used for removing minor surface contamination by submerging the sheets in a Nitric-Fluoride solution for a period of 45 to 90 seconds. Once the sheets are cleaned they can be handled normally with the use of cloth gloves. It's important not to contaminate them during printing. Boeing made all these cleaning procedures. When the sheets were contaminated, they were sent back for cleaning.

## 2.2 Characterization of the Ceramic Powder Obtained by MIT.

In order to obtain a material where the particle size was smaller and more homogeneous, other samples of yttria were obtained. Low-Risk printing experiments will determine the size of the particles to use in the High-Risk approach. From picture 2.1.1 we can see that only 8% of the original powder lies below 20 microns. This means that

92% of the material would be unusable for slurry printing. Ideally, the smaller size the better. It is part of this research to determine the minimum particle size that can be used, in either the High-Risk and Low-Risk approaches. The Low-Risk will help determine some of the particle size characteristics needed for the High-Risk.

Yttria is available in several particle sizes and purity levels. The purity level used for these tests is 99.9%. Powder with particle size -20 microns and -10 microns were obtained for testing. The supplier of these powders is the Johnson Matthey Company located in Wardhill MA. The powder with particle size of 10 μm and below is directly listed in the Company's catalog, while the powder with particle size -20 μm has to be specially bought. The quote for the stock number can be found in Appendix D at the end of this document. The next 2 pictures show SEM photos of these samples.

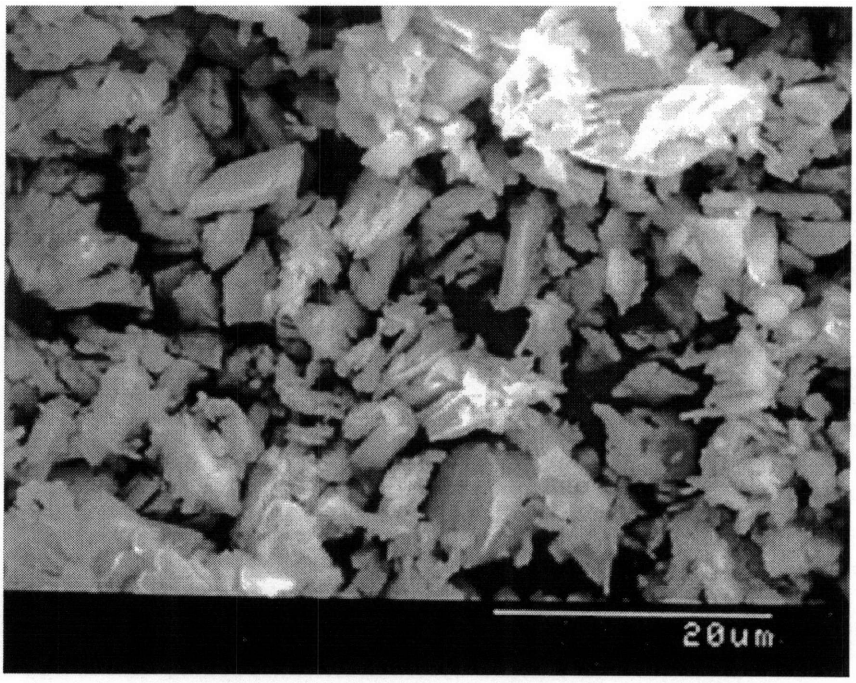


**Figure 2.2.1**
**Yttria Powder with particle size of 10 microns and below. Vendor: Johnson Matthey**

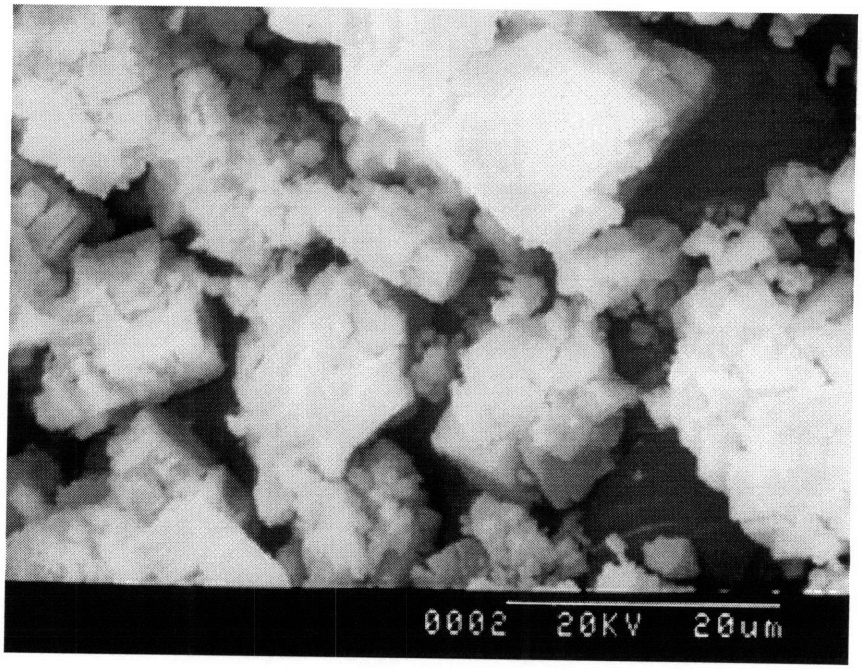


**Figure 2.2.2**
**Yttria Powder with particle size below 20 microns.**
**Vendor: Johnson Matthey**

This series of SEM photographs shows us the advantages of obtaining material, which has been previously classified and selected. Some of these benefits are that the sieving operation is eliminated and there is waste of ceramic powder. In conclusion, Boeing's yttria will be sieved for printing experiments with particles above 20 μm.; and for tests below that size the pre-selected commercial powder.

## 2.3 Packing and Apparent Densities

Packing and apparent densities of all the powders were studied. This was done by measuring the final volume of a certain amount of powder introduced into graduate cylinder. In the particular case of the packing density, the powder was mixed with water. After all the particles settled in the bottom, the mass was divided by the final volume. The results for the packing density experiments are presented in the next table.

| Yttria Powder Sieved (μm) | Grams of Yttria | Volume (ml) | Density of powder | Packing Density |
|---|---|---|---|---|
| Original | 5.23 | 2.65 | 1.97 | 39.4% |
| > 37 and < 45 | 2.08 | 0.95 | 2.18 | 43.7% |
| > 20 and < 37 | 5.63 | 2.8 | 1.94 | 38.7% |
| < 20 Johnson Matthey powder | 1.67 | 1 | 1.67 | 33.4% |
| <10 Johnson Matthey powder | 2 | 2.5 | 0.8 | 16% |

**Table 2.3.1 Packing densities for the powders depicted in sections 2.1 and 2.2.**

These results clearly stated that the slurries were not dispersed. In other words particles arrange themselves in a way where many voids are left between them making the packing density very low. In addition, as the particle size got smaller the packing density also did because smaller particles tend to agglomerate more than bigger ones. The next figure illustrates this principle [Rahaman 1996].

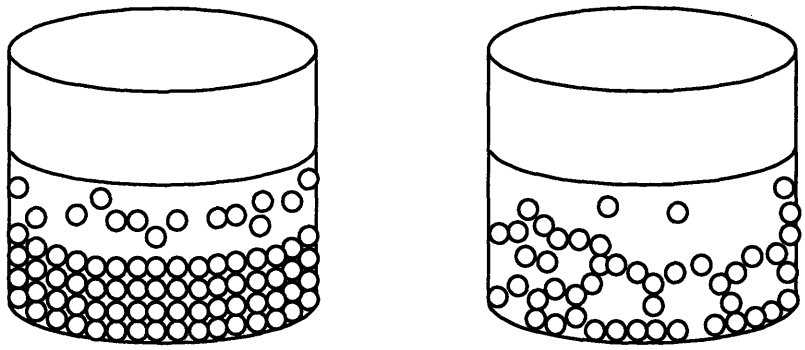


**Figure 2.3.1 A. Stable dispersed suspension B. Flocculated suspension.**

In the case of the apparent density the same operation is performed with the exception that no liquid is added. Again a certain mass of material is dropped into a graduated cylinder where a volume read is obtained and the apparent density is calculated.

In similitude with the packing density, the apparent density decreased with the particle size. Table 2.3.2 shows the apparent densities.

| Yttria Powder Sieved (μm) | Grams of Yttria | Volume (ml) | Density of powder | Apparent Density |
|---|---|---|---|---|
| Original | 9.5 | 5 | 1.9 | 38% |
| > 37 and < 45 | 9 | 5 | 1.8 | 36% |
| > 20 and < 37 | 7.6 | 5 | 1.52 | 30% |
| < 20 Johnson Matthey powder | 7 | 5 | 1.4 | 27% |
| <10 Johnson Matthey powder | 4.4 | 5 | 0.88 | 17% |

**Table2.3.2 Apparent densities and Packing densities for the powders depicted in sections 2.1 and 2.2**

## 2.4 Description of the Low Risk Printing Process.

As explained in chapter 1, this approach consists in printing binder on top of a sheet with ceramic powder. The idea is that the binder will dry and fix the powder onto the sheet only on the printed areas. The unprinted powder can then be easily removed with a blast of air. As indicated in the specifications in Appendix B, a nominal thickness of 0.003 in. is required so the amount of powder added should be controlled.

In order to achieve the desired layer thickness, a weight technique was used. This method consists of spreading powder with a sieve over a known area (3X5 card). Then, measure the weight of powder and using the packing density information from table 2.3.2, we can determine the thickness of the layer by calculating the volume.

Several printing tests were made in order to find the best printing sequence. Primarily, 3 ways of printing were explored using the Low-Risk approach. The first one and maybe the simplest, is to print binder on the titanium sheet using a 3D-Printing machine and the deposit a layer of powder. The second consists in spreading the correct layer and then print the binder on top. The third method spreads a very thin layer of powder followed by the printing of the binder and finally while the fluid is still wet, a final spread of powder. The advantage of method 1 is that no powder is introduced in the printing machine, but

unfortunately the binder flows before the powder comes into play making the edge definition very poor. Figure 2.4.1 shows this effect.

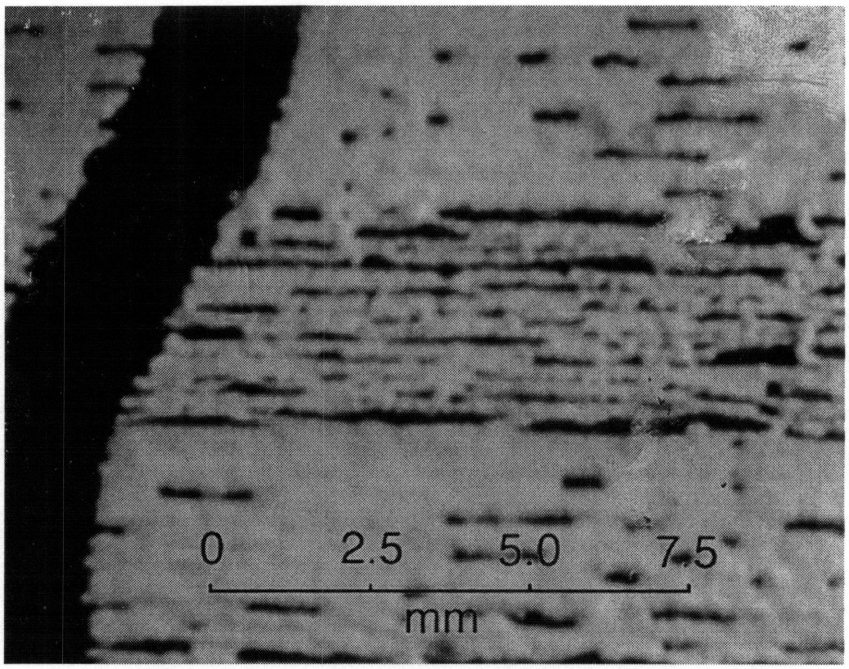


**Figure 2.4.1**
**Detail of Sheet printed by Low-Risk Approach Using method 1 Particle size 20 μm and below**

The second method has the disadvantage that the lines of powder shrink producing enormous defects in the printed areas. Figure 2.4.2 illustrates the effect.

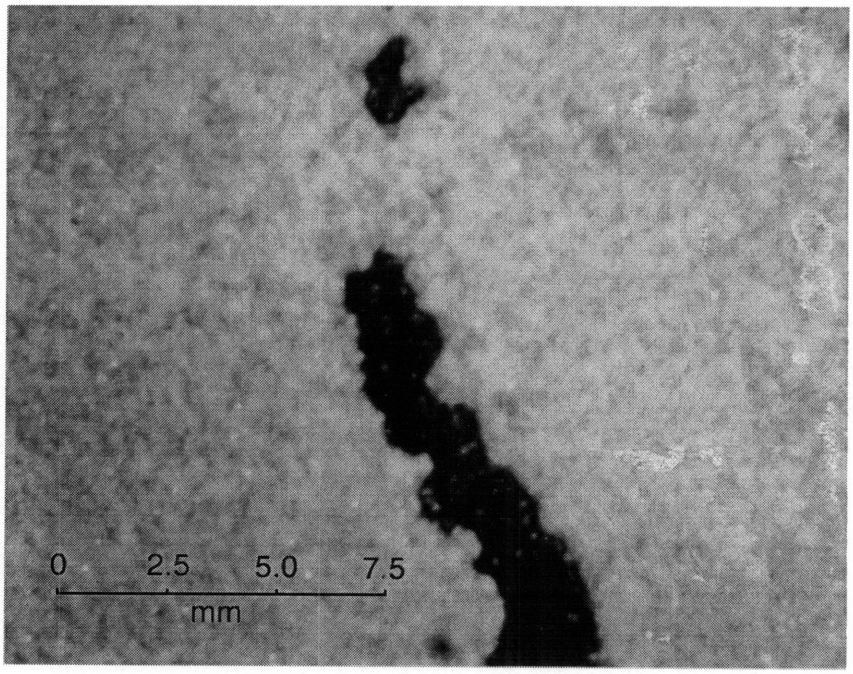


**Figure 2.4.2**
**Detail of Sheet printed by Low-Risk Approach Using method 2 Particle size 53 μm and below.**

The third solves both problems by locking the fluid with a very small amount of powder and also avoiding shrinkage. After that a last powder deposition comes into place covering all the defects and giving the pattern the desired thickness.

The steps to follow (Figure 2.4.3) in order to print a titanium sheet using the low risk approach are the following:

1.The first step is to spread the Yttria powder on to the titanium sheet using a sieve with 53 μm mesh. In this part of the process it has been found that if too much powder is placed on the sheet, the acrysol will be very quickly absorbed producing severe warpage and a uneven distribution of the powder in the sheet. This shrinkage may be avoided by barely dusting the sheet in first place. In other words, after depositing this first layer the titanium should still be visible. It doesn't matter that the area is not completely covered with powder, although it is important to have a uniform dusting.

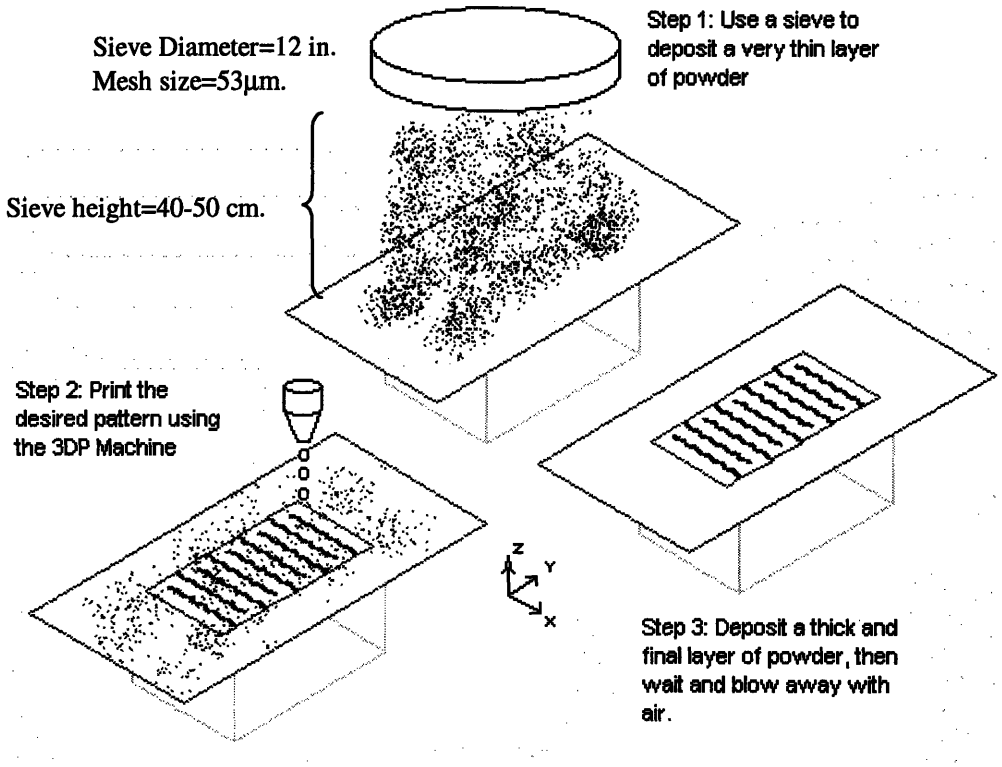


**Figure 2.4.3 Low Risk Approach Process**

2. The second step is to take the sheet to the Alpha machine where the CAD program should be ready as a 3DP file. The binder used in the machine was acrysol 25 Vol. %, while the flow rate was 0.85 cc/min. per jet. The nozzles used for printing were 47 microns. The sheet is then placed on the machine and the printing process starts. Once the machine finishes printing the layer it is very important to remove it quickly and go to step # 3.

3. In the third step we dust the sheet again but this time we add a lot of powder because the binder is still wet.

4. Finally the sheet is dried and the unprinted powder is removed. It is necessary to wait for at least 20 minutes before removing the loose Yttria. After the binder is completely dried, compressed air can be blown directly to the sheet in order to remove the excessive powder.

A total of 10 sheets were printed using the Low-Risk approach. The procedure used for printing all the sheets is the same as the one described previously. The binder used for all the tests was acrysol (25-weight %) with a flow rate of 0.85 cc/min. per jet. The 3D-Printing machine has a total of 8 jets printing at the same time.

Figures 2.4.4 through 2.4.7 show different sheets printed by the Low Risk Approach.

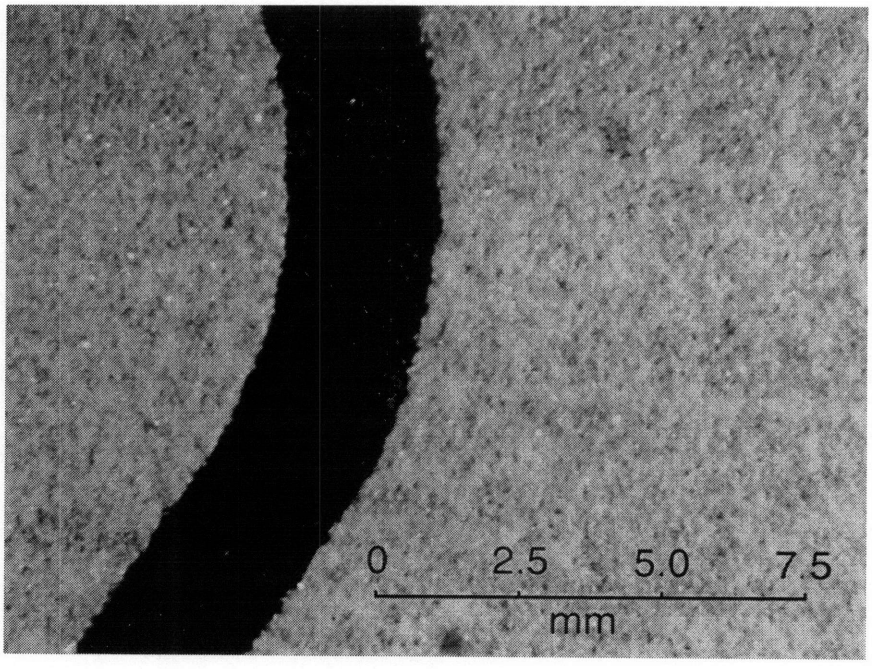


**Figure 2.4.4 Detail of sheet printed with particles 53 μm and less from the sample provided by Boeing Method 3**

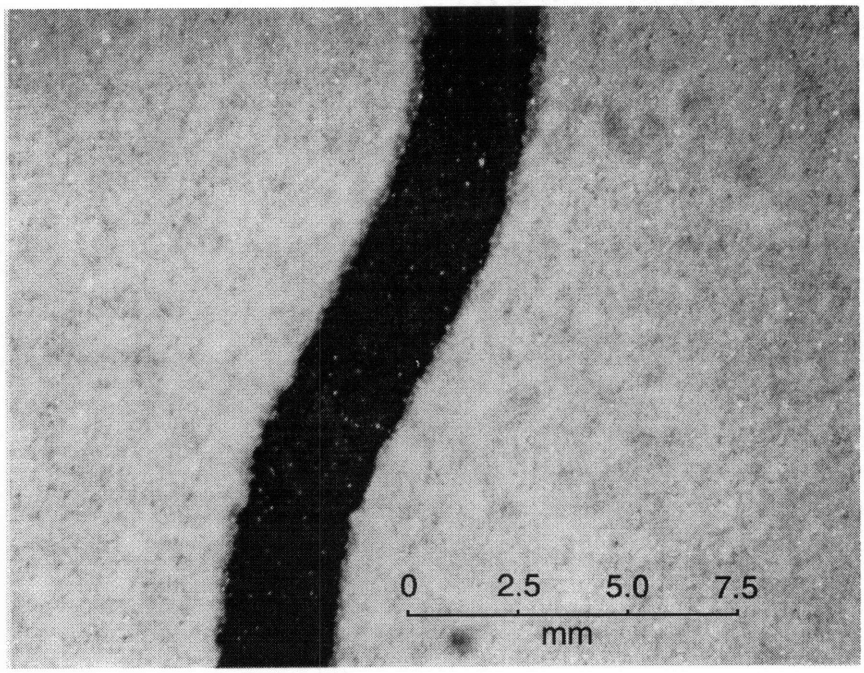


**Figure 2.4.5 Detail of sheet printed with particles 20 μm and less. Johnson Matthey Powder**
**Method 3**

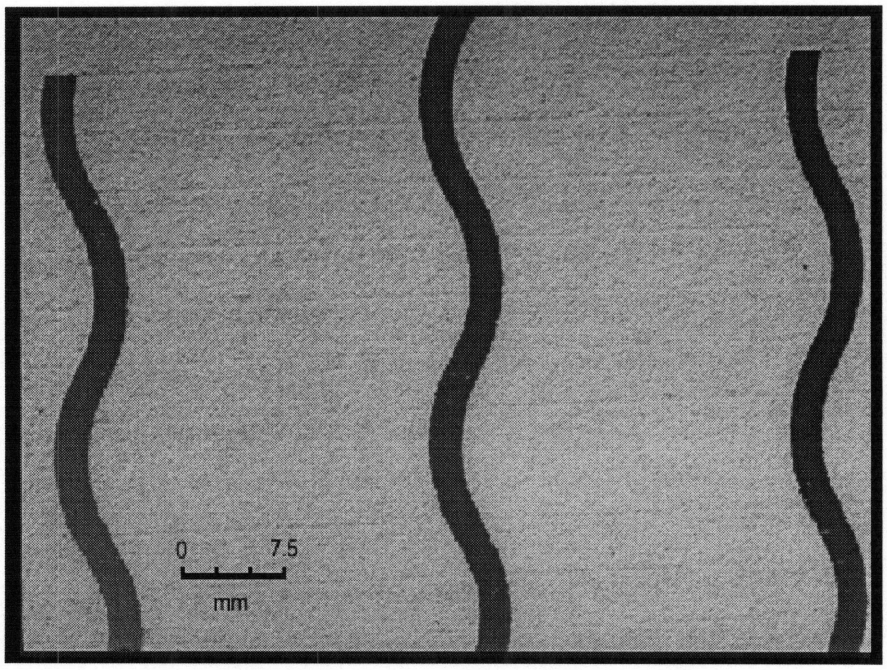


**Figure 2.4.6 Detail of sheet printed with particles 53 μm and less from the sample provided by Boeing**
**Method 3**

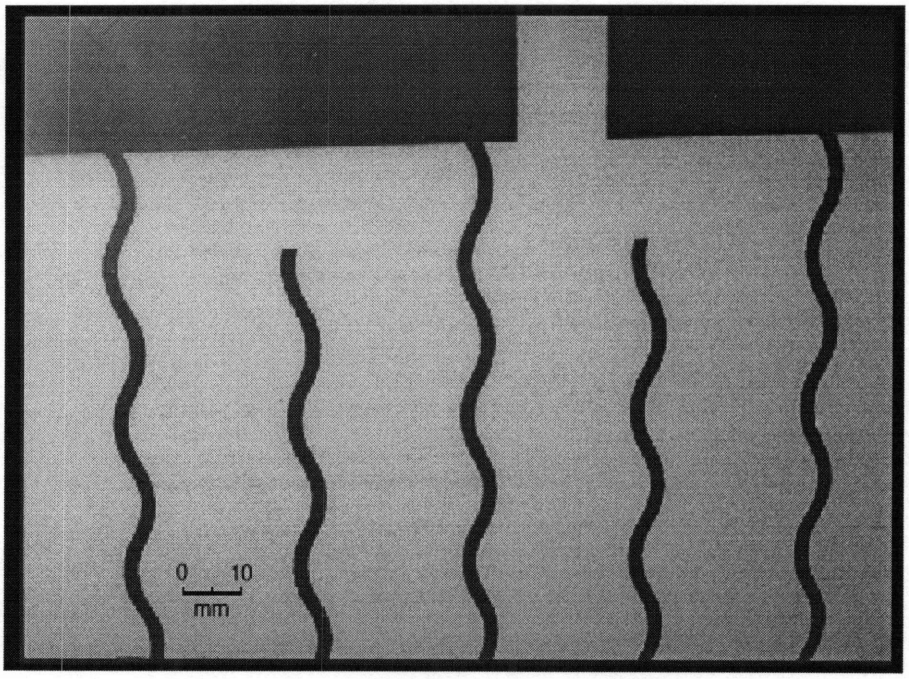


**Figure 2.4.7**
**Detail of sheet printed with particles 53 μm and less from the sample provided by Boeing**
**Method 3**

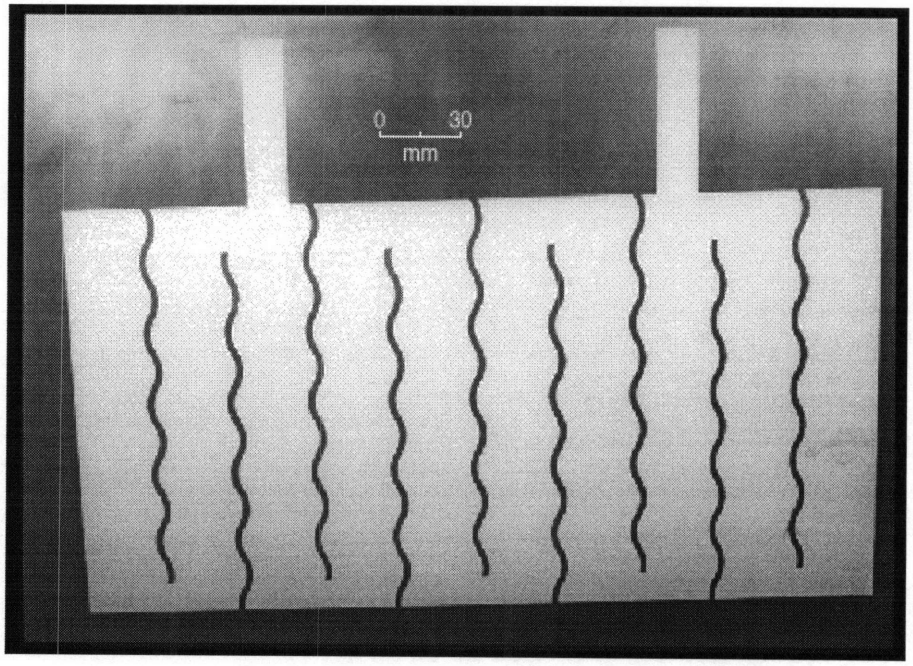


**Figure 2.4.8 Entire sheet printed with particles 53 μm and less from the sample provided by Boeing**
**Method 3**

## 2.5 Description and Measurement of the Printed Titanium Sheets

After printing the sheet and cleaning it with air, the layer thickness was measured. An Olympus microscope model BH2 with magnification of 10X up to100X was used. The depth of field of the microscope was less than two microns.

It is important to remark that the human eye comes into play introducing small errors. Any way, a very good feel of the thickness value can be obtained using this technique. Several measures were taken in different parts of the printed pattern. This was done to see the uniformity of the layer. Figure 2.4.1 show the 6 points that were selected.

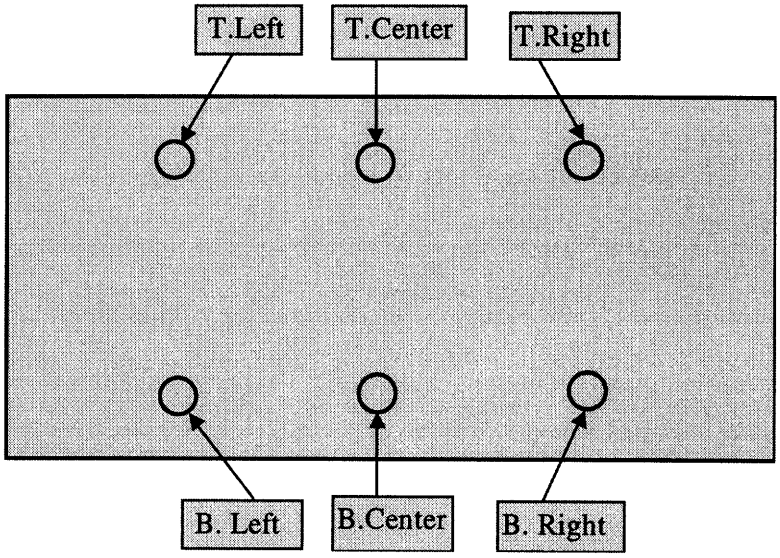


**Figure 2.5.1 Thickness measurements Positions**

In order to measure every point, the sheet was placed under a microscope and the procedure was the following:

- Place the light spot of the microscope over a zone that covers at the same time a printed and unprinted area.
- Focus the image on the bare titanium and make a measurement.
- Focus the image over the printed pattern trying to focus in point where most of the powder can be clearly seen. Take the second measure.

- Because of the scale of the focus knob is in μm. the difference between both annotations will result in the actual thickness of the yttria layer.

The next table presents a description of the printed sheets specifying particle size, average thickness and extra comments.

**Printed Sheets:**

| Sheet number: | Particle size: | Layer Thickness: | MIT Comments: | Boeing Comments: |
|---|---|---|---|---|
| 1 | 53 μm and less | 0.00316 in. | Ok. | Ok. |
| 2 | 20 to 37 μm | 0.00268 in. | Ok. | Ok. |
| 3 | 20 μm and less | 0.00284 in. | Ok. | Ok. |
| 4 | 10 μm and less | 0.00271in. | Bad looking | Failed |
| A | 53 μm and less | 0.00330 in. | Ok. | Ok. |
| B | 20 μm and less | 0.00305 in. | Ok. | Ok. |
| A1 | 53 μm and less | 0.00318 in. | Ok. Rectangles Added | Ok. |
| B1 | 20 μm and less | 0.00330 in. | Ok. Rect. (2 layers) | Ok. |
| Double A Side 1 | 53 μm and less | Not available | Ok. Sinusoidal edges | Ok. |
| Double A Side 2 | 53 μm and less | Not available | Ok. | Ok |
| Double B Side 1 | 20 μm and less | Not available | Ok. Sinusoidal edges | Ok. |
| Double B Side 2 | 20 μm and less | Not available | Ok. | Ok. |

**Table 2.5.1 Characteristics of the printed sheets**

The first 6 sheets have the same pattern. The next 2 have 2 rectangles added for easier post processing. The final 2 sheets have modified patterns and were printed on both sides. Due to this factor no thickness measurements were taken in order not to affect the printed patterns. The MIT comments refer to the appearance of the sheet, while the Boeing's comments refer basically to the good performance of the sheet in the actual post processing. The CAD drawings of the patterns can be seen in Appendix B.

## 2.6 Conclusions and Recommendations for the Low-Risk Approach

As we can see from the table, with the exception of 1 sheet all of the others met the expectations. Sheet # 4 was printed using powder presented in figure 2.2.1. The problem with this particular sheet was the fact that spreading a layer of very small powder presented serious problems. Particles join in such way that agglomerates form making it impossible to use a small sieve to spread it. On the other hand, the use of a bigger sieve to spread it will result in chunks falling down to the sheets.

In respect to particle size, the feedback received from Boeing determined that there was no problem in using the commercial powder with a particle size of -20 μm. Sheets 3, B, B1, and Double B were printed using this powder. The rest of the sheets were printed using the original yttria with a particle size of 53μm and less. The best sheets manufactured by this approach were the ones that used bigger particle size. Spreading was very easily performed and very good layers of yttria were obtained.

In the future, if the Low-Risk approach is pursued, it is very clear that particles of 53 μm. and below give very good results and are easy to handle and spread. It is also clear, that the development of a better and more reliable spreading technique is required.

One possible solution to this problem is to place a sieve at about 1 or 1.5 meters above the sheets and then proceed to spread. This will make the powder to spread evenly throughout the titanium sheet because as the particles fall down they have more time to disperse throughout the whole printing area. Spreading tests were made with very successful results. Yttria of 53 μm and less spread perfectly. Particles of 20 μm and less also spread much better using this technique. In the case of the -10 μm and less the results were not good due to the formation of agglomerates. Figure 2.5.1 depicts this spreading concept. The technique was not used because the sieve used for spreading was not big enough to cover the entire area where the pattern was printed. In the future, a special sieve could be constructed. This sieve would be the same in size as the area of the pattern to be printed.

Another idea can be the use a close volume on top of the sheets where a known amount of powder is placed. Then a series of fans can be introduced creating a cloud of

powder. Finally gravity will do the rest of the work depositing a good and even layer of Yttria.

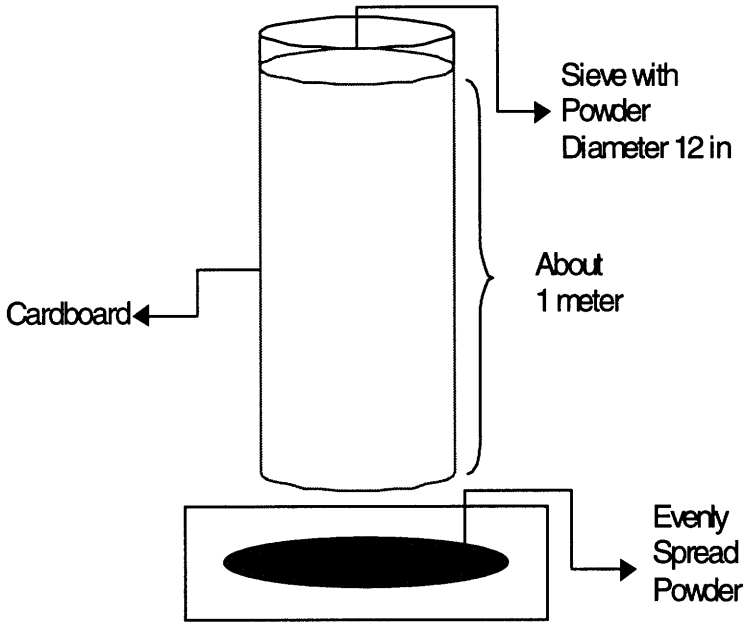


**Figure 2.6.1 Spreading powder form higher position**

Other ideas can be implemented and studied, but this research effort will try to focus on the High-Risk approach, which is the subject of the next chapters.

## Chapter 3: High-Risk Approach, Slurry Studies.

### 3.1 Introduction

As stated in section 1.2, one of the most important goals of this research is to print slurry based fluids with the current 3D-Printing technology. In this case, no powder has to be spread, and no feed piston is needed. The process will consist of directly depositing a layer of slurry in the titanium sheet. The concept of the "binder selectively joining powder" disappears. Instead, the binder and the powder are mixed together forming fluid with rheological behavior. This fluid or so-called slurry has to be jetted through a small nozzle and then selectively deposited on a titanium sheet. In principle, the smaller the nozzle the better, but many restrictions apply. The size of the particles is critical for these experiments. It is impossible to jet particles that are bigger than the nozzle, and it is very difficult to jet slurries with particles close in size to the nozzle diameter. The use of filters is essential but the most important factor of the process is to have completely dispersed slurry.

The dispersion process varies depending on the particles and the liquid media that are going to be used. Good dispersion is required to separate all the particles and prevent agglomeration. This helps enormously when jetting slurry because it assures that the particles will be completely separated in the liquid. In the particular case of this project, Yttria and water were the principal elements that formed the slurry. All the experiments done with the Low-Risk approach helped determine the minimum particle size that could be used in the High-Risk approach.

### 3.2 First Jetting Experiments of Yttria Slurries

The first jetting experiments done in this area consisted in mixing just water with 20μm. and below Yttria powder. Several slurries with different volume fractions were tested. After a good mixing, the suspensions were rapidly jetted through several nozzles and needles. This jetting was done before any settling occurred, and in most of the cases

the syringes were shaken while jetting in order to avoid settling. In other cases the jetting was done in an upward position to prevent settling at the tip of the nozzle. The fundamental purpose of these experiments was to observe which volume fractions could be jetted through the different orifice sizes. Six nozzle diameters were used to jet the various slurries and the results are presented in the next table.

| Volume % | 330μm. | 254 μm. | 203 μm. | 152 μm. | 127 μm. | 102 μm. |
|---|---|---|---|---|---|---|
| 7.5 % | XXX | XXX | XXX | XXX | Jets | Jets shaking |
| 10 % | XXX | XXX | XXX | XXX | Jets shaking | Clogs |
| 12.5 % | XXX | XXX | XXX | XXX | Jets Shaking | Clogs |
| 15 % | Jets | Jets | Jets | Jets Shaking | Jets Shaking | XXX |
| 20 % | Jets | Jets | Jets Shaking | Jets shaking ↑ | Clogs | XXX |
| 25 % | Jets | Jets | Jets Shaking | Clogs | XXX | XXX |
| 30 % | Jets | Jets | Jets Shaking | XXX | XXX | XXX |
| 35 % | Jets | Jets | Jets Shaking↑ | XXX | XXX | XXX |
| 40 % | Immediate clogging | Immediate clogging | XXX | XXX | XXX | XXX |

**Table 3.2.1 First jetting experiments for Yttria slurries (Yttria and water) using the powder in the sample provided by Boeing**
**Particle size below 20 μm.**
**(XXX means not tried)**
**(↑ means jetting upwards)**

The results show that a concentration of more than 7.5 volume percentage will clog the 2 smallest nozzles, which are the most important ones. The bigger the nozzle size, the harder it would be to print. Therefore it is critical to find a way of jetting higher volume percentages through the smaller nozzles. Moreover, the higher volume fraction will deposit more ceramic material over the titanium sheet.

## 3.3 Development of Slurry Formulation

### 3.3.1 Dispersion Studies with pH and Steric Control

Attractive surface forces, generally referred to as the van der Waals forces, exist between all atoms and molecules regardless of any other forces that may be involved. They also exist in macroscopic bodies such as particles. These forces make particles agglomerate into bigger bodies, therefore it is necessary to find a way of dispersing them.

There are 3 ways for trying to disperse a solution [Rahaman 1996]:

1. Electrostatic stabilization: Consists in adjusting the pH of a solution to achieve electrical repelling. Particles can be deflocculated by creating mutually repelling charged double layers.
2. Steric or polymeric stabilization: In this method a substance is added to the slurry. The repulsion is produced by polymer molecules adsorbed (or chemically attached) onto the particles surfaces.
3. Electrosteric: This type of stabilization is a result of both electrostatic and steric repulsion.

Once the ceramic particles are suspended in the liquid, they will agglomerate. One of the methods described above should be used to disperse them. Following method 1, when modifying the pH of a slurry, repulsion between particles is achieved by electrostatic charges on the particles. An electrical double layer of charge is produced between the particles, and the repulsion occurs as a result of the interaction. The

measured potential associated with the electrical double layer is called the zeta potential [Rahaman 1996]. This potential is an important guide to the stability of a slurry. The pH at which the zeta potential is zero is termed the isoelectric point (IEP). Raising or lowering the pH from the IEP will increase the absolute value of the zeta potential, therefore electrical charging may stabilize slurries in polar liquids. The IEP of Yttria lies in the range of 6.5 to 7 pH, so in order to electrically disperse the slurry we have to modify the pH towards the acid part or basic part. The following diagram depicts how the zeta potential changes with the pH for Yttria slurry.

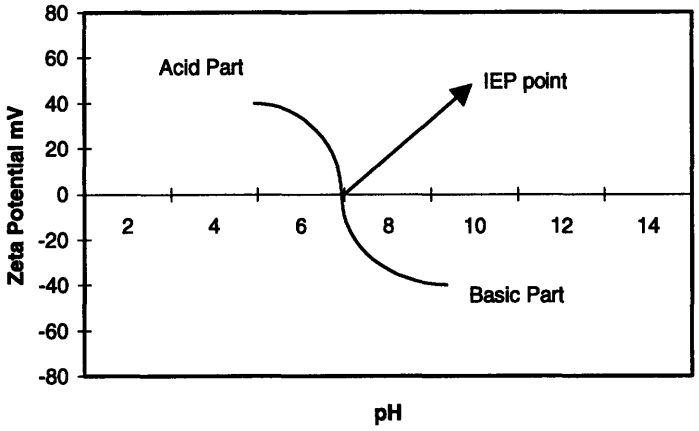


**Figure 3.3.1 pH versus zeta potential for Yttria slurry**
**Test performed with slurry of 5-volume % and a particle size of –10 μm**

Experiments were conducted using Yttria powder with particle size of 10 microns and less. Once slurry with this particle size could be dispersed the next step would be to use 20 μm. Several approaches have been followed based on the methods described above.

Slurries were prepared by combining the right amounts of liquid, powder and dispersant. Various mixing sequences were investigated in order to obtain the most suitable slurry. The sequences were:

- Powder was added to mixtures of dispersant and water
- Dispersant was added to mixtures of powder and fluid
- Water was added to mixtures of powder and dispersant

After several experiments and research [Galla 1994], it was found that the first sequence is the most appropriate one, because the powder is slowly added to liquid avoiding the formation of big agglomerates. This method was the one used for preparing all of the slurries tested in this work.

The first slurry prepared was 20-volume fraction following the steric method. Fifty five ml of slurry were prepared and Darvan C was the surfactant used. The amount of Darvan added was 1.5% of the weight of the ceramic powder. The initial pH of the solution was 7.6. The slurry was placed on the ball mill in order to reach a complete dispersion. After 2 hours a paste was formed. The pH of the slurry was 10.4. The change in pH occurs because as the agglomerates break in the mill more powder comes in contact with the liquid causing the pH to change. Also Darvan C contains ammonia, which helped the increase in pH.

Several efforts were made to formulate slurry with a different pH. Again 20 volume percent slurry was prepared and the pH was set to 4 using a 2M solution of nitric acid. The slurry was then placed on the mill for 2 hours. After milling the pH measured was 6.8 and the appearance of the slurry was not good. Yttria seems to react with the acid when the last is added in large concentrations, making the pH of the slurry very hard to control. In fact, the pH stays low for some time and then it tends to go to the IEP. Other efforts were made using different concentrations of nitric acid (0.5 M, 1M) and the results were very similar to the ones obtained with a concentration of 2M.

New 20 volume fraction slurry was made with nitric acid without the addition of Darvan C. The amount of slurry prepared was 55 ml. The nitric acid was added in small quantities. Only 3-ml (2M) of nitric acid were used. After milling, it was found that the pH of the suspension lied around 9. The appearance of the slurry was good and for the first time fully liquid slurry was obtained.

Comparing the slurries with and without Darvan, we could see that the particles in the slurries without Darvan settled during the course of the day. In contrast, the slurries containing Darvan remained for days in the same pasty form.

With the exception of the last slurry prepared, The first set of slurries failed because they were not stable and after several hours thick pastes were formed. Also, jetting was not successful and no improvements were made in comparison to the first experiments. Darvan C was abandoned completely and the only dispersant agent used was nitric acid.

In the beginning, dispersions were made using nitric acid and -10 μm powder. Later the -20 μm powder obtained from Johnson Matthey was utilized. Very small amounts of nitric acid in a 2M solution were used to disperse the slurries by modifying the pH. The important concept here is to control the pH of the slurry in some point between 8 and 9. The 20 volume fraction slurries were successfully jetted through 127 μm nozzle.

It was then observed that the slurries did not adhere to the sheet after the vehicle was dried, therefore another formulation had to be developed. It is of fundamental importance that once the slurry is deposited in the titanium sheet, it will significantly adhere so post-processing operations could be performed. Any successful jetting is useless if no good contact between both materials is made.

Instead of using nitric acid, it was decided to use polyacrylic acid (PAA). This binder was chosen for several reasons. First, since it is an acid, it could be used as electrosteric dispersant. Second PAA it is a strong binder that it's available in different molecular weights, making it very easy to experiment. Finally it is soluble in water and is very easy to handle.

### 3.3.2 Poly Acrylic Acid

Because of the very poor adherence seen between the slurry and the sheets, some extra research had to be developed. PAA was used because it could perform 2 functions at the same time. These functions were dispersing and binding. Unfortunately, the binding function was very poor. Again the search for a new and better binding agent was imperative. In the beginning small concentrations of PAA were used. Then larger

amounts of binder were added. The viscosity of the liquid media of the slurry increased when the concentration of PAA grew.

A viscosity graph was obtained for PAA Molecular weight 2000 and Molecular weight 5000. Figure 3.3.2 represents the viscosity of the liquid for a 20 volume fraction Yttria slurry varying from 20 up to 60 volume percent of PAA per ml of Yttria. This means that the amount of PAA added is a function of the amount of ceramic in the slurry. For example, to prepare 10 ml of liquid media for a 20 volume percent Yttria slurry with 20 volume fraction of PAA MW 2000 per ml of ceramic, we can the following:

For 10 ml of a 20 volume fraction Yttria slurry we have 2 ml of ceramic and the rest is liquid. The 8 ml remaining containing PAA and water are what we are considering the liquid media. To determine the amount of PAA to add, we simply multiply the volume of the ceramic powder by 20%, which is the concentration of binder per ml of ceramic. We can also use a mass relation. Finally we multiply the previous number by the weight fraction of the PAA 2000 (Density very close to 1 gr./cc). The remaining number is the amount of PAA in grams we have to add.

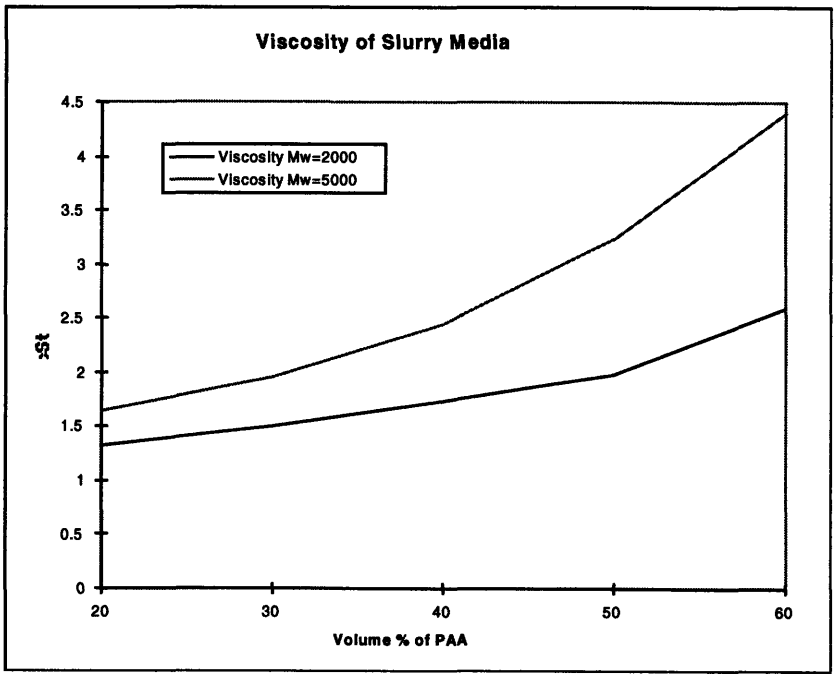


**Figure 3.3.2 Viscosity versus binder concentration for PAA MW 2000 and PAA MW 5000**

We can clearly see that the viscosity or the PAA Mw 5000 is higher than the 2000, but neither binder has produce good results yet. All the different types of PAA were obtained from Aldrich Chemical Company.

Another important issue is fact that PAA dissolves in water. This means that if we add 10 cc of water and 10 cc of PAA we are not going to get 20 cc of mixture, so some tests were made to determine if the difference in volume was such that it would be important in the volume fraction calculations. An experiment was made to determine the importance of this effect. For 52 ml of a 15 Volume fraction Yttria slurry with 25% PAA 2000 (per ml of ceramic) we mix the following components:

- 8 ml of Yttria (the powder will not be added for this experiment)
- 3.25 ml of PAA 2000 (65 weight %) with density very close to 1 gr/cc
- 41.5 ml of water

The mixture was poured into a graduate cylinder and a volume read was taken. The volume of the liquid containing water and binder was 44 ml. The theoretical volume for the liquid assuming PAA would not dissolve in water was 44.5 ml. From these results, we can conclude that is safe to assume that the volume of PAA can be added to the volume of water and the volume of powder.

It has been observed, that the adherence changes depending on the concentration of PAA and the milling process. For slurries using 20 percent PAA (2000, 5000) up to 35percent, some adherence to the sheets but not significant was observed before and after the milling process. For 40 volume percent and higher concentrations of binder results were better as the concentration increased. However for the same slurries, after milling, results were not so good and in fact poor. In addition, the jetting process is hardly affected as the concentration of the PAA increases. Furthermore, foaming became a big factor for high concentrations of PAA. As a rule to control foaming a single drop of Octanol was always added.

In the next photograph, we can see a 20 Volume %. Yttria slurry with 40 % PAA 2000 before milling. This slurry stuck quite well to the sheet, while the same slurry did not after having been milled. In the photo we can see that a film of binder was formed to the right of the Yttria. When this film formed, the process worked and the slurry adhered

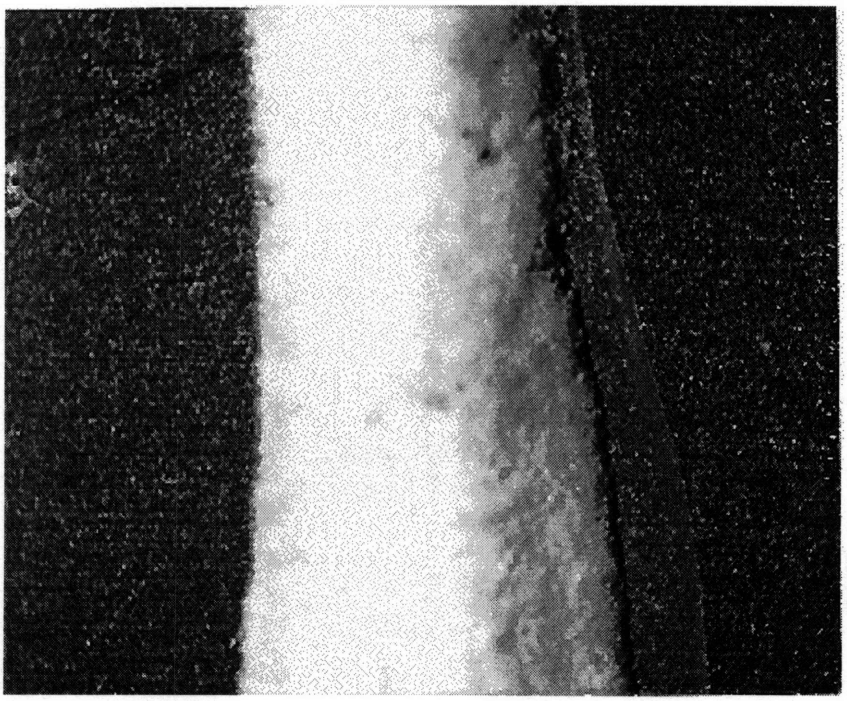

**Figure 3.3.3 20 Volume percent slurry with 40 volume percent of PAA**

to the sheet. So other tests had to be made in order to determine why the milling process was affecting the adherence.

In order to find the correct amount of PAA to use and a possible explanation to the problem of the no adherence after milling, some calculations were made in order to estimate the thickness of the film of PAA covering the surface of the ceramic particles. If the layer of PAA forming around the particles was only a monolayer, it is possible that this layer might have undergone a chemical change due its proximity to the powder surface. If this was not to be the case, the layer would be thick and it would be unlikely for the entire layer to through a chemical change.

The area of a PAA molecule was calculated approximately. The calculation was done by using the atomic radius of the elements that compose a molecule, and also by estimating the lengths of the bonds between the different elements. For practical reasons

these lengths were considered as 1 Å. Also, it was considered that the carbon has a tetrahedron arrangement in space so the molecule is not flat. We can see this calculation below along with the picture of a molecule, its chemical formula and the atomic diameters of Hydrogen, Oxygen and Carbon [Askeland 1985].

| Element | Atomic Radius | Molecular Weight |
|---|---|---|
| Carbon | 0.77 Å | 12 |
| Oxygen | 0.6 Å | 16 |
| Hydrogen | 0.46 Å | 1 |

**Table 3.3.1 Characteristics of the elements composing PAA**

Therefore the molecular weight of the monomer is 72 gr./mol, because the chemical formula of the PAA is:

$$-\left[CH_2CH(COOH)\right]_n-$$

In the next picture we can see an arrangement similar to a PAA molecule, we can see the tetrahedron structure of Carbon.

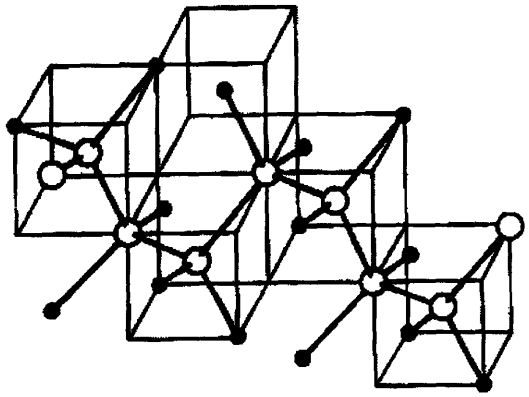

**Figure 3.3.4 Tetrahedron structure of Carbon.**

Once we had the area of one molecule, we can estimate the area of a polymer chain. Therefore, by the amount of PAA (MW 2000) that we add we can see calculate the total area of a certain amount of PAA for a particular molecular weight. After making the calculations with the minimal area a molecule can occupy, the results say that there was enough PAA to cover at least 250 times the surface area of the Yttria. Thus, it seems that the layer of PAA is fairly thick and it is unlikely that a chemical reaction between the powder and the PAA is able to substantially alter the PAA.

In consequence, to see if the PAA will behave as acrysol did in the low risk method, a printing experiment using the low risk approach was used. A solution of PAA and water was prepared and jetted to a nozzle to a sheet dusted with Yttria. After that a second layer of powder was placed and after dried, the results were observed. The adherence of the powder to the sheet was good, but not as good as with acrysol. When printing in the Alpha machine 25 Vol. % acrysol was used, while the PAA solution used in this experiment was 7.6 Vol. %.

Another experiment done was to prepare a normal 20 Volume percent Yttria slurry with 20 Volume percent PAA and then mill it. The slurry was taken to the centrifuge, which separated the denser solids from the liquid and then extract the latter. After that the liquid was jetted to observe whether or not it would adhere to the sheet. In parallel a solution was prepared with the same characteristics as the one used in the slurry and jetted in the same way. After the experiment was concluded, the milled solution did not stick and was easily removed with a finger while the original stuck to the sheet.

Due to the lack of good results using PAA as a binder, the possibility of using acrysol in the slurry was studied. A 20 % acrysol by volume on 20 volume percent Yttria slurry was prepared with and the results were discouraging. Clogging was observed continuously and the slurry was clearly not well dispersed. Other combinations were tried without any good results. Therefore acrysol was abandoned as a binder to be used in the high-risk approach. Once again, the need to find a binder that would make the slurry adhere to the sheet was imperative, for this reason PEG (Polyethylene glycol) was the next polymer to explore.

### 3.3.3 Poly Acrylic Acid and Polyethylene Glycol

Following the same steps as before, different slurries were prepared starting with 20 volume percent of PEG (MW 20,000 Vendor Fluka) on 20 volume percent ceramic slurry. An eyedropper was used to spread some slurry onto a titanium sheet. After drying, the material presented some adherence to the sheet but the adherence was weak. The pH of the solution was very close to 8. The next step was to increase the amount of PEG, so solutions with 25, 30, 35 and 40 volume percents were prepared and spread onto titanium. The 35 and 40 percent slurries presented a strong bond with the sheet. In the same way, a significant amount of material was prepared in order to be milled and spread afterwards. The experiments were done and the slurry adhered reasonably well to the sheet. These results were encouraging but we still needed to jet the slurry through a 102 μm nozzle. The viscosity of the liquid media using PEG increases significantly as the volume percent goes up, therefore we couldn't use high concentrations of PEG.

Another very important issue is the fact that we still need an acid agent to disperse powder in the liquid. The PEG by itself doesn't create an acid media so it was impossible to jet through the nozzle. Because all the previous work done with PAA, and the fact that that doesn't affect the viscosity in a significant way when added low concentrations, PAA was chosen as the acid dispersant. Good results were immediately obtained with this combination. Several different slurries were prepared fixing the amount of PEG at 35% per ml of Yttria and varying the PAA from 10 to 30 volume percent of the ceramic.

A set of final expressions can be derived in order to calculate the amounts of PAA and PEG. In contrast with all the previous calculations, the amount of additives added will be related to the amount in grams of Yttria contained in the slurry. For a 7% PEG per gr. of Yttria (corresponds to a 35% PEG per ml of Yttria) and 5% PAA (corresponds to a 25% PAA per ml of Yttria) the expression is as follows:

$$PEG_{[gr]} = Yttria_{[gr]} * 0.07$$

$$PAA_{[gr]} = Yttria_{[gr]} * \left( \frac{0.05}{Weight\%_{of\,PAA}} \right)$$

From the slurries prepared, it was found that the best dispersions are the following:

For a 20 vol. % Yttria Slurry:

| De-ionized Water |
|---|
| 7 % PEG (Per gr. of ceramic) |
| 6 % PAA (Per gr. of ceramic) |
| 1 drop of Octanol to avoid foaming |

**Table 3.3.2Componensts for a 20 vol % slurry**

For a 15 vol. % Yttria Slurry:

| De-ionized Water |
|---|
| 7 % PEG (Per gr. of ceramic) |
| 5 % PAA (Per gr. of ceramic) |
| 1 drop of Octanol to avoid foaming |

**Table 3.3.3 Components for a 15 vol % slurry**

Once the slurry was carefully prepared, it was placed on a nalgene bottle and milled for at least 5 hours. The milling media used were alumina balls of about 3/8 of an inch in diameter.

## 3.4 Jetting Setup, first continuous jetting experiments

Continuous jetting experiments were conducted with different slurries. These first experiments consisted on simply jetting fluid continuously. Filters, a pressurized vessel and a magnetic stirrer to keep the slurry in continuous movement were the equipment used. The pressures used were between 30 and 50 psi, and the filters sizes were 104 and

74 μm for a 127 μm nozzle. For the case of a 102 μm nozzle the filters used were 88 and 60 μm. Figure 3.4.1 depicts in a simplified way the arrangement to jet the slurries.

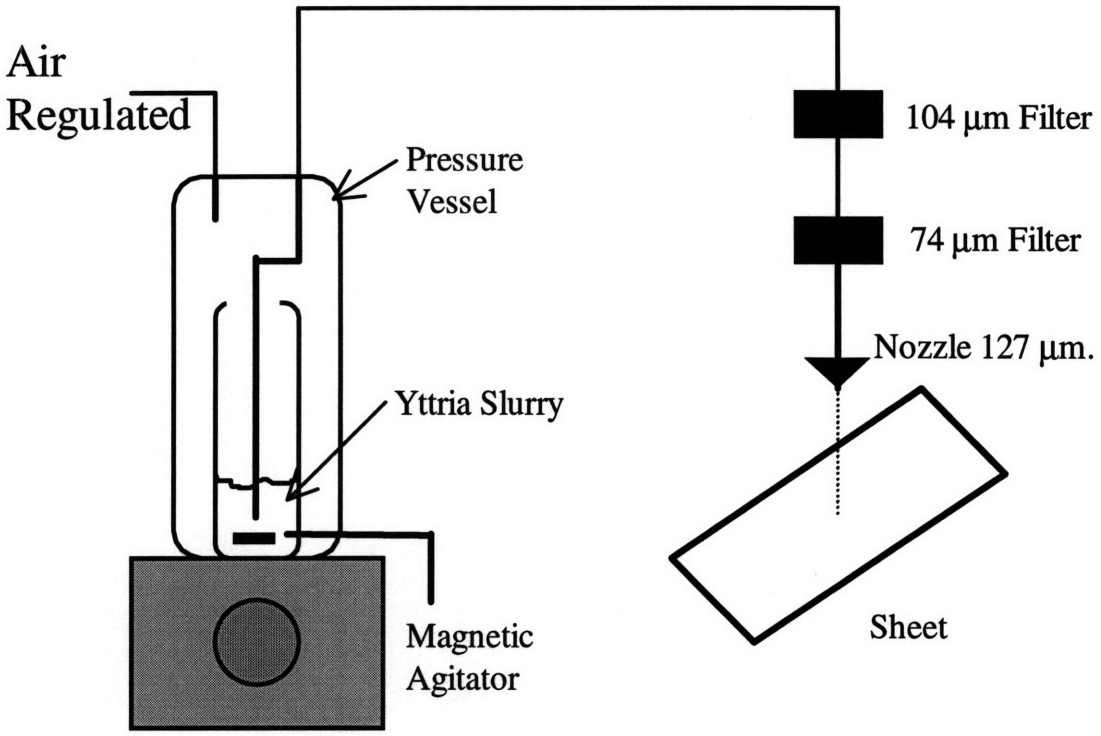


**Figure 3.4.1 Fluid system for jetting slurries.**

Table 3.4.1 includes the most important slurries that were using -20 μm powder. We can see the volume concentration as well as the components of each particular case and the final results.

## Yttria Slurries Used in Continuous Jetting Experiments

| # | Yttria Below 20μm (gr.) | Water (ml) | Nitric Acid 2M (ml) | Darvan (ml) | PEG MW 20000 | PAA MW 2000 65 weight % (ml) | pH | Comments |
|---|---|---|---|---|---|---|---|---|
| 1 | 55 | 40 | 7 | 4 | xxx | xxx | 10.4 | 18Vol% Turn into Paste |
| 2 | 55 | 40 | 3 | xxx | xxx | xxx | 9.2 | 20.4Vol%. Jets 127 μm nozzle |
| 3 | 55 | 40 | 7 | 3 | xxx | xxx | 9.9 | 18Vol% Turn into Pasty Form Jets for 30 seconds |
| 4 | 55 | 40 | 4 | xxx | xxx | xxx | 9.0 | 20.4Vol%. Jets 127 μm nozzle |
| 5 | 75 | 40 | 5 | xxx | xxx | xxx | 9.2 | 25 Vol% Clogs 127 μm nozzle |
| 6 | 55 | 40 | xxx | xxx | xxx | 1 | 4.2 | 21Vol%. Jets 127μm nozzle Poor adherence |
| 7 | 55 | 40 | xxx | xxx | xxx | 2 | 4.2 | 20.7Vol%.Jets 127 μm nozzle Poor adherence |
| 8 | 35 | 28 | xxx | xxx | 2.4 | 3.2 | 5 | 18Vol%.Jets 127 μm nozzle Good adherence |
| 9 | 30 | 31.6 | xxx | xxx | 2.1 | 2.3 | 4.8 | 14.5Vol%.Jets 102 μm nozzle Good adherence |

**Table 3.4.1 Jetted Slurries of several volume fractions**

**Powder commercial –20 μm Yttria**

It is very important to say that the slurries need to be milled for certain time. A minimum milling time should be 5 hours but they can be placed in the mill and left overnight with the same jetting results. Milling is needed to break all the agglomerates and to mix all the components in the slurry.

In order to verify that we are jetting 20 volume % slurry, a very simple test was made. This test consisted of jetting a certain mass of slurry. Once the mass is known, we wait for 1 day for the water to evaporate and then we weighted again. The remaining mass is just Yttria and binder, and we can see if we are jetting the slurry adequately. The following experiment was developed using slurry # 7 from the table above.

The complete data of Slurry 7 is the following:

- 20.75 Volume % Yttria.
- 57.11 Mass % Yttria.
- Theoretical Density 1.8169 gr./cc.
- Measured Density 1.9 gr./cc.

The data of the flow and nozzle:

- Flow rate 3.57 cc./min.
- Flow rate (mass) 6.5 gr./min.
- Velocities of stream 4.7068 m/s.
- Diameter of nozzle 127 μm.
- Area of nozzle 1.26E-08 $m^2$

Experiment

- 6.5 grams were jetted in a minute.
- 3.7 grams remained after drying giving us a 56.9 weight % of Yttria, which is really close to the theoretical 57.11 weight %. This confirms that we are indeed jetting above 20 volume % slurries with average particle size of 20 μm.

### 3.5 The generation of Droplets

After being able to jet 20 volume % slurries, the next step was to create drops. Drops are necessary for 3Dprinting, and a piezo crystal is used for this purpose. A boa jet [Serdy Private Communication 1996] was adapted to a 102 and 127 μm ceramic nozzles and used in the jetting tests. The arrangement can be seen in figure 3.4.1 with the exception of the piezo adapted to the nozzle.

A frequency generator was used to drive the piezo and induce the creation of droplets. Also a power amplifier was connected to the system in order to achieve an electric potential range of 60 to 100 Volts. This voltage was required to obtain a good break off of the jet. Finally in order to know for certain that drops were forming, a CCD video camera was used with an LED (Light Emitting Diode) flashing at the same frequency as the one applied in the stream.

Several flow rates were used, varying from 3 to 2 cc/min. It was very important to see that the break off of the jet doesn't occur at the theoretical Raleigh frequency. The break off of the stream happened at much lower frequencies than the ones expected. The table below shows a relation between the Raleigh frequencies, the observed break off frequencies, the velocity and the flow rate for a 102 microns nozzle. The slurry used was dispersed with PAA and had a density of 1.7 gr/cm3.

| Flow rate (cc/min.) | Velocity (m/s) | Raleigh (kHz) | Observed (kHz) |
|---|---|---|---|
| 3.0 | 6.1 | 13.3 | 6-8 |
| 2.5 | 4.8 | 10.6 | 2-4 |
| 2.0 | 3.8 | 8.4 | 1.5-3 |

**Table 3.5.1 Jetting parameters for a 102 μm nozzle**

### 3.6 Comparing the amount of Yttria printed by the High-Risk method to the One Printed by the Low-Risk Method

In order to see if the 20 volume % slurry we are using in the High Risk Approach is comparable to the amount of Yttria that is deposited in the sheet using the Low Risk, we can do the following calculations

From all the previous sheets printed we can estimate that the average layer thickness is about 70 μm. Also by doing a simple settling test to the 20 μm. or less powder we found that the packing density of it is about 25 %. From table 2.4.1 we can see that the average layer thickness obtained by the Low-Risk approach is around 0.003 inches which corresponds to 0.07 mm. We can obtain the volume of this layer by multiplying the area it covers times the thickness. For the particular case of the volume of the layer covering a square cm we can use the following expression:

$$Vol_{\substack{Over \\ 1cm^2}} = (1E-2cm)^2 * 0.07mm = 70E-10m^3$$

Thus, the mass of the layer of Yttria covering 1cm² can be determined by:

$$Mass_{Yttria} = Vol_{\substack{over \\ 1cm^3}} * \delta_{yttria} * Packing\ density \qquad \text{so,}$$

$$Mass_{yttra} = 5000\,{}^{kg}\!/_{m^3} * 70E-10 * 0.25 = 8.75E-6kg$$

Now for the High-Risk approach assuming a flow rate of 3 cc/min and a print speed of 1 m/s we can determine the volume of a line of length 1 cm by:

$$Vol_{line} = Flowrate * time \ \ where \ \ time = {}^{\text{distance}}\!/_{\text{print speed}} \qquad \text{thus}$$

$$Vol_{line} = 0.05\,{}^{cc}\!/_{s} * \left(1E-2{}^{m}\!/_{1m/s}\right) = 0.0005cc$$

Now, using a line spacing of 400 μm, we have that we need 25 lines to cover 1 cm, therefore the total volume of slurry over 1 square cm is:

$$Vol_{\substack{over \\ 1cm^2}} = Vol_{line} * 25 = 0.0125cc$$

Finally we know that the slurry is 20 volume % and the density is 5 gr./cc so these numbers cancel and the mass is 1.25E-5 kg. The ratio between the High Risk and the Low Risk is:

**1.25E-5/8.75E-6= 1.42**

Clearly we can see that the High Risk Approach gets about 42% more material to the sheet than the Low Risk. The same calculations were made for 15 Volume % slurry finding out that the material deposited by the high risk is about 7 % more than the low risk. The point is that after looking at the results obtained from the low-risk it is feasible to reduce the volume concentration in some amount to make the jetting not only easier, but above all more reliable.

## Chapter 4 High-Risk Approach, Line Printing.

### 4.1 Experiment Setup

Printing lines is possibly the most important part of this research project. Lines form by depositing many drops next to each other. The nozzle moves in a linear direction depositing the material in the sheet. When a certain feature has to be created, lines are stitched together. As explained in chapter 3 section 5, the drop formation is determined by the flow rate and controlled by the piezo frequency.

In order to print straight lines with a repeatable print speed a bicycle wheel setup was used. Previous 3DP students constructed this setup which is very suitable for printing single lines with specific characteristics. Figure 4.1.1 illustrates the experimental setup [Arthur 1996]:

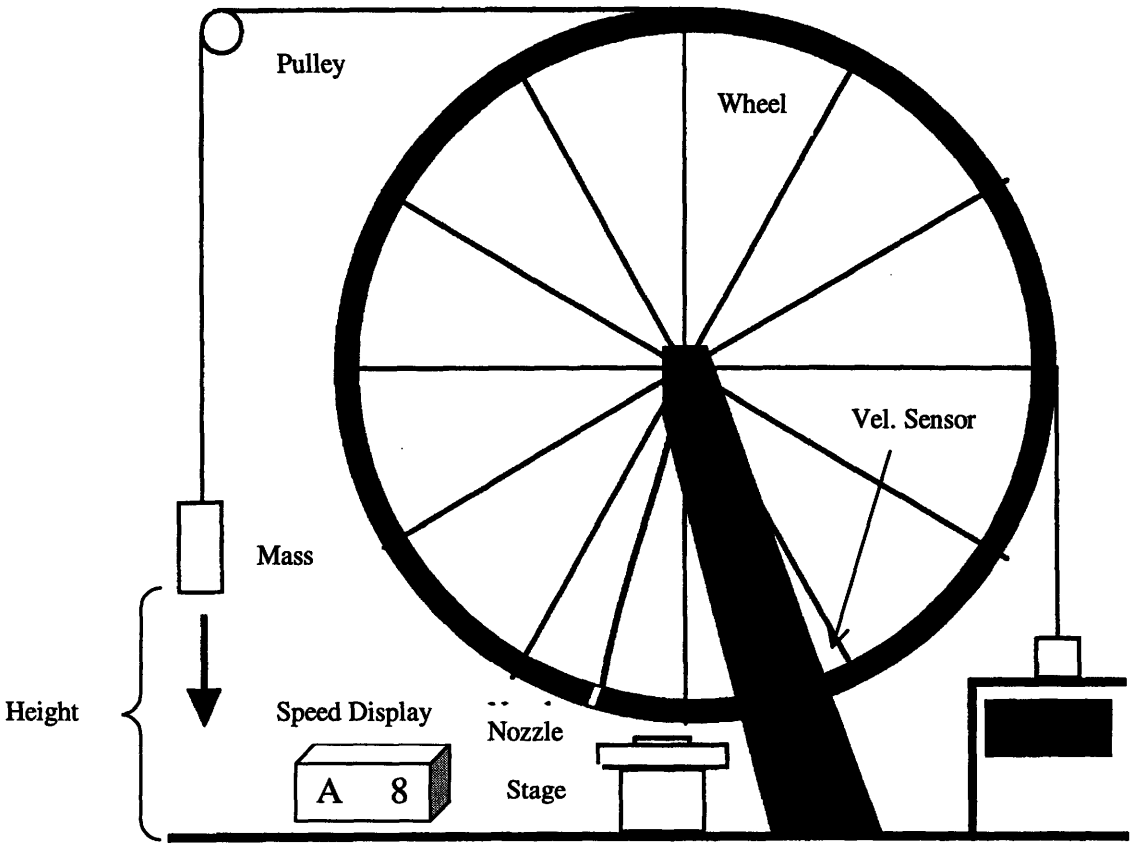


Figure 4.1.1 Line Printing Setup

We can vary the printing speed by changing the height and mass in the setup and then by using some dynamics we can estimate the print speed. Assuming that the mass of the wheel is concentrated in the hoop, we can use the following expressions to calculate the velocity:

$$\tau = I\alpha \quad \text{and} \quad \alpha = \frac{a}{R_{wheel}} \tag{4.1}$$

Where $a$ represents the acceleration, $\tau$ the torque, $\alpha$ the angular acceleration, $I$ the moment of inertia of the wheel and $R_{wheel}$ the radius.

When the mass is released from a fixed altitude and it hits the bottom just before printing, making the nozzle travel at a constant speed while printing. The speed just before printing is determined by the following expressions:

$$a = \frac{m_{fall} g}{m_{fall} + m_{wheel}} \tag{4.2}$$

Thus

$$V = \sqrt{2ah_{fall}} \tag{4.3}$$

Where $g$ represents the gravity, $V$ the printing velocity, $h_{fall}$ the altitude of the mass, $m_{fall}$ the mass of the falling object and $m_{wheel}$ the mass of the wheel.

Because the friction is small, we can consider that once the mass reaches the ground, the wheel travels at constant velocity.

## 4.2 Development of a Digital Velocity Sensor

One new feature that was adapted to the wheel setup was a velocity meter. This was done to be certain that the print speed used was in fact the predicted one. The meter was made using an optical sensor and some electronics. Basically, the optical sensor detects the presence of a known distance object for a certain amount of time. Then, using

counters and an oscillating circuit, we can count the number of electronic clocks that occur in the time it takes the known length object to cross the optical sensor. We can display this count on a set of hexadecimal displays and use arithmetic to obtain the speed in meters per second. This circuit uses two 4-bit counters in cascade giving us a resolution of 256 counts. The circuit also has an oscillator with adjustable frequency for different ranges of print speeds. The frequency of the oscillator was set at 10 kHz. The speed can be obtained by multiplying the number of counts by the duration of each count in seconds. Then, divide the fixed distance (in meters) of the object that crosses the sensor by the total time. Finally, a reset button was added in order to set to 0 every time a line was printed. The next diagram is a simple representation of the electronic circuit.

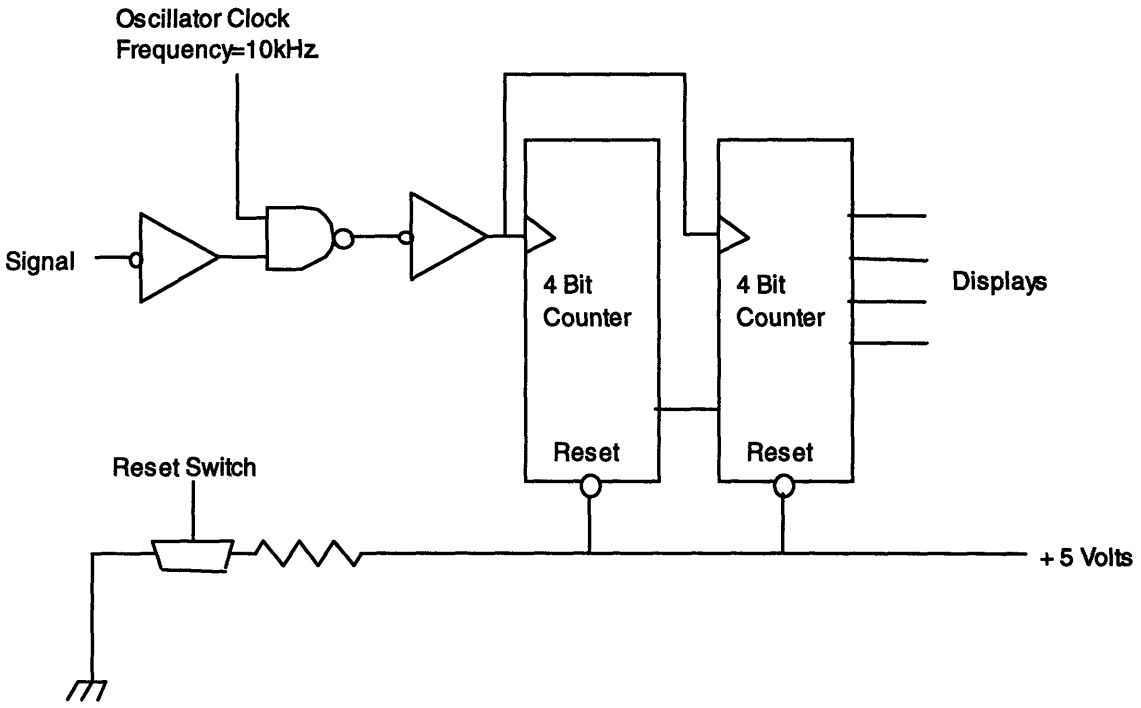


**Figure 4.2.1 Electronic circuit for measuring printing velocity**

The repeatability of the experiments showed that the electronic velocity sensor worked well. The speeds measured were very close to the ones predicted using the formulas of section 4.1.

For example, if we want to print with a velocity of 1 m/s we can do the following:

Select the mass to use in the bicycle setup and calculate the acceleration using equation 4.2. For this example the mass is going to be 200 gr. The mass of the bicycle wheel is 1.1 kg therefore the acceleration is:

$$a=\frac{m_{fall}g}{m_{fall}+m_{wheel}}=\frac{0.2*9.8}{1.1+0.2}=1.5\frac{m}{s^2} \tag{4.4}$$

Then we can use expression 4.3 to determine the height.

$$h_{fall}=\frac{V^2}{2a}=\frac{1}{2(1.5)}=0.333m \tag{4.5}$$

After setting the mass of the fall and the height, we connect the velocity sensor and measure the velocity. From the displays we read a hexadecimal number. This value has to be converted to decimal base. The result is the number of counts registered during the time the optical sensor was obstructed. Then to obtain the speed in m/s we use the following expression:

$$V=\frac{L_{Obstruct}}{f*N_{counts}} \tag{4.6}$$

Where $L_{obstruct}$ [m] is the length of the object crossing the optical sensor, $N_{counts}$ is the number of clock counts registered in decimal base and $V$ [m/s] is the printing speed.

For the example presented above ($m_{fall}$=0.2 kg and $h_{fall}$=0.333 m) 3 measurements were made with the sensor. The next table shows the results:

| Hexadecimal Number | Decimal Number | Speed (m/s) |
|---|---|---|
| 8A | 138 | 0.92 |
| 88 | 136 | 0.94 |
| 89 | 137 | 0.93 |

**Table 4.2.1 Speeds measured with digital velocity sensor for a predicted speed of 1m/s. Clock frequency=10 kHz $L_{obstruct}$ =0.0128 m Speed**

## 4.3 Printing Experiments and Results

Lines were printed using different flow rates, speeds and separations from the nozzle to the sheet. The first experiments were made using a distance of about 2 inches from the tip of the nozzle to the sheet. A piezo was used and it was verified that the stream was breaking off adequately before reaching the sheet. The results obtained were poor and the lines were crooked and discontinuous. However, some important things were learned like the distance between the nozzle and the sheet was too big. Also, from these first experiments it was seen that the best flow rate to work with is about 3 cc/min for a 102 μm nozzle. Lower flow rates produced worse lines and splashing was observed when the flow rate was higher. Better lines were obtained using speeds of 0.7 m/s or less, higher speeds produced very discontinuous lines. For these printing conditions, it is clear that the binder dose is determinant in creating continuous lines.

In the second round of experiments the sheet was placed closer to the nozzle. A distance of about 1.5 cm was used, and the flow rate was held at 3 cc/min. Again, it was verified that the stream was breaking off adequately before reaching the sheet.

As explained before, the frequency of the piezo was much lower, almost half, of the Rayleigh frequency. Instead of using 13.3 kHz, 7.5 kHz was the frequency used. Droplets were observed in the range between 8 and 6 kHz for this flow rate. For a 2.5 cc/min or less flow rate, the range was between 2 to 4 kHz.

In order to find a possible explanation for this phenomenon, the viscosity of the slurry was measured. The formulation of the slurry was the same as # 9 form table 3.4.2. First, the viscosity of the liquid media was measured using a viscometer. The viscosity of the liquid media was 6.2 cP. Then using a capillary tube, the viscosity of the slurry was measured. The value obtained was 9.1 cP. Bruce 1976 determined that the results presented by Rayleigh are accurate up to a viscosity of 10 cP, so this was not a possible explanation for the problem. However, the behavior of viscoelastic fluids obtained by the addition of high molecular weight polymers may cause the Rayleigh frequency to change noticeably [Bruce 1976].

In the second round of line printing experiments, individual lines were printed as well as lines next to each other. Speeds ranging from 0.8 m/s up to 2 m/s were used. All

the lines printed were much better looking than the ones printed in the first round. Figures 4.3.1 through 4.3.4 show the most representative examples.

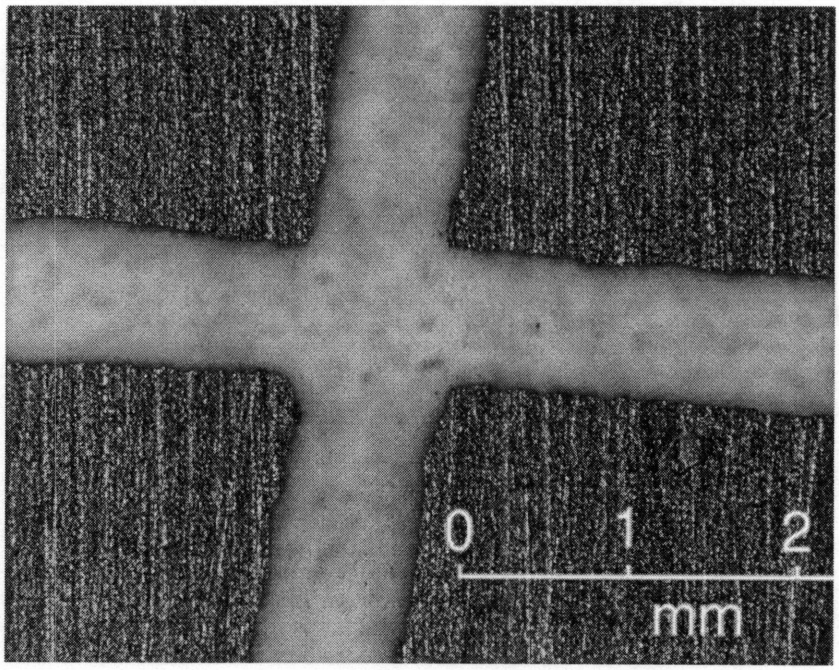


**Figure 4.3.1**
**Two lines printed in cross together.**
**Flow rate 3cc/min.**
**Freq. 7.5 kHz.**
**Vertical speed 1m/s**
**Horizontal speed 0.8 m/s**

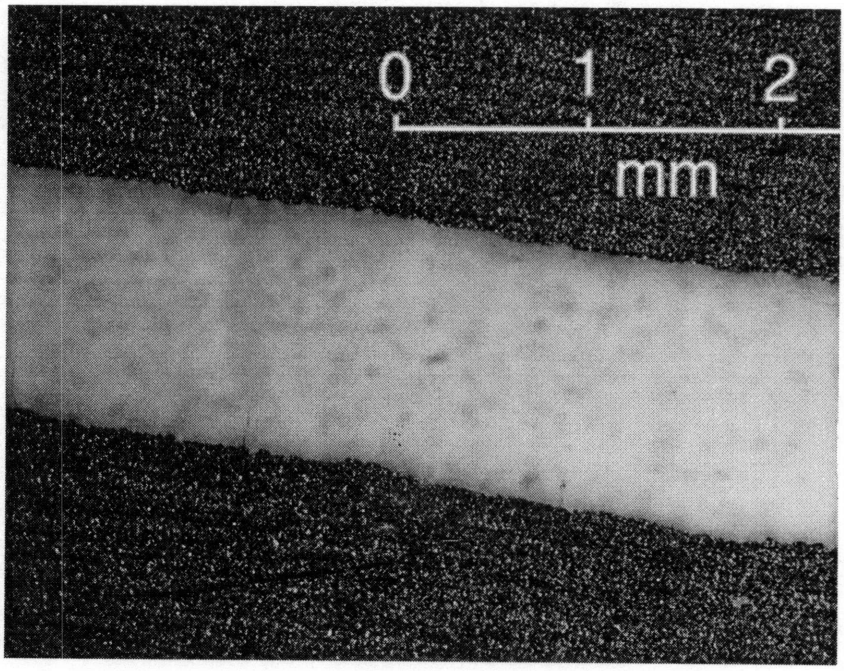


**Figure 4.3.2**

**Two lines printed.**
**Flow rate 3cc/min.**
**Freq. 7.5 kHz.**
**Speed 1 m/s**
**Line widths close to 0.8 mm.**

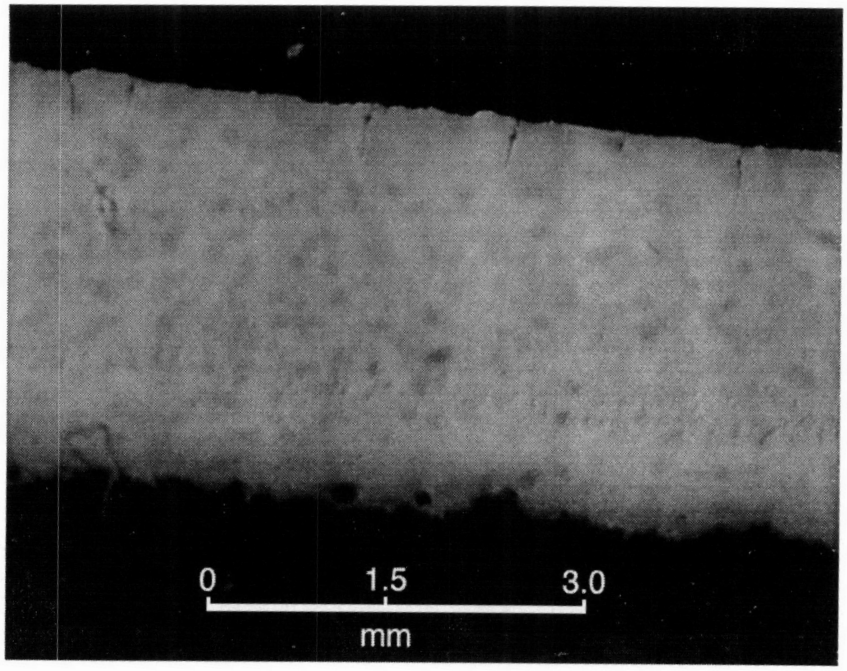


**Figure 4.3.3**

**4 lines printed together.**
**Freq.=7.5 kHz.**
**Q=3 cc/min.**
**Separation 600 μm.**
**First line printed in the top of the figure**

Another important issue was to print separate droplets. This was important to verify that droplets were reaching the sheet. Also, we can observe the size and appearance of individual droplets. This printing was accomplished by printing at high speed with low frequency. We can see that using 2 kHz and a speed of 1.8 m/s the separation between drops would be of:

$$t = \frac{1}{f} \quad t = 0.0005s$$

Hence:

$$d = V * t \qquad d = 1.8 * 0.0005 = 900\mu m = \text{Separation between drops}$$

Tests were made by printing droplets over absorbent paper and titanium. The results were practically the same. The flow rate used for these experiments was very low making it sometimes unstable. In the future, it is recommended to print with at least 3 cc/min.

Below can see a picture of these droplets depicted below:

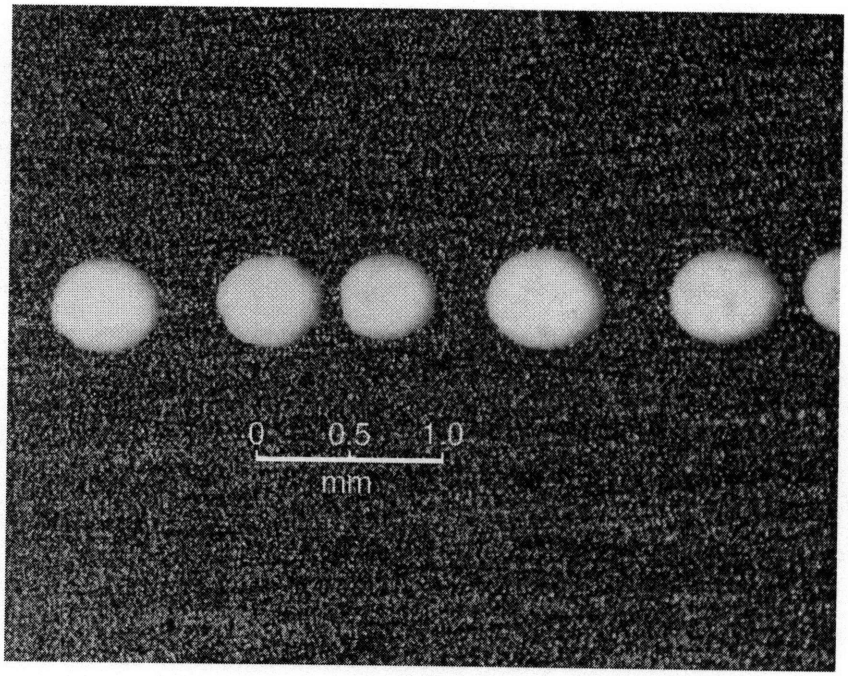


**Figure 4.3.4**

**Flows rate 2 cc/min.**
**Freq. 2 kHz.**
**Speed 2 m/s**
**Diameter of drops 0.450 mm.**
**Average spacing around 0.8 mm**

It was clear that lines could be printed together with good results. For a flow rate of 3cc/min, and a printer speed of 0.8 or 1m/s the spacing between lines can lie in the range of 0.5 to 0.7 mm. If we separate the lines more, problems will begin and gaps will start to form.

With all the previous work, it was now possible to print a pattern using slurry. The next step would be to print a rectangle (1*6 inches) proposed by Boeing. After testing this sample we can find out whether the High-Risk approach fulfills the planned goals and if it does then a direct printing of a pattern would be the next step.

## 4.4 Line Width predictions

A series of lines were printed on different substrates. The purpose was to see if the thickness of the lines varied from substrate to substrate under the same printing conditions. At the same, we could determine experimentally the size of every line and how it changed depending on the material system. Figure 4.4.1 shows the line width of printed lines over, normal paper, glass, inkjet printing transparency and titanium.

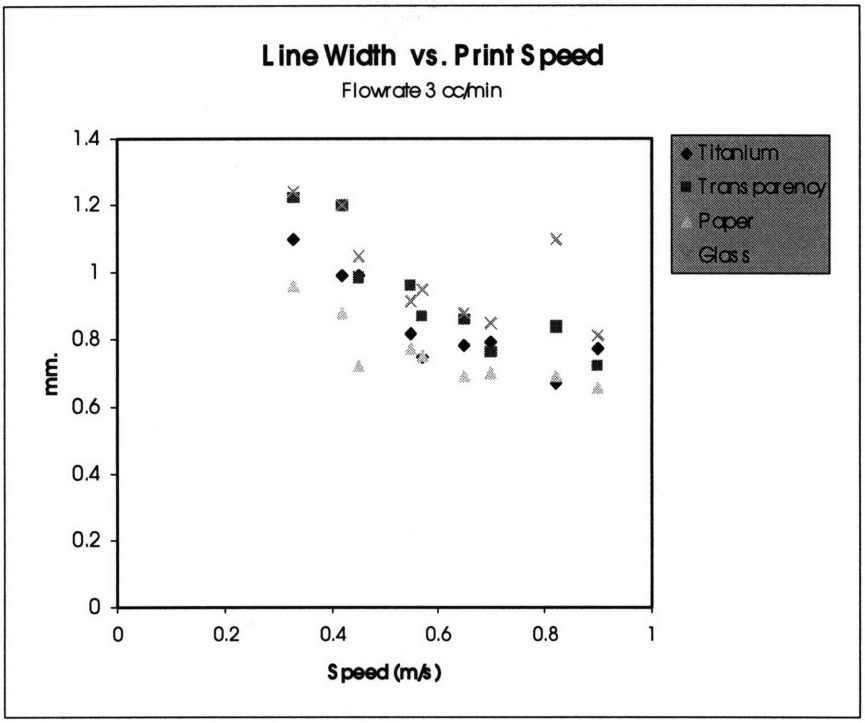


**Figure 4.4.1 Line width versus print speed.**
**Slurry 20 Vol. % Nozzle size 102 μm.**

As expected, low printing velocities produce very thick lines while higher speeds create thinner lines. The quality of the low speed lines is better than that of the high-speed lines. For titanium, lines are acceptable at all ranges keeping in mind that it is very important to have a stable jet with constant flow rate.

In general, all the material systems behave in the same form. Lines are wider in glass and transparency while smaller in paper.

In order to be able to predict a certain line width, a physical model that uses the angle of contact (β) between the liquid and the solid was used [Sachs 1995]. Based on the conservation of mass, the model calculates the area of the cylinder (formed by the line printed) which is lying on top of the sheet. The area of the cylinder is a function of the angle of contact and the volume of liquid. The expression used for estimating the width of a line is:

$$Width = 2 * \sqrt{\left(\left(\frac{\sin^2(\beta)}{\beta - \sin(\beta)\cos(\beta)}\right)\right)\left(\frac{V}{Lenght}\right)}$$

The next photograph we can see the angle β that forms at the interface of the titanium sheet and the slurry.

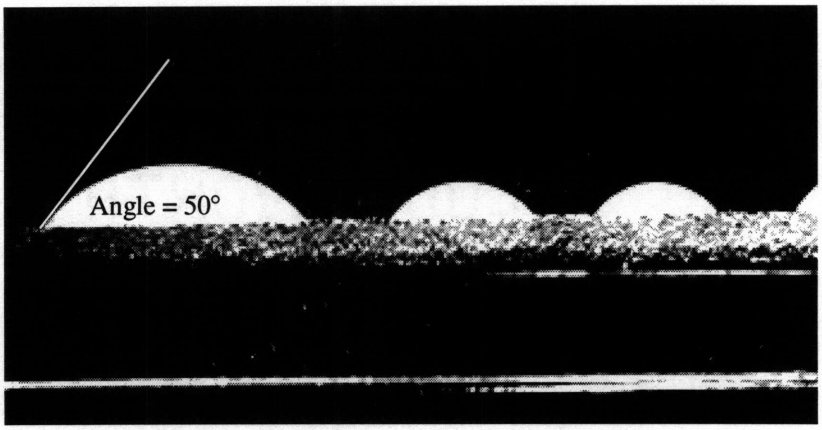


**Figure 4.4.2 Contact angle between a 15 Volume percent slurry and titanium.**

Once the angle was estimated, some lines were printed and the predicted values were calculated. The flow rate used for all the lines is 3 cc/min. Figure 4.4.3 depicts the theoretical and experimental width versus speed. The results are similar with some error in certain cases. In general, once we know all the printing conditions, an estimate of the width can be formulated.

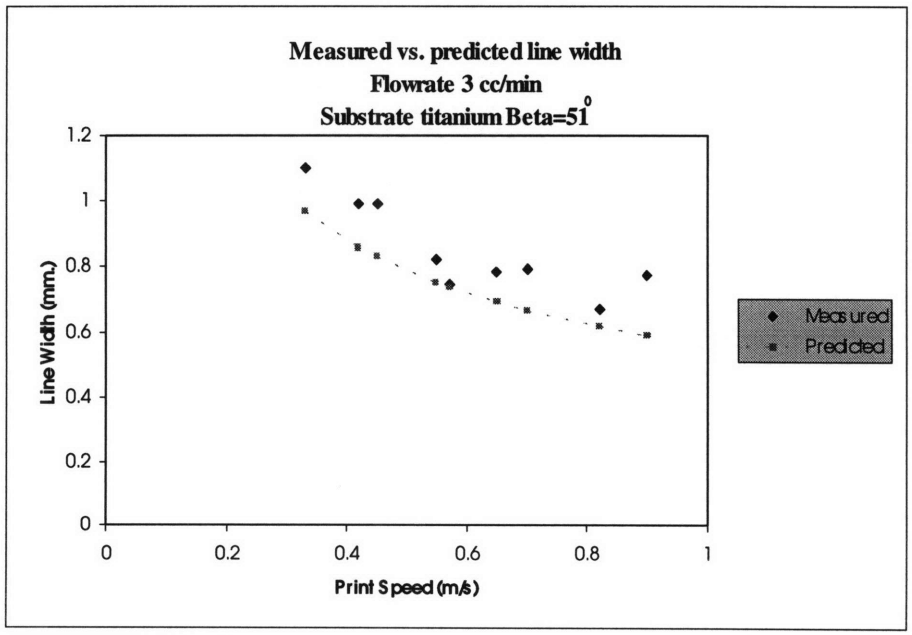


**Figure 4.4.3 Print speed versus line thickness for a 15 Vol. % Slurry**

## Chapter 5 Line Printing Experiments with the Alpha Machine.

### 5.1 Introduction

As explained in the end of section 4.3 in order to test the High-Risk approach a pattern had to be printed onto a titanium sheet. Boeing proposed a rectangle of 1 by 6 inches as the experimental pattern. The pattern had to be created by printing a series of lines next to each other. In the previous chapter lines were printed using the setup depicted in figure 4.1.1. This setup was not capable of printing the length of the rectangle described above therefore the use of the Alpha Machine was necessary. This machine gave us the possibility of printing with different line spacing and several print speeds. A series of experiments were conducted and the results are presented in Section 5.3.

### 5.2. Fluid System

Two different fluid systems were studied before printing:

The first one was the same as the one used in chapter 4. A 15 volume fraction slurry made with Yttria (20 μm and less) was pre-filtered through a 47 μm filter before pouring it into the container inside the pressure vessel. A magnetic stirrer avoided settling of the particles in the bottom of the container. The slurry was then filtered through an 88 and 60 μm filters before reaching the nozzle.

The system worked well, however two problems were identified for long term use. The first problem and the most important was the fact of the material settling in the filters. This problem occurred because of the small flow rate flowing through the filters. The second problem relates to the fact that the pressure vessel is a closed container, therefore there is no way of refilling the inside container when printing.

The second system used a pressurized tank with a bladder inside [Serdy 1997 Private communication]. The slurry (with the same characteristics as the one above) was placed inside the bag, which had a feed line placed at the bottom of the bag, and a return

line at the middle of it. These lines were connected to a peristaltic pump. The fluid was pumped from the bottom of the bag through a filter and then returned into the bag. This system did not require the use of a magnetic stirrer. All the system was pressurized and a printing line with the nozzle was attached to the principal line. The principal idea was to keep the slurry in continuous motion in order to avoid settling. Also, because the pump handles larger flow rates, the solid contents of the slurry did not settle inside the filter (60 μm). Moreover, the line with the nozzle was placed in the recycling line just at the outlet of the filter, so the slurry was completely filtered before reaching the nozzle. Another advantage is that the system can be easily refilled.

The problem with this setup was the changes in pressure due to the presence of the peristaltic pump. This effect was seen at the tip of the nozzle. Figure 5.2.1 depicts the system.

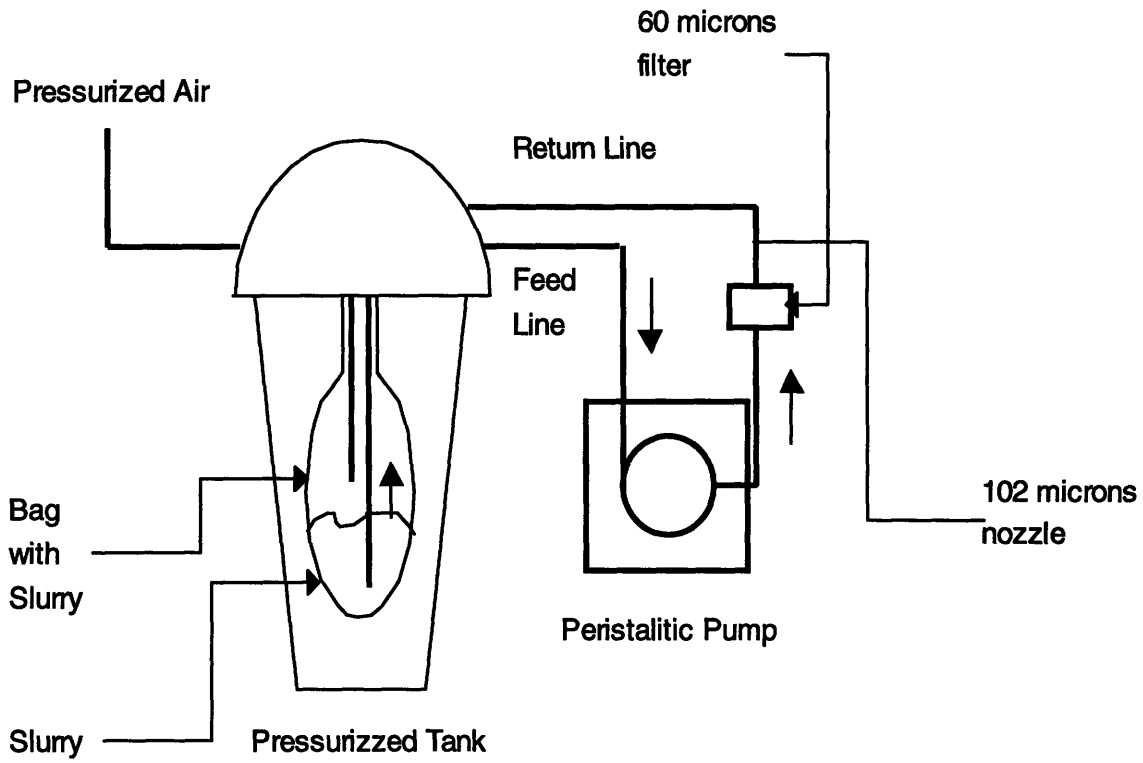


**Figure 5.2.1 System for jetting Slurries with a recycling pump**

## 5.3 Printing

A detailed drawing of the rectangle selected to be printed can be seen in Appendix B. The pattern was printed by masking the 2 short edges with scotch tape. Then the printhead rastered the area. Figure 5.3.1 shows the arrangement.

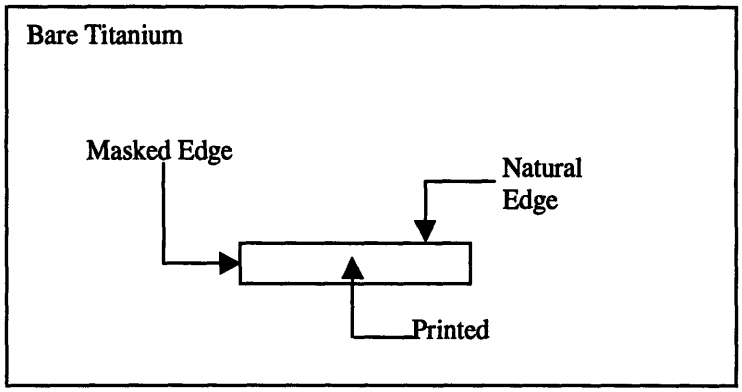


**Figure 5.3.1 Test Pattern for the High-Risk Approach**

Based on the experiments of Chapter 4 several files were prepared in order to print the selected area. Lines spacing of 500, 600, 700, 800 and 900 microns were studied along with several print speeds. The distance between the nozzle and the titanium sheet was 2.5 cm, and no piezo was attached to the nozzle. The printing velocity range lied between 0.7 m/s up to 2m/s.

For speeds below 1 m/s the line printing was not successful because too much material was placed onto the sheet. A moment after printing, the pattern looked good but after drying the ceramic cracked and the sheet was useless.

The next step was to print higher speeds. Printing was done with a speed of 1 m/s with much better results, but still too much material was printed and a pool of slurry formed on top of the sheet. Figure 5.3.2 shows this case. In the photo we can see that the material is concentrated in the center. This happened because the material flowed to the center as it dried. When the spacing between lines was 700 μm, some individual lines started to form however they joined in many points.

Finally a speed of 2 m/s was used to print. The distance between the nozzle and the sheet was still 2.5 cm. Lines could be distinguished when the separation between

them was 600 μm. Again some lines merged and the material formed a small pool leaving some areas unprinted. Figure 5.3.3 shows this particular case. For a line separation of 700 μm very few necks formed and for a spacing of 800 μm completely individual lines were printed. At this line spacing no merging points were observed.

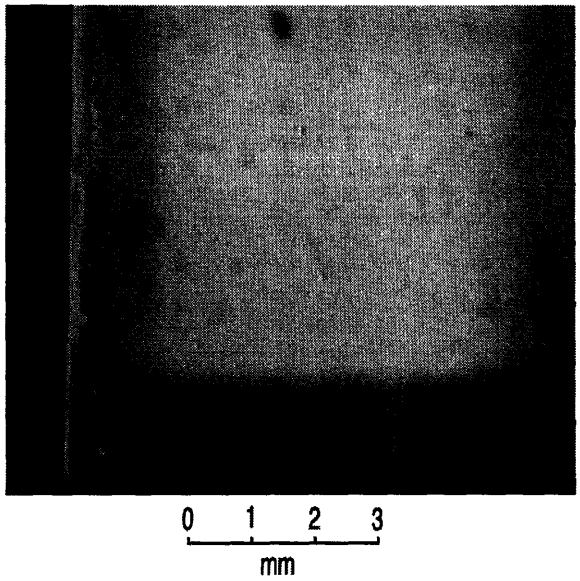


Figure 5.3.2 Slurry Printed with a Line Spacing of 500 μm, flow rate 3cc/min and speed of 1m/s

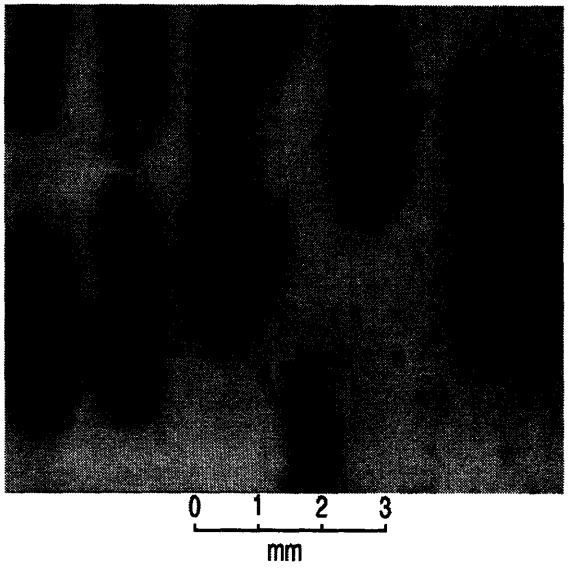


Figure 5.3.3 Slurry Printed with a Line Spacing of 600μm, flow rate 3cc/min and speed of 2 m/s

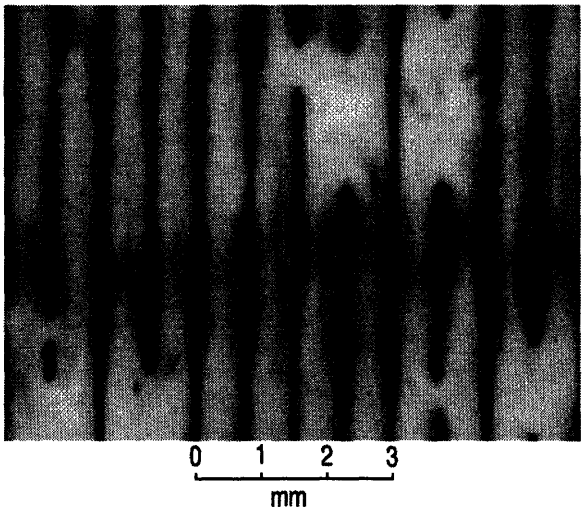


Figure 5.3.4 Slurry Printed with a Line Spacing of 700 μm, flow rate 3cc/min and speed of 2 m/s

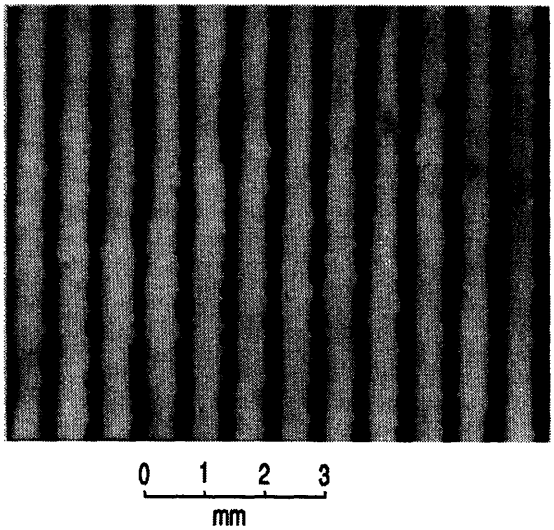


Figure 5.3.5 Slurry Printed with a Line Spacing of 800 μm, flow rate 3cc/min and speed of 2 m/s

Figure 5.3.5 shows that individual lines can be printed, however the separation between them is such that some areas are still unprinted. The fact of increasing the separation between lines avoids pooling but made the pattern useless, therefore something else had to be done. In order to solve this problem, printing was done in three separate steps.

The first step consisted in printing lines with a separation between 400 and 450 μm. The next step was to dry the lines printed in step one by using heating lamps. Step 3 consisted in printing lines in between the lines printed in step # 1. The next diagram depicts the process.

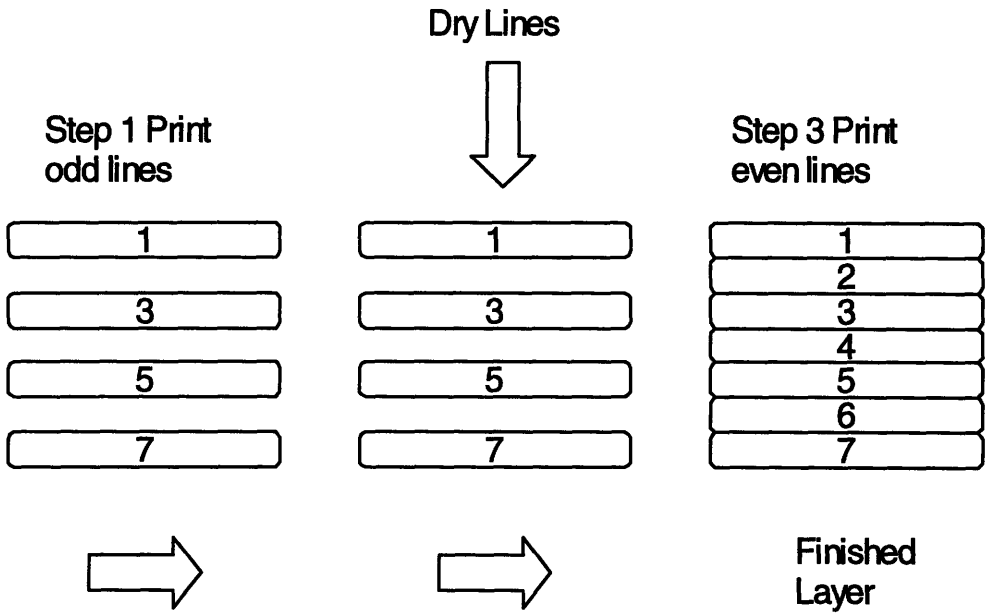


**Figure 5.3.6 Printing Sequence in the High Risk Approach**

Several print tests were made following this approach with good results. The optimal line spacing for printing with a 15 volume fraction slurry (20 μm and less in particle size) with a flow rate of 3 cc/min and a speed of 2 m/s was between 800 and 900 μm.

Figure 5.3.7 shows a part of final rectangle.

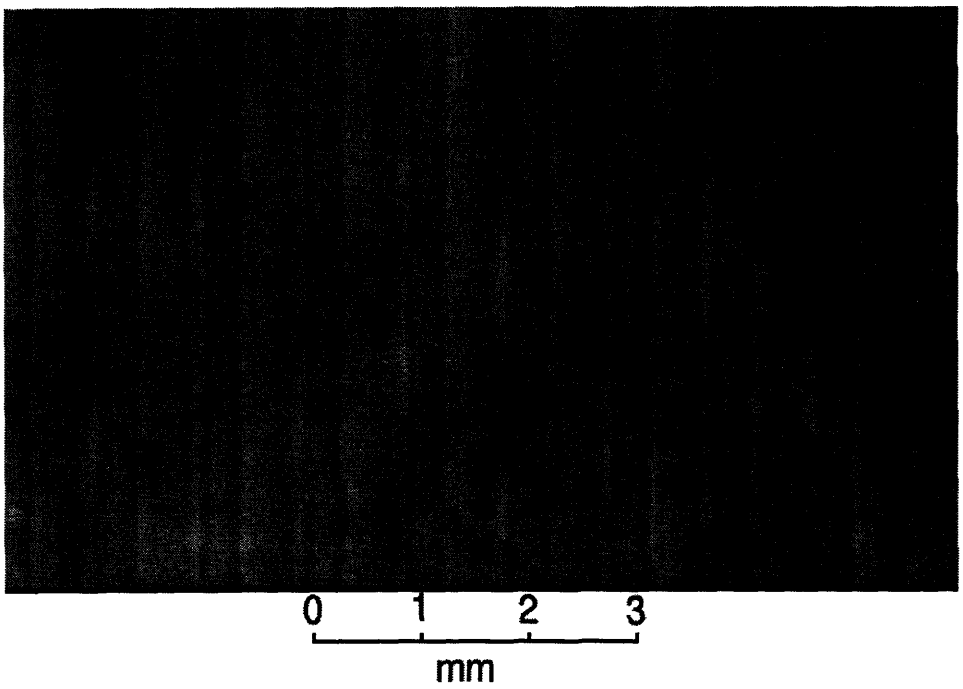


**Figure 5.3.7 Area printed with a Line Separation of 450 μm.**
**Flow Rate=3 cc/min and speed =2 m/s**
**Distance between nozzle and sheet 2.5 cm.**

In the figure above we can observe that the thickness of the layer is not uniform. The thickness was measured using the same microscope and the same method as the ones in section 2.5. The table below shows the results.

| Top Lines | Bottom Lines | Difference |
|---|---|---|
| 55 | 43 | 12 |
| 66 | 51 | 15 |
| 63 | 47 | 16 |
| 65 | 49 | 16 |
| 55 | 44 | 11 |
| 60 | 46 | 14 |
| 54 | 42 | 12 |

**Table 5.3.1 Thickness of Printed Rectangle Shown in figure 5.3.7.**
**Units in microns**

A total number of 14 measurements were made (7 in the top lines and 7 in the bottom lines). The average layer thickness for the bottom lines was 46 μm while the average for the top lines was 60 μm.

Although the layer thickness had an average roughness of 14 μm, the area of the rectangle is completely covered with Yttria. In other words, no areas remained unprinted and the layer looked the same throughout the whole pattern. In addition, the edge of the larger side of the rectangle presented good edge definition.

In the future, if a thicker layer is needed, a second layer could be printed repeating the steps described in this section.

## Chapter 6 Printing with Deflection

### 6.1 Current Problems for Printing with Deflection

Some tests were made in order to print with the actual print head. Unfortunately, the current print head was designed to print with smaller nozzles (47 μm) making it hard to print with larger ones (70-120 μm). The clearance between the jet and the charging cell walls was small making it very hard to center the jet in the cell, and at the same time clear the deflection cell.

Another problem was the break off length. In contrast with 47 μm nozzles the break off length for larger nozzles was longer. The break off length for a 102 and 120 μn nozzle occurred outside the charging cell making it impossible to charge the droplets for deflection.

In the case of the deflection cell, the current cell was not wide enough. Again any failure in centering the jet made the distance between stream of droplets and the walls very small. In most of the cases just placing the block that holds the deflection and the charging cells in position made the stream hit the deflection cells.

### 6.2 Printing a Test Pattern with deflection

After carefully centering the jet and by placing the nozzle in a higher position so that the break off would fall in the charging cell. A circle of 1 cm in diameter was printed using a 120 nozzle. The frequency used was 7 kHz and the flow rate was 4.5 cc/min. The line spacing used for this print test was 200 μm. Figure 6.2.1 shows that the edge definition was very poor. Also no lines were identified indicating that a pool of slurry was created while printing. In the same figure we can also see that the material is concentrated in the center of the circle leaving a very thin layer around the edge. Finally, because too much material was printed the layer cracked completely when it dried.

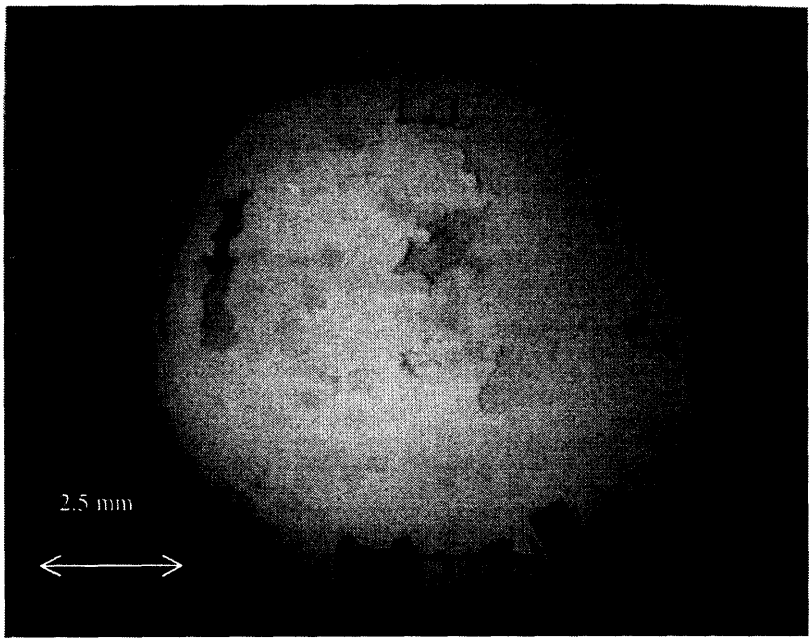


**Figure 6.2.1 Circle printed with Yttria Slurry (15 %) Particle size 20 μm and less Line spacing 200 μm. Frequency of 7 kHz and a nozzle diameter of 120 μm.**

## 6.3 Modifications to the Actual Print Head in order to Handle Larger Nozzles

In order to avoid the problems described in section 6.2, some modifications have to be made to the actual print head. Appendix A discusses some of the important issues to take into account while designing a new print head geometry.

In order to handle a larger nozzle, the geometry of the charging cell has to be modified. The length has to be increased in order to assure that the break off the stream will occur inside the charging cell. Also, the spacing between the walls of the charging cell needs to be enlarged.

Appendix A shows that a separation of 0.030 inches reduces the charge in the droplets by 15 percent, but makes the centering of the jet in the deflection cell easier. Finally, the change in length compensates the previous reduction.

The defection cells used for printing slurries can be the same as the one shown in Appendix A. These cells are wider than the actual ones and their shape tries to follow the path of the droplets all the way into the catcher.

Using the excel spreadsheet designed by Chris Shutts, the length and width of the charging cell was modified, and the new printing conditions were studied. The width of the charging cell was set at 0.030 inches while the length was increased from 0.080 to 0.120 inches. Figure 6.3.1 shows the deflection path for the following conditions:

- Flow rate=3 cc/min
- Nozzle size = 102 μm
- Charging cell voltage = 135 Volts
- Deflection Cell voltage = 2000 Volts
- Fluid slurry 15 volume fraction
- Deflection cell profile same as the one depicted in Appendix A

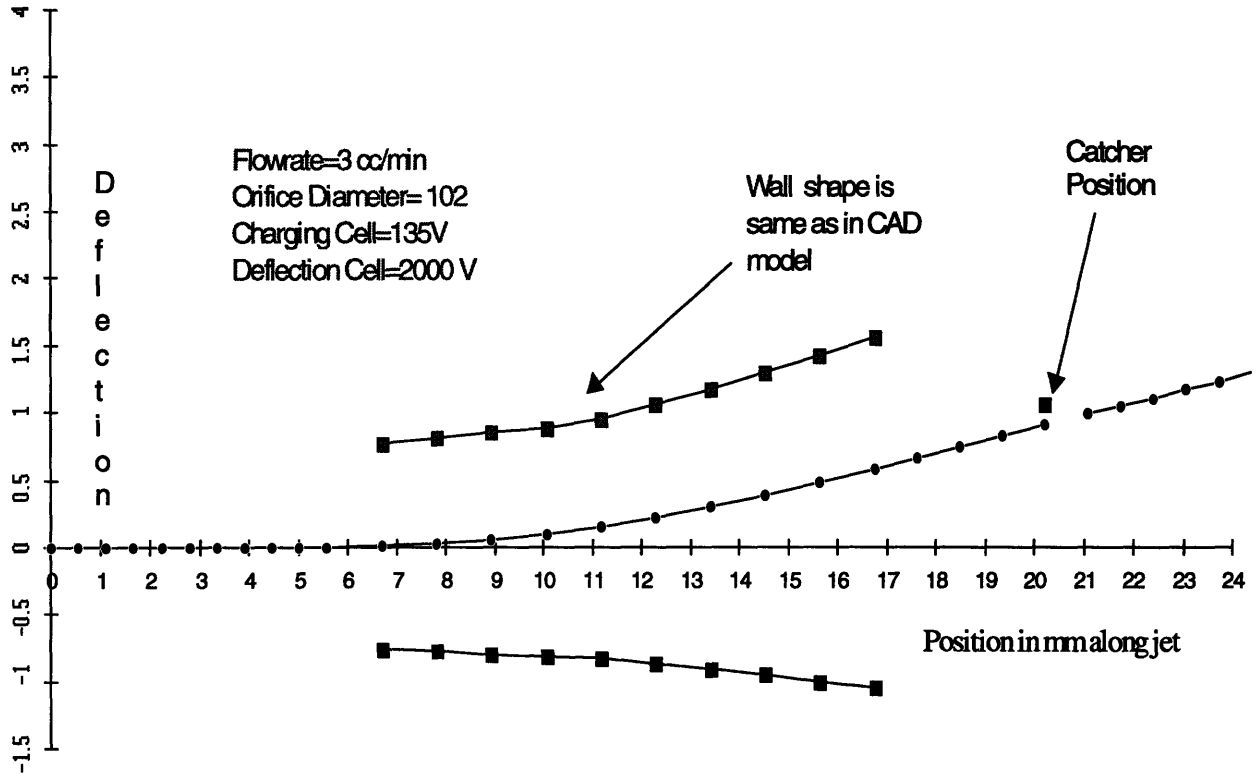


**Figure 6.3.1 Position versus deflection using a charging cell of 0.030 by 0.120 inches Nozzle size 102 μm.**

Finally, another thing that can be done to obtain a good trajectory into catch. The catcher could be placed a couple of mm below its current position. This would help in reducing the risk of getting the stream close to the deflection walls. At the same, charging voltages and deflection voltages could be reduced.

# Chapter 7 Conclusions

## 7.1 Low-Risk Printing

The Low-Risk results demonstrated that it was possible to print sheets that performed adequately. Boeing evaluation of these test parts stated that the printed titanium sheets fulfilled the expectations. Single side printed sheets as well as double side worked well. Also, it was determined that a particle size of 20 μm and less is adequate to endure the test process. As explained in Section 2.5 the best sheets manufactured by the Low-Risk printing method were the ones with particle size of 53 μm and less. With the use of this powder, the edge definition is very good and the thickness of the layer is very uniform, therefore this project has demonstrated that the Low-Risk Approach is a viable method for printing titanium sheets with Yttria powder.

## 7.2 High-Risk Printing

TheHigh-Risk approach has demonstrated the possibility of using slurry to print a sheet. Chapter 3, 4, and 5, describe in detail the materials, systems and parameters needed to print areas without deflection. Chapter 6 discusses the problems and recommendations for printing with deflection. The problems to be solved in order to achieve success using the High-Risk approach are:

- The construction of a new print head with larger and wider charging cells is needed. Also, the possibility of using higher deflection voltages and charging voltages has to be explored.
- A better fluid system has to be developed in order to stand continuous hours of operation. The system has to be able to keep the slurry in motion and avoid settling in the filters.
- The problem of pooling has to be solved either by printing separated lines and then printing in between them, or by heating the titanium sheet while printing in order to dry the droplets as the hit the sheet.Another problem to be solved is to obtain a short break-off of the jet without the presence of satellites.

If these issues were to be solved a reliable print head could be developed and the printing of patterns onto titanium sheets could be easily performed.

## References


Askeland, Donald, The Science and Engineering of Materials, PWS Publishers, USA, 1985.

Arthur, Tara, "Factors Limiting the Surface Finish of Three Dimensional Printed Parts," Masters Thesis, MIT, June 1996

Curdeau, Alain, "Three Dimensional Printing of Ceramic Molds with Accurate Surface Macro-Texture for Investment Casting of Orthopedic Implants," Ph. D. Thesis, MIT, September 1995.

Horowits, P. and Hill, Winfred, The Art of Electronics, Cambridge University Press, NY 1989.

Moritmer, Charles, Chemistry A Conceptual Approach, Van Nostrand Company, NY 1979.

Rahaman, M., Ceramics Processing and Sintering, Cambridge University Press, NY 1996.

Reed, James, Introduction to the Principles in Ceramic Processing, Wiley & Sons, NY, 1988.

Shutts, Christopher, "Development of a Reliable Electrostatic Multijet Printhead for Three Dimensonal Printing," Masters Thesis, MIT, May 1995.

Sachs, E., Cima, M., Williams, P., Brancazio, D., Cornie, J., "Three Dimensional Printing: Rapid Prototypes Directly from a CAD Model," Accepted publication in the Journal of Engineering for Industry.

Stockham, J., Fochtman, G., Particle Size Analysis, Ann Arbor Publisher, Michigan, 1979.

# Appendix A

# Print Head Study

## Appendix A Print Head Study

### Introduction:

This appendix studies the error observed between the experimental and theoretical deflection of the binder stream. It looks for the plausible causes of the error and focuses on a new deign that will minimize this problem. Several deflection and charging cells were studied including the current printhead and the next generation. The principal objective is to design a cell geometry that would make the difference between the observed deflection and the predicted one, very small. After several experimental runs and simulations the final shape for the deflection cells was chosen, and at the same time a series of charging cells can be selected. Experimental tests including video and measurement of charges, currents and voltages were made. At the same time a theoretical excel spreadsheet, developed by Chris Shutts, was used to compare results with the real world. Numerical analysis was used to help understand the behavior of the deflection cells, as well as the charging cells. The study is divided into 2 sections. The first one deals with the charging cells, while the second one deals with the study, simulation and new design of the deflection cells.

### Droplet Charge Measurement

Several measurements were made to determine the droplet charge in the alpha machine. The next graph shows these results:

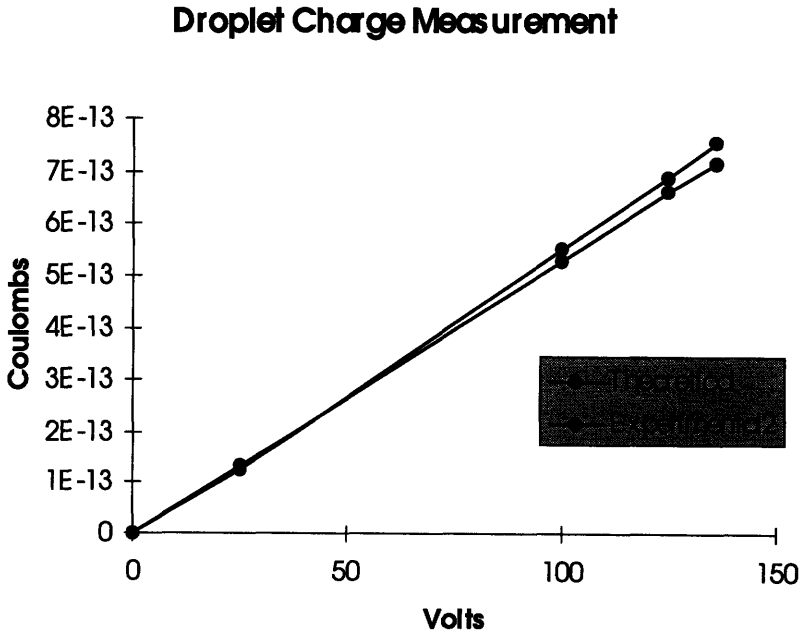


**Figure A-1 Charge versus voltage**

A piezo frequency of 40 kHz. was used while the voltage in the 8 charging cells was varied from 0 to its maximum value. A 50 microns nozzle was used to make these tests. The currents measured with the picoammeter are very similar to the ones estimated with the theoretical spreadsheet. The theoretical value was calculated without the effect of the preceding droplets. This means there is still and unexplainable error of about 20% between experimental charge value and the theoretical one.

**Other Tests:**

In order to know more about the charging process, several fluids were tested finding out that it does not affect at all the use of different binders the charge in the droplets is the same (As expected).

Another important issue that comes into play is the mathematical model used to estimate the droplet charge. We take this model as a parallel plate system with a stream of fluid grounded in the center, so to find out if the break off point makes a difference in the charging process a series of experiments were made. The break off length was varied and no substantial change in the current was observed.

Also, the charge in the droplets was measured with the deflection cell on and the cell off. Again no change was observed between these 2 conditions.

Finally using the picoammeter, currents were measured in the 8 jets. The voltages in the charging cells were also measured being the same at each particular condition. The results are on the next table (currents in nanoampers):

| Voltage | c | u | r | r | e | n | t | s |
|---|---|---|---|---|---|---|---|---|
| | jet 0 | jet 1 | jet 2 | jet 3 | jet 4 | jet 5 | jet 6 | jet 7 |
| 100 | 21 | 22 | 22 | 22 | 21 | 22 | 21 | 22 |
| 136 | 30 | 27 | 30 | 28 | 29 | 28 | 29 | 30 |

From the table above, the charge in the droplets doesn't vary enough from jet to jet, in fact they are very similar. Also, the changes in binder didn't affect the charge in the droplet. In conclusion, these additional tests didn't provide any information that could explain the difference between the theoretical and experimental values.

**Wider Charging Cells:**

Another problem is the fact that centering the stream in the charging cell is very difficult, therefore if the charging cell gap is increased, a big centering error can become a much smaller one. The actual charging cells have 0.020 inches between plates. When the charging cell gap is increased, the capacitance decreases and therefore the charge in the droplets also, but this reduction in capacitance can be compensated either by using more deflection voltage or more charging voltage. The next table shows a relation between the actual distance and the possible new distances. The charging voltage is 100 V; the nozzle size is 50 μm. and the flow rate 1 cc/min. Another set of conditions can be chosen and the values of capacitance and droplet charge will change but the relationship between them will stay constant for the same charging and flow rate conditions.

| Cell Width | Capacitance (e-11) | Droplet Charge (e-13) | Relation (%) |
|---|---|---|---|
| 0.02 | 2.19 | 4.95 | 0 |
| 0.03 | 1.89 | 4.27 | 15.92 (less) |
| 0.035 | 1.8 | 4.05 | 22.2 (less) |
| 0.04 | 1.72 | 3.88 | 27.5 (less) |

An important issue is the fact that when we increase the charging cell gap, the electrical field from the deflection cell can affect the charging cell. A wider charging cell is more vulnerable to having filed inside influenced by the field from the deflection cell.

In order to see if the deflection voltage will affect the increase of cell width a Pdease simulation of actual conditions was developed. Pdease is a 2 dimensional finite element program that can be easily programmed. From Pdease a series of charts were obtained. From this charts (Can be seen at the end of the appendix figures A-16 to A-19) we can see that the deflection cells affect more the charging cells as they become wider. Nevertheless, the electric field that forms inside the cells presents a very week field force. It is a trade off; easier to machine cells and less centering problems against formation of undesired electric fields inside the charging cells. From the tests and simulations it is possible to thin that a 0.030 to 0.035 distance can be the best choice.

**Deflection Cells:**

After measuring the droplet charge, the next step was to analyze the deflection cells. First the current printhead was studied. For this purpose video was taken in order to measure the position and the angle of the stream at the end of the defection cell. Several conditions were studied including 2 jets at the same time. Jets # 4, and #5 were the ones used for this test. The fluid printing conditions were the following:

- Fluid $\Rightarrow$ Water with density = 1 gr./cc
- Frequency of piezo $\Rightarrow$ 39 kHz
- Flow rate $\Rightarrow$ 1.07 cc/min.

It's important to notice that the charging cell voltage was different for each of the jets. The charging voltage in Jet #4, was higher than the charging voltage in Jet #5. The deflection voltage was the same for both jets every time. Once the test were made the video was studied. Measurements of deflection including position and angle were taken for further studies. This data was compared with the data produced by Chris Shutts spreadsheet. It is important to mention that the values of deflection obtained from the theoretical spreadsheet don't take into account the capacitance that exists between particles. The value of the capacitance used for estimating the charge in the droplet is just the capacitance of the charging cell with a stream in the center. In table A-1 we can see and compare the theoretical and experimental values of the deflection.

As we can see in the table, we have a great difference between the predicted values and the actual ones. The measurements were made in the bottom edge of the deflection cell. We can see that we have different magnitude of errors depending on the jet we are comparing. Jet #4 presents an average error of about 30%, while jet #5 shows an error of about 50%. This is very hard to explain and the only difference observed is that jet #5 was not centered in the charging cell. Another important issue is the fact that the deflection error increases as we get close to the corner of the deflection cell. The concentration of the electrical field in the final corner of the deflection cell makes the stream of droplets deflect much more than the predicted value. If we take a percentage of the deflection cell used (In fact half of the deflection cell from the center to the wall) we can see that the

error grows as we get closer to the final corner of the deflection cell.. This error goes from about 20 %, when using 60 % of the deflection space, to about 40 % when using 95%. In other case the error goes from 45 to 70%. This is clearly a factor to consider in the future.

After testing the old printhead, the new printhead was studied. This printhead is wider in all of its sections and the percentage of cell use is smaller than the previous printhead. The stream can go into catch without getting too close to the final corner of the cell, therefore the errors encountered are smaller. In Table A-2 the results are presented.

**Design:**

Using Chris Shutts spreadsheet, the cell geometry was modified in order to get a flight path that would follow the cell wall. The geometry selected for the new deflection shape was one that will follow the jet in the best possible way. Also a finite element program was used to model the whole cross section of the printhead. Again, Pdease was programmed to model a 2 dimension simulation Several diagrams were obtained from the simulation including equipotential lines, vector fields and a picture showing lines of constant electric fields. We can see the results in a series of 17 pictures at the end of the appendix. In parallel to the Pdease analysis, the same parameters were used in the spreadsheet. The electric fields of different points along the deflection cell were studied and compared. The results show a lot of similarities throughout the deflection cell. The points of interest in where some substantial difference is seen are at the beginning of the cell and especially at the end of it. There is an area where the Electric field strength grows substantially. This is seen in pictures A-14 and A-15. This area covers the last 2 mm in height of the deflection cell and most important covers about 0.6 mm if the distance between electrodes. *The voltage used in the simulation is 1500 V.* From this set of pictures we can discover that it is important to stay away from the cell corner. Wider cells will be better than narrow ones in matters of predicting deflection. After reviewing all this data and graphs, the geometry chosen for the cells was to follow the jet so that the distance from the wall to the center of the stream will be as constant as possible when deflecting to the catcher. A series of excel charts showing the path of the droplets is presented at the end of this appendix. Graphs A-2 to A-5 illustrates the same trajectory

into the catcher. The travel path is exactly the same for all the different printing conditions. In other words we can vary nozzle size and flow rate, but at the same time compensate these changes by modifying charging and deflection voltages. As stated before, its important to stay at least 0.6 mm away from the cell wall, that is why this design tries to make the droplets fly keeping a distance of 0.8 mm to the wall.

**Conclusions:**

**The results of the practical experiments and the simulation show that the spreadsheet is not very far from reality if we follow the next rules:**

- **Make the correction for the charge in the droplet.**
- **Be sure to have jet correctly centered in the charging cell.**
- **A wider cell can be used although some problems may arise.**
- **For this particular configuration of cell, leave 0.6-mm distance between the stream and the deflection wall.**
- **For future cells use about 60% as maximum deflection between the center of the stream and the wall.**

In the next pages we can see the tables, the excel charts showing the same flight path for a series of different nozzle sizes and printing parameters, the drawings for the deflection cells, and all the Pdease pictures.

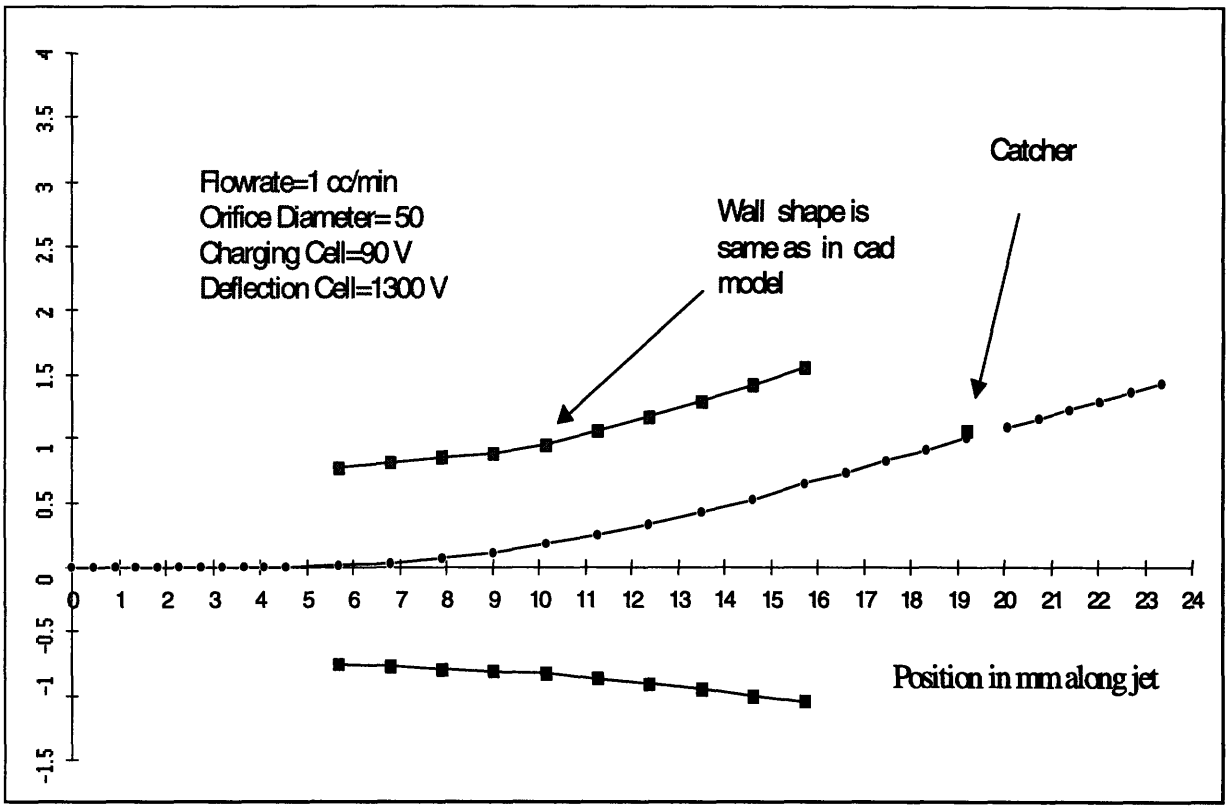


**Figure A-2 Deflection Path for Water. Nozzle 50 μm Flow rate 1 cc/min**

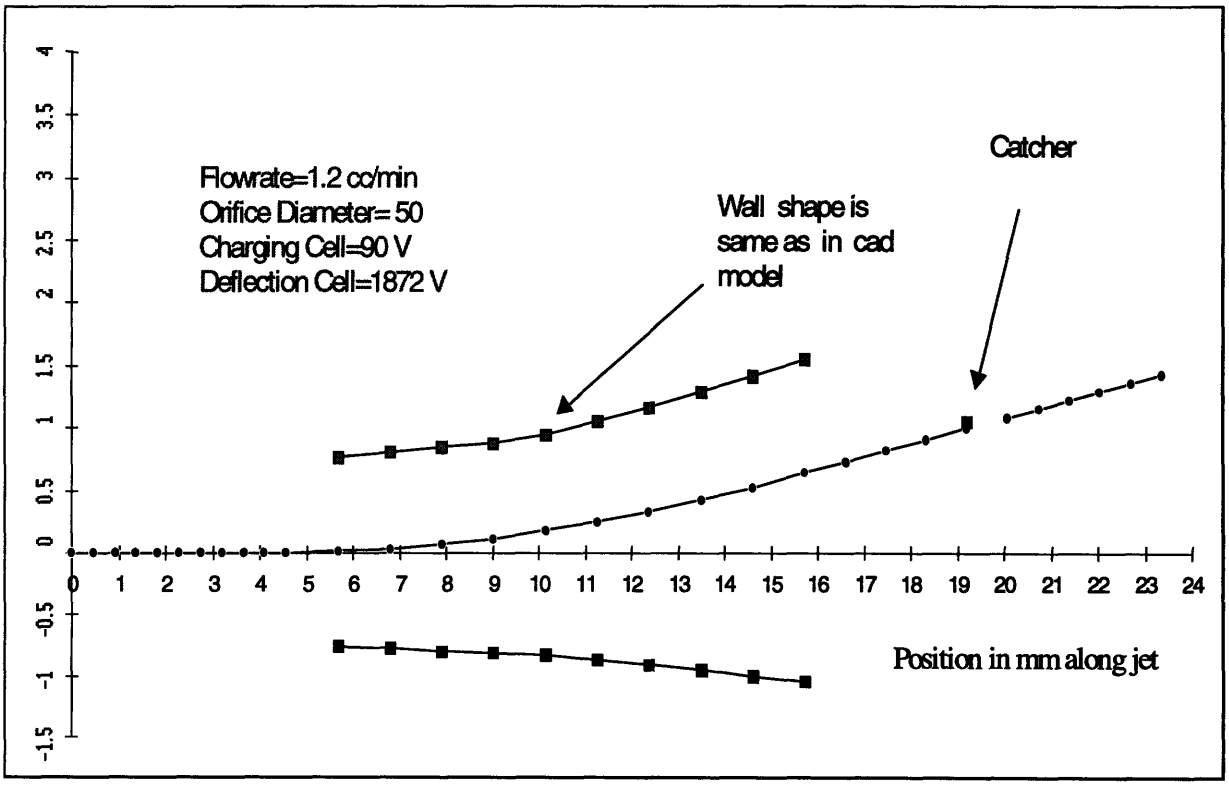


**Figure A-3 Deflection Path for Water. Nozzle 50 μm Flow rate 1.2 cc/min**

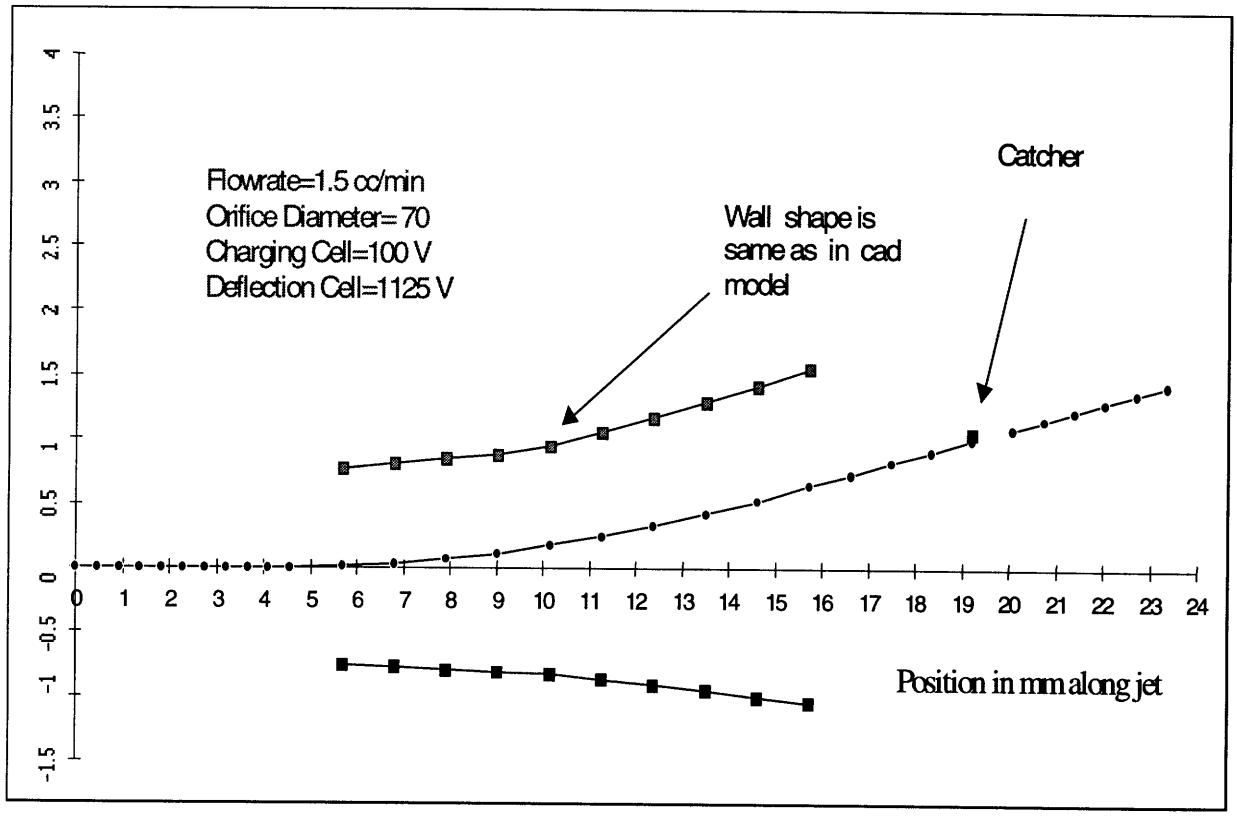


**Figure A-4 Deflection Path for Water. Nozzle 70 μm Flow rate 1.5 cc/min**

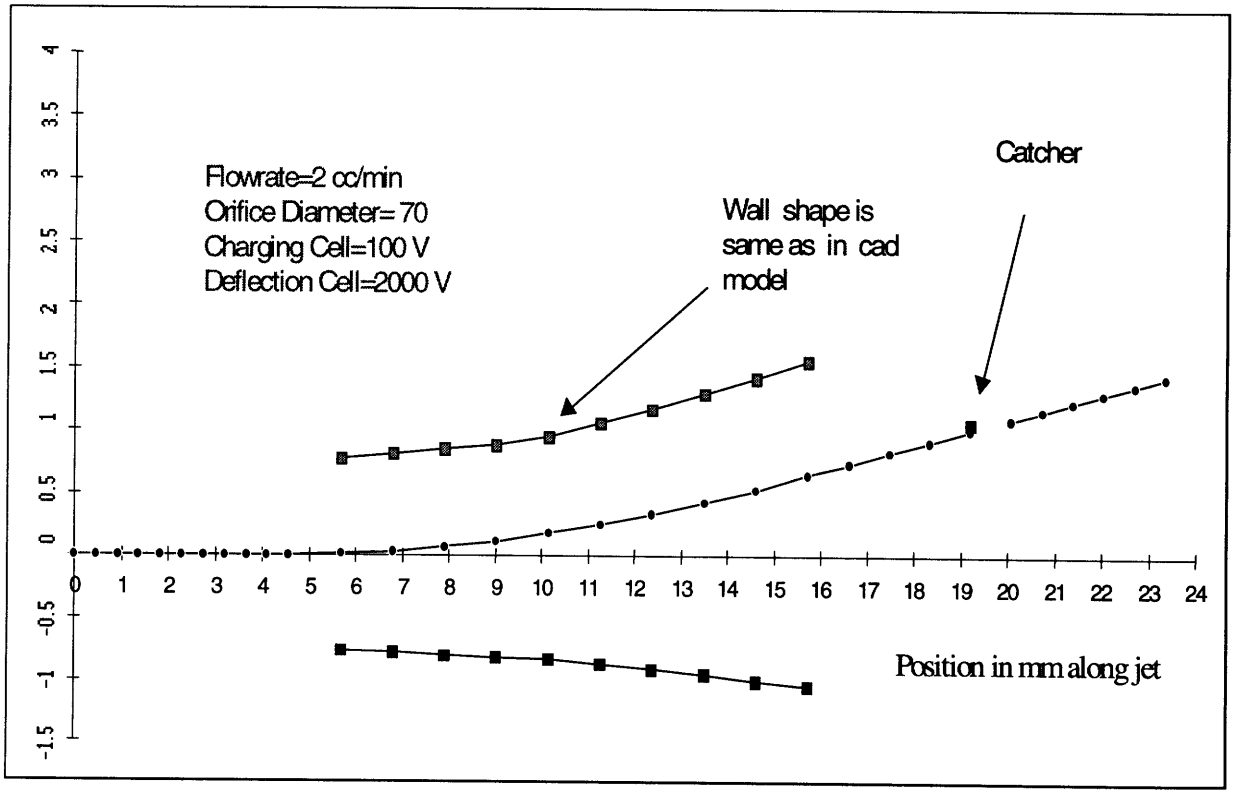


**Figure A-5 Deflection Path for Water. Nozzle 70 μm Flow rate 2 cc/min**

## Table 1Tests made with old Print head

| Charging Cell Voltage[V] | Deflection cell Voltage[V] | Experimental Deflection [mm] | Theoretical Deflection [mm] | Ratio Exp/Theoretical | | % of cell use | Exp. Angle | Theoretical Angle |
|---|---|---|---|---|---|---|---|---|
| 85.70 | 575.00 | 0.7933 | 0.6049 | 1.3115 | L | 0.6667 | 10 | 7 |
| 70.90 | 575.00 | 0.7933 | 0.5005 | 1.5851 | R | 0.6667 | | |
| 85.70 | 816.00 | 1.1333 | 0.8123 | 1.3952 | L | 0.9524 | 14 | 11 |
| 70.90 | 816.00 | 1.1333 | 0.6704 | 1.6905 | R | 0.9524 | | |
| 55.30 | 886.00 | 0.7344 | 0.6015 | 1.2209 | L | 0.6171 | 10 | 6 |
| 46.40 | 886.00 | 0.7344 | 0.5047 | 1.4551 | R | 0.6171 | | |
| 55.30 | 907.00 | 0.7933 | 0.6157 | 1.2885 | L | 0.6667 | 8 | 7 |
| 46.40 | 907.00 | 0.7933 | 0.5166 | 1.5357 | R | 0.6667 | | |

Comments:

Right stream was not centered as well as the left stream.

Angles measured in degrees and in respect to a vertical line in the center of the deflection cell.

Jets #4 and #5 were the jets used for the tests.

## Table 2 Tests made with New Print Head

| Test 47 µm<br>Charging Cell Voltage[V] | Deflection cell Voltage[V] | Experimental Deflection [mm] | Theoretical Deflection [mm] | Ratio Exp/Theoretical | % of cell use |
|---|---|---|---|---|---|
| 103.50 | 800.00 | 0.4079 | 0.4078 | 1.0002 | 0.2632 |
| 103.50 | 1200.00 | 0.6526 | 0.6117 | 1.0668 | 0.4211 |
| 103.50 | 2000.00 | 1.1013 | 1.0200 | 1.0797 | 0.7105 |
| 120.00 | 800.00 | 0.4895 | 0.4730 | 1.0348 | 0.3158 |
| 120.00 | 1200.00 | 0.7342 | 0.7090 | 1.0356 | 0.4737 |
| 120.00 | 2000.00 | 1.3053 | 1.1890 | 1.0978 | 0.8421 |
| Test 102 µm | | | | | |
| 120.00 | 2000.00 | 0.8388 | 0.8006 | 1.0478 | 0.5412 |

# Pdease Program

```
{
This Program model the new
geometry of the print head with different
charging cells
}

title 'Deflection Cells'
 Select
 nodelimit=1500

 Variables
   v(range=0,1500)

 definitions

   Ex=-dx(v)
   Ey=-dy(v)
   Eabs=sqrt(Ex**2+Ey**2)
   eps0=8.854e-12
   eps
   DEx=eps*Ex
   DEy=eps*Ey
   Dabs=sqrt(DEx**2+DEy**2)
   zero=1.e-15

 equations
   div(-eps*grad(v)) = 0

 boundaries
   Region 1
     eps=eps0

         natural (v)=0

         start (-7,-7) line to (18.178,-7)
         to (18.178,18.176) to (-7,18.176) to finish

         value (v)=0

         start (0.4,0) arc(center=0.4,0.4) to (0,0.4)
         line to (0,10.776) arc(center=0.4,10.776)
         to (0.4,11.176) line
         to (2.31,11.176) arc(center=2.31,10.776) to
         (2.71,10.776) line to (2.695,10.0584)to
         (2.68, 8.9408) to
         (2.666,7.8232) to
         (2.641, 6.7056) to
         (2.604,5.588) to
         (2.562, 4.4704) to
         (2.518,3.35282) to
         (2.473,2.2352) to
         (2.421,1.1176) to
         (2.38656, 0.3843) arc(center=1.98686,0.4) to
```

(1.98686,0) line to finish

value (v)=0

start (10.778,0) arc(center=10.778,0.4)
to (11.178,0.4) line
to (11.178,10.776) arc(center=10.778,10.776) to
(10.778,11.176) line to (8.868,11.176)
arc(center=8.868,10.776) to (8.468,10.776) line to
(8.483,10.0584)to
(8.498, 8.9408) to
(8.512,7.8232) to
(8.537, 6.7056) to
(8.574,5.588) to
(8.616, 4.4704) to
(8.66,3.35282) to
(8.705,2.2352) to
(8.757,1.1176) to
(8.79144, 0.3843) arc(center=9.19144,0.4) to
(9.19144,0) line to finish

value (v)=1500

start (4.234,10.776)
arc(center=4.634,10.776) to
(4.634,11.176) line to
(6.544, 11.176)
arc(center=6.544,10.776) to
(6.944, 10.776) line to
(6.8932, 9.779) to
(6.8678, 8.9408) to
(6.8424, 8.3566) to
(6.817, 7.4422) to
(6.7154, 6.223) to
(6.6392, 5.1562) to
(6.563, 4.318) to
(6.4614, 3.3274) to
(6.3852, 2.5146) to
(6.309, 1.8542) to
(6.2328, 1.3208) to
(6.1566, 0.6096) to (6.1242,0.350386)
arc(center=5.72729,0.4) to
(5.72729,0) line to
(5.45071,0)
arc(center=5.45071,0.4) to
(5.0538,0.350386) line to
(5.0214, 0.6096) to
(4.9452, 1.3208) to
(4.869, 1.8542) to
(4.7928, 2.5146) to
(4.7166, 3.3274) to
(4.615, 4.318) to
(4.5388, 5.1562) to
(4.4626, 6.223) to
(4.361, 7.4422) to
(4.3356, 8.3566) to

```
        (4.3102, 8.9408) to
        (4.2848, 9.779) to finish

        value(v)=0

        start(4.311,-4.318)
        arc(center=5.589,-4.318) to (5.589,-3.04)
        to (6.867,-4.318) to (5.589,-5.596) to finish

        value (v)=100

        start (-.508,13.97) line to (3.218,13.97)
        to (3.218,16.002) to (-.508,16.002) to finish

        value (v)=100

        start (3.725,13.97) line to (7.452,13.97)
        to (7.452,16.002) to (3.725,16.002) to finish

        value (v)=100

        start (7.96,13.97) line to (11.682,13.97)
        to (11.682,16.002) to (7.96,16.002) to finish

monitors
  contour(v)
plots
  contour(v) as "Potential" pause
  contour(v) zoom (5,10,5,5) as "Potential" pause
  contour(v) zoom (4,-2.5,6.5,7) as "Potential" pause
  vector(dx(v),dy(v)) as "Electric Field" pause
  vector(dx(v),dy(v)) zoom (5,10,5,5) as "Electric Field" pause
  vector(dx(v),dy(v)) zoom  (4,-2.5,6.5,7) as "Electric Field" pause
  contour(Eabs) as "Constant Deflection Fields" pause
  contour(Eabs) zoom (5,10,6,5) as "Constant Deflection Fields" pause
  contour(Eabs) zoom  (4,-2.5,6,6) as "Constant Deflection Fields" pause
  contour(Eabs) zoom  (6.5,6,4,6) as "Constant Deflection Fields" pause
  contour(Eabs) zoom  (5.5,-1,6,7) as "Constant Deflection Fields" pause
end
```

# Cad Drawings for the Print Head

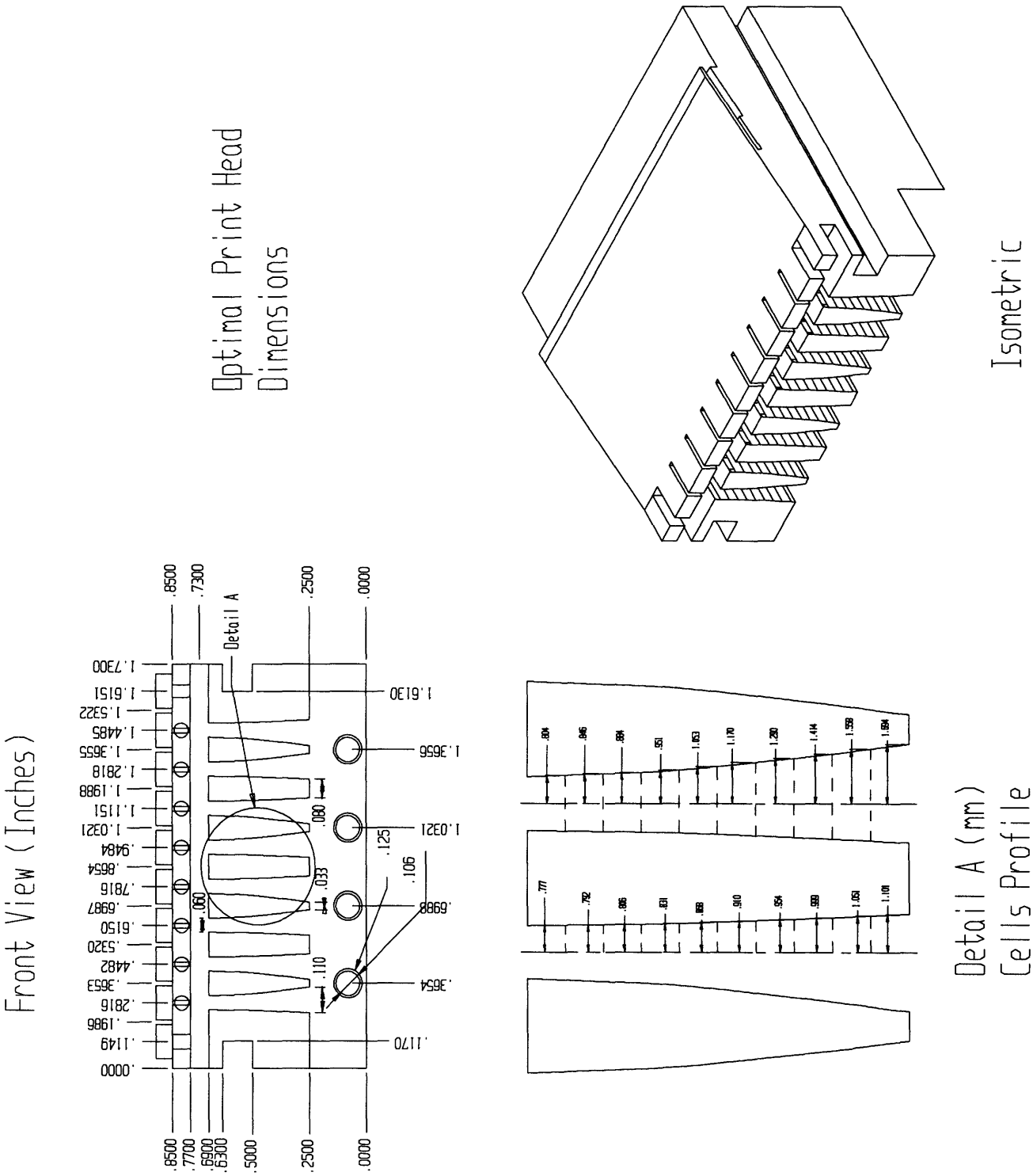

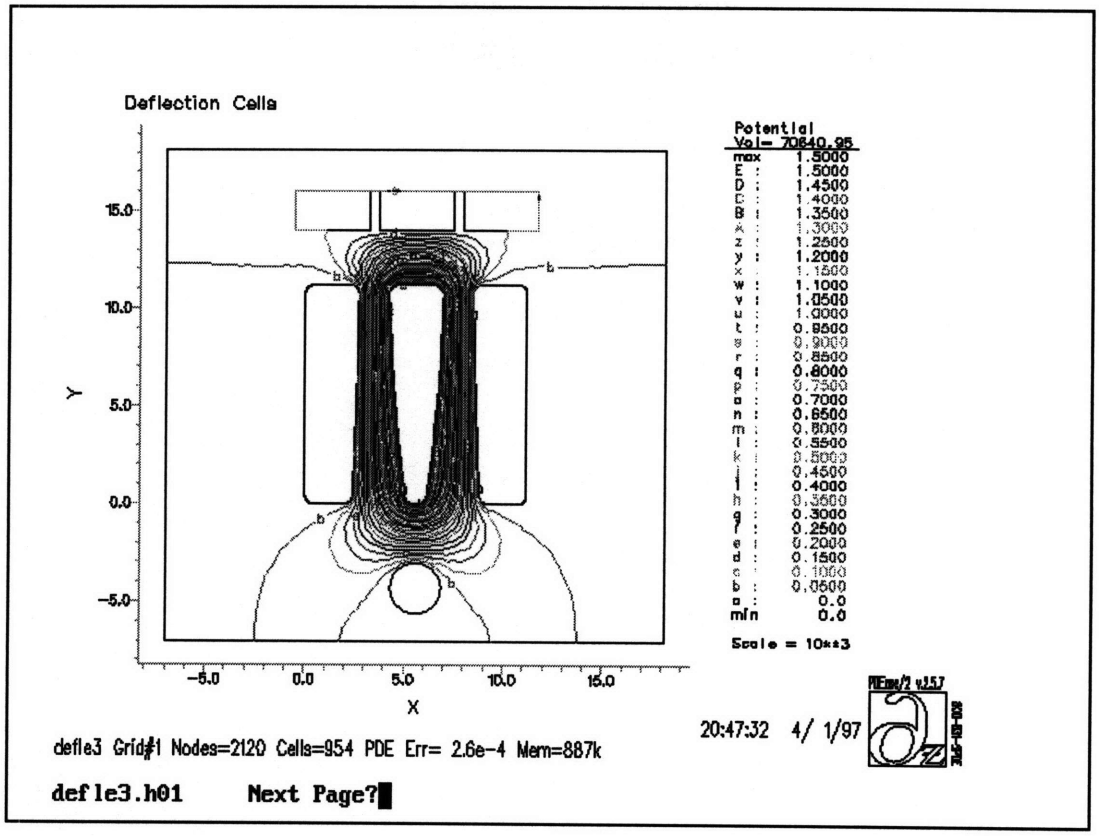


**Figure A-6 Equiotential Lines. Charging Cell Voltage 100 V. Charging Cell gap 0.020 inch**

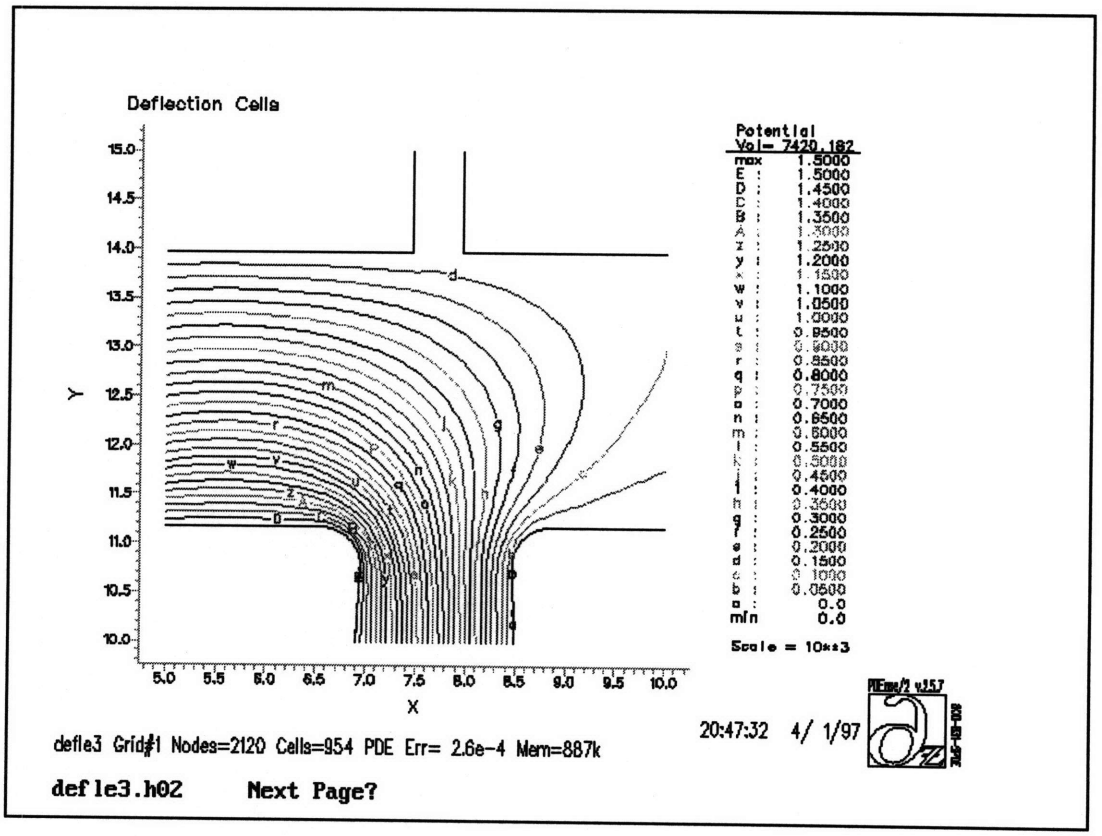


**Figure A-7 Equiotential Lines. Charging Cell Voltage 100 V. Charging Cell gap 0.020 inch**

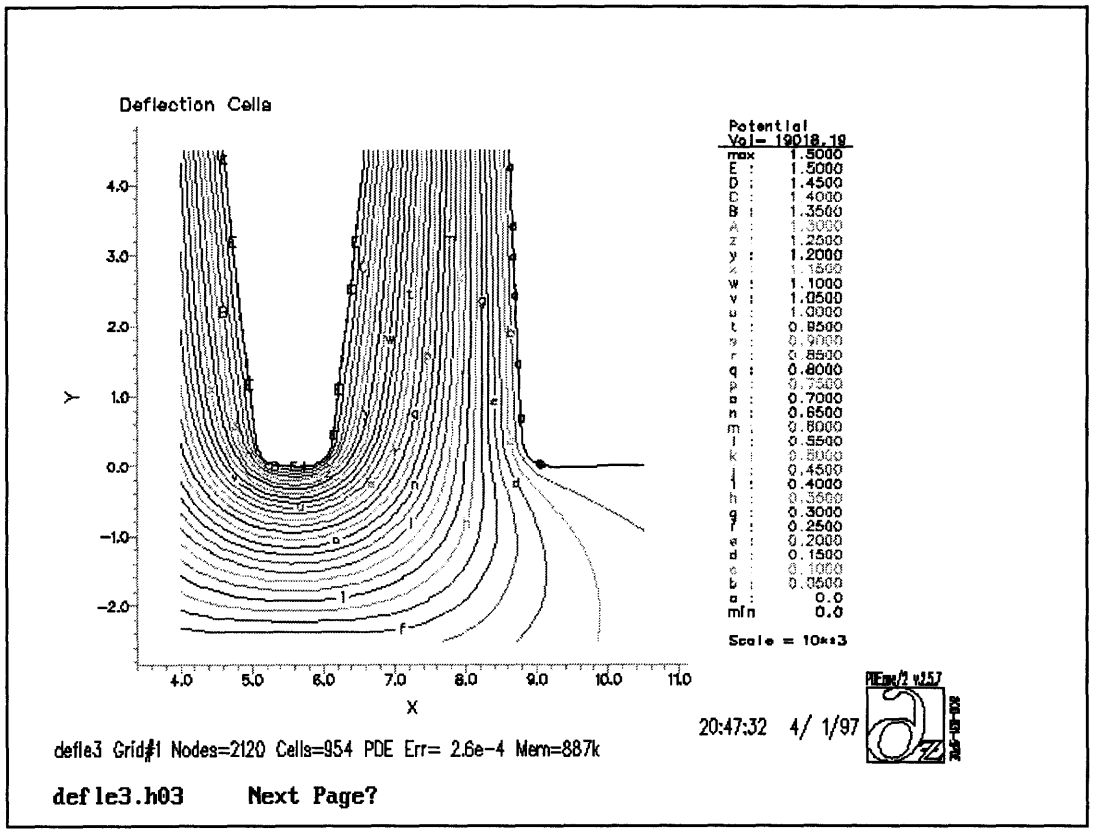


**Figure A-8 Equiotential Lines. Charging Cell Voltage 100 V. Charging Cell gap 0.020 inch**

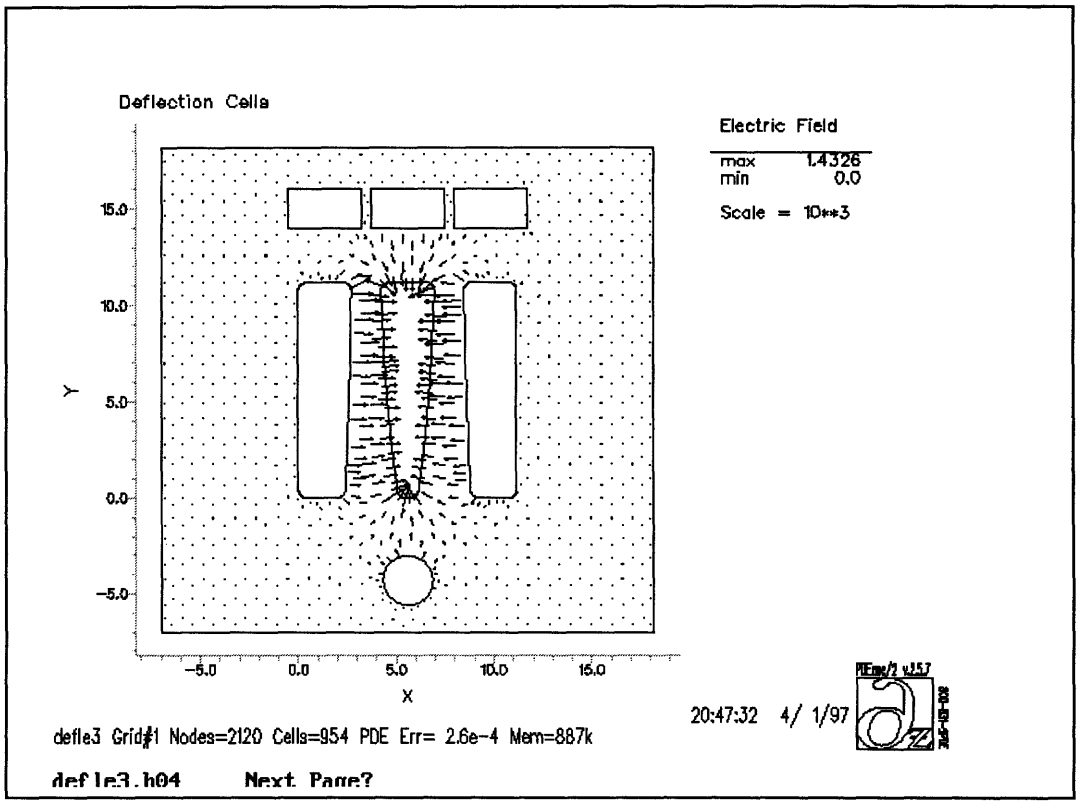


**Figure A-9 Electric Field. Charging Cell Voltage 100 V. Charging Cell gap 0.020 inch**

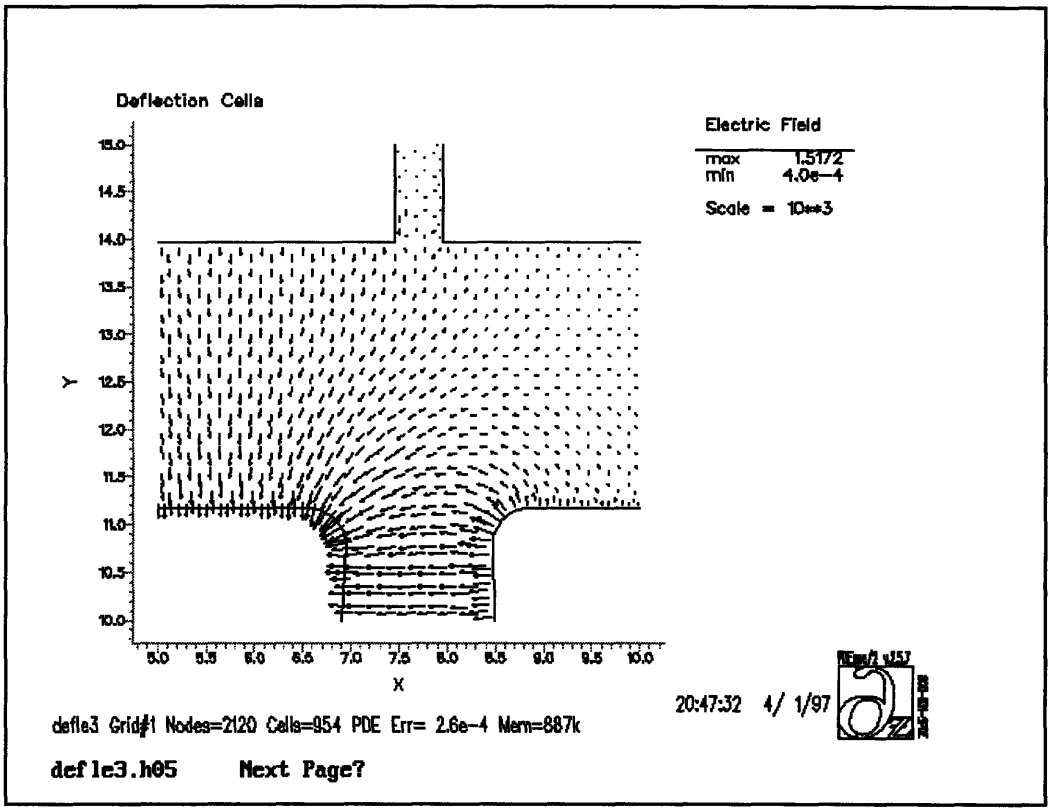


**Figure A-10 Electric Field. Charging Cell Voltage 100 V. Charging Cell gap 0.020 inch**

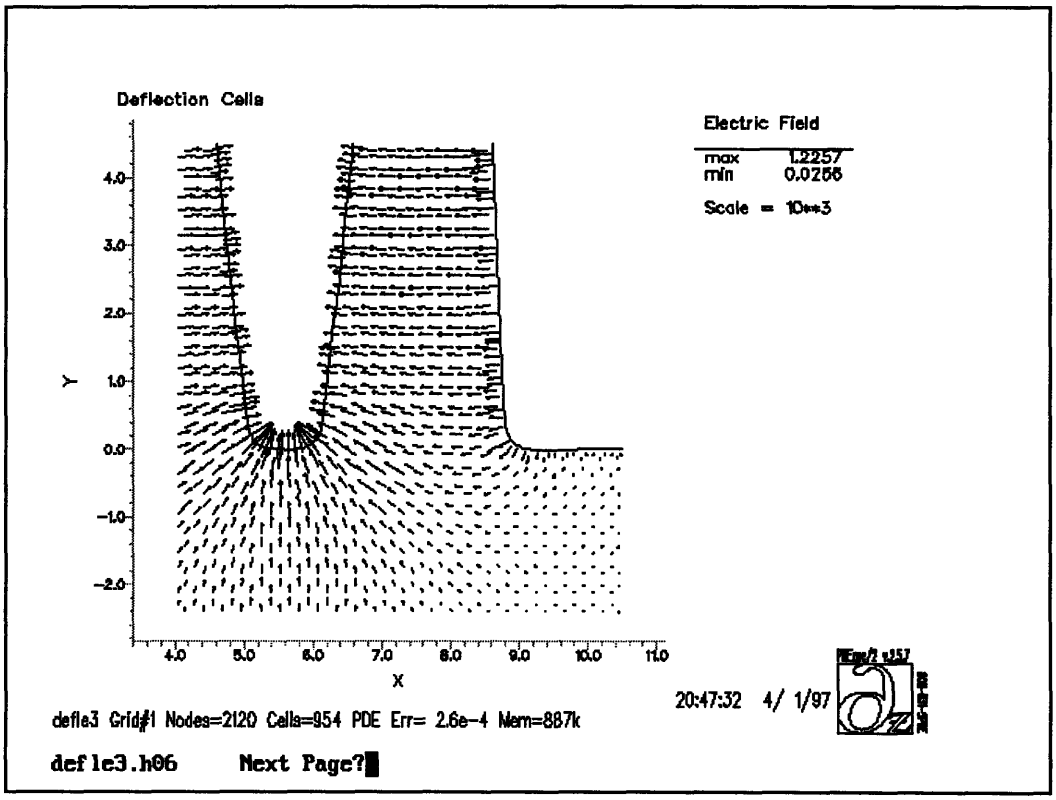


**Figure A-11 Electric Field. Charging Cell Voltage 100 V. Charging Cell gap 0.020 inch**

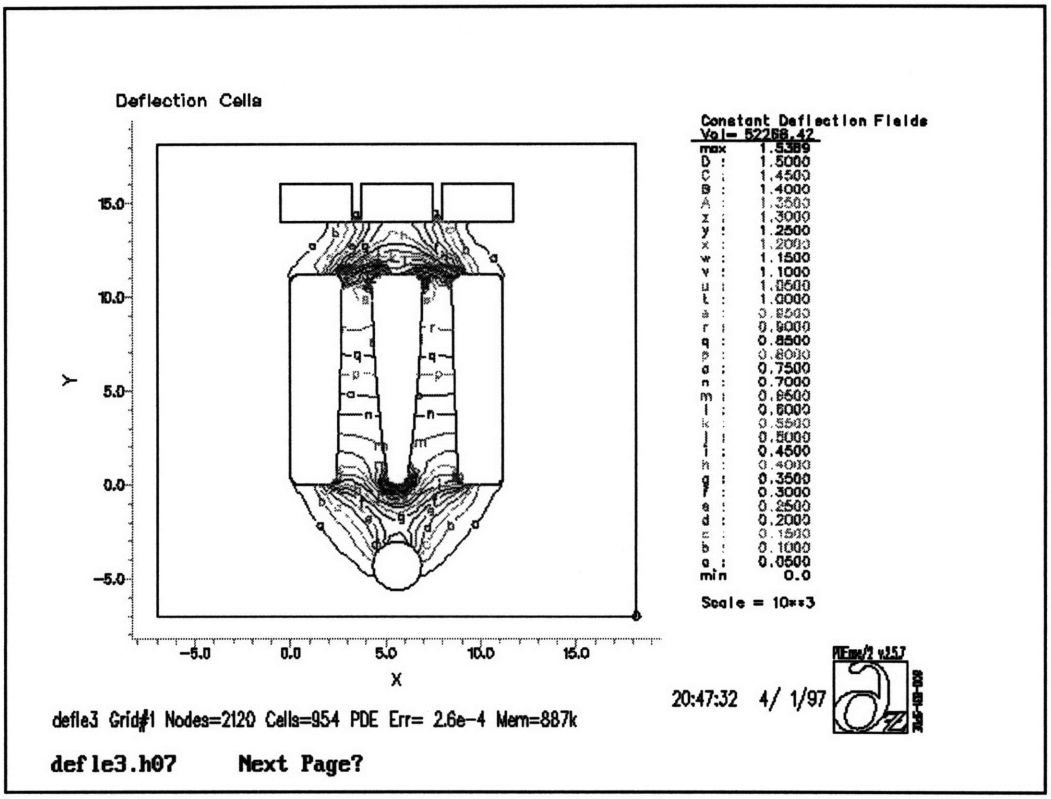


**Figure A-12 Constant electric field lines. Charging Cell Voltage 100 V. Charging Cell gap 0.020 inch**

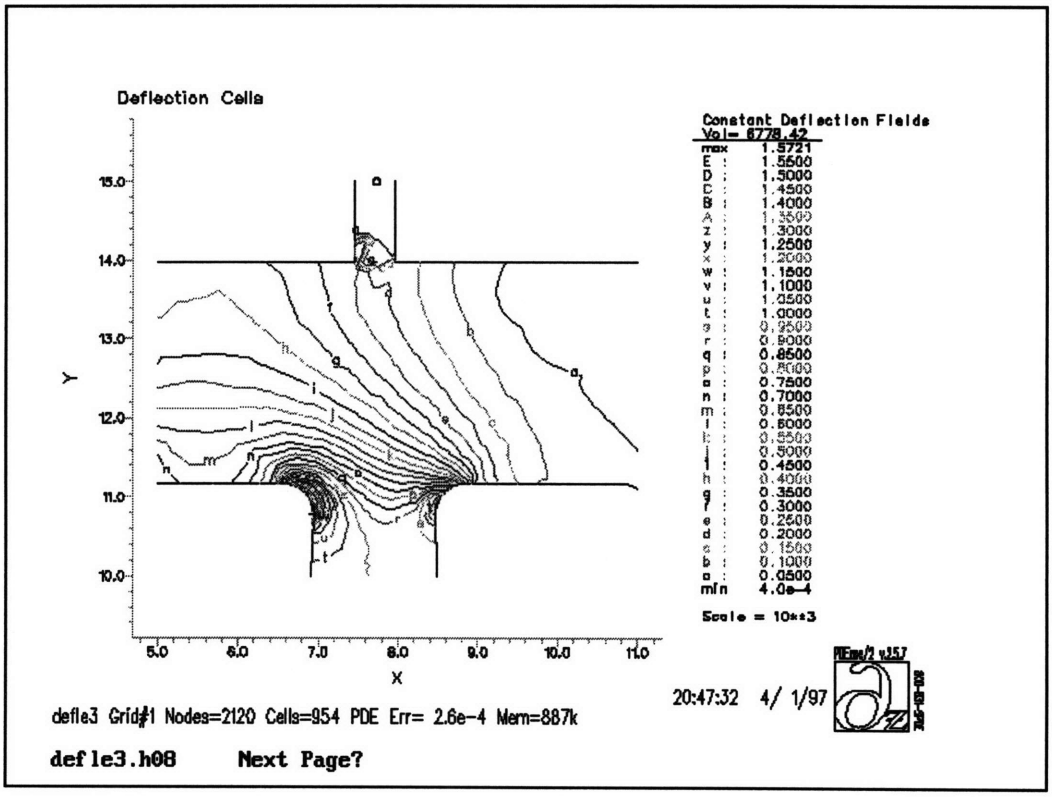


**Figure A-13 Constant electric field lines. Charging Cell Voltage 100 V. Charging Cell gap 0.020 inch**

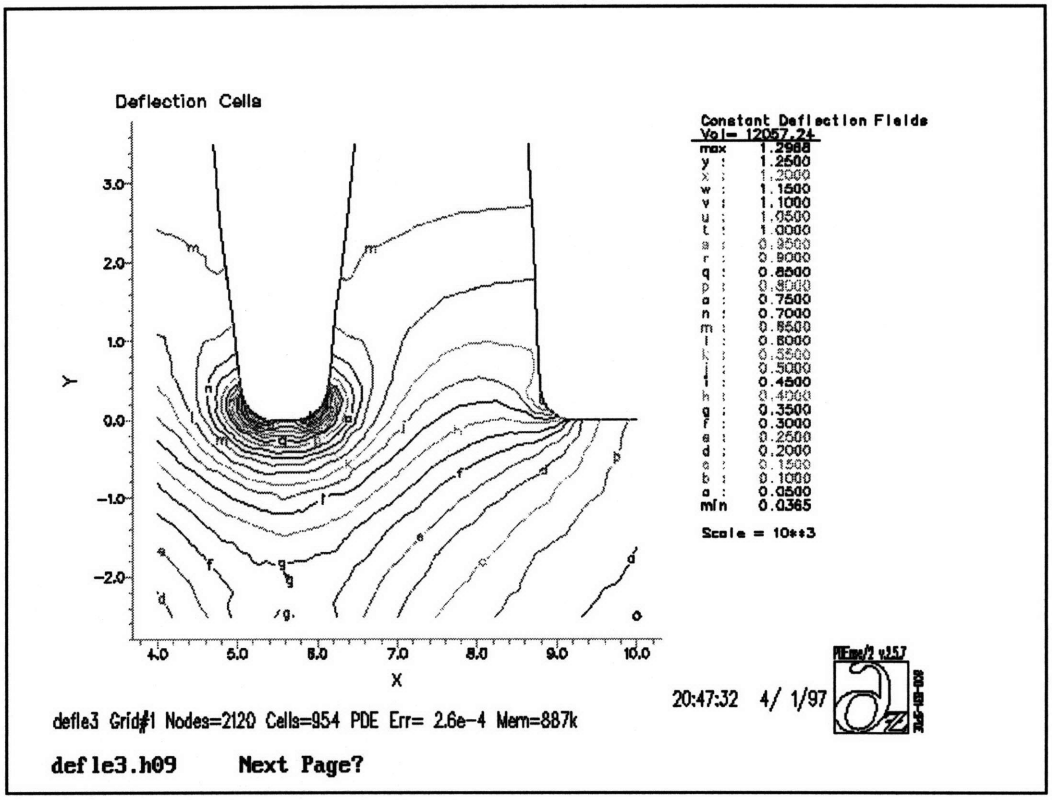


**Figure A-14 Constant electric field lines. Charging Cell Voltage 100 V. Charging Cell gap 0.020 inch**

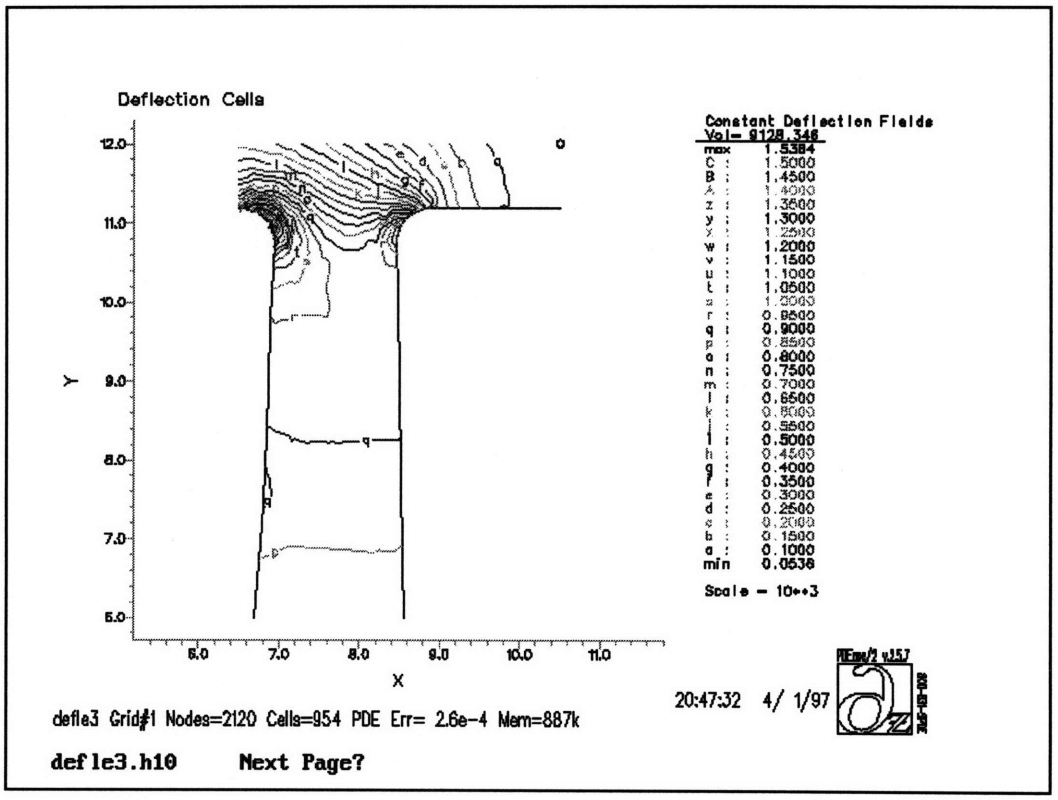


**Figure A-15 Constant electric field lines. Charging Cell Voltage 100 V. Charging Cell gap 0.020 inch**

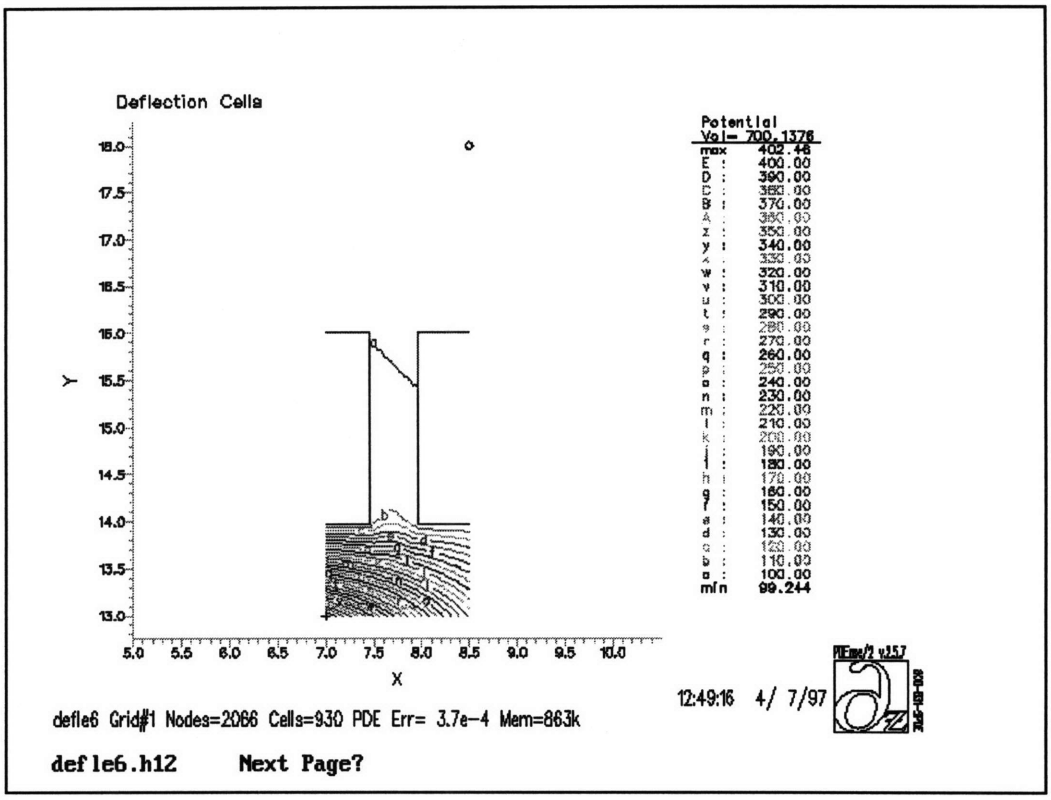


**Figure A-16 Equipotential lines. Charging Cell Voltage 100 V. Charging Cell gap 0.020 inch**

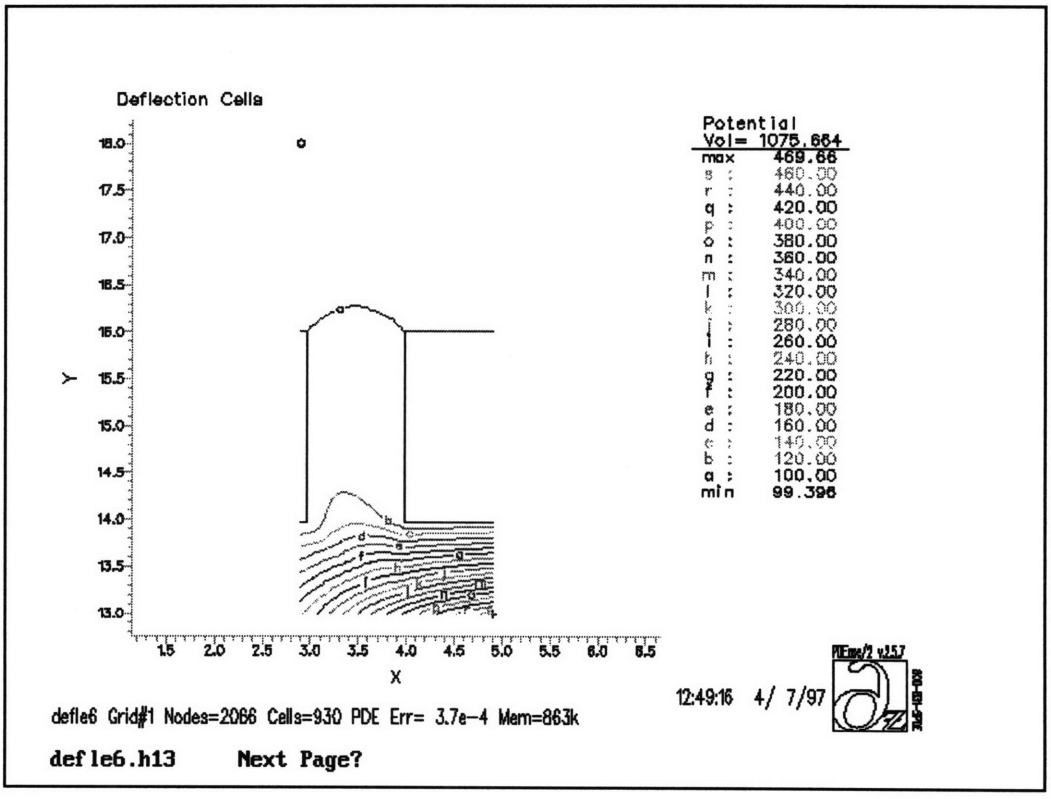


**Figure A-17 Equipotential lines. Charging Cell Voltage 100 V. Charging Cell gap 0.035 inch**

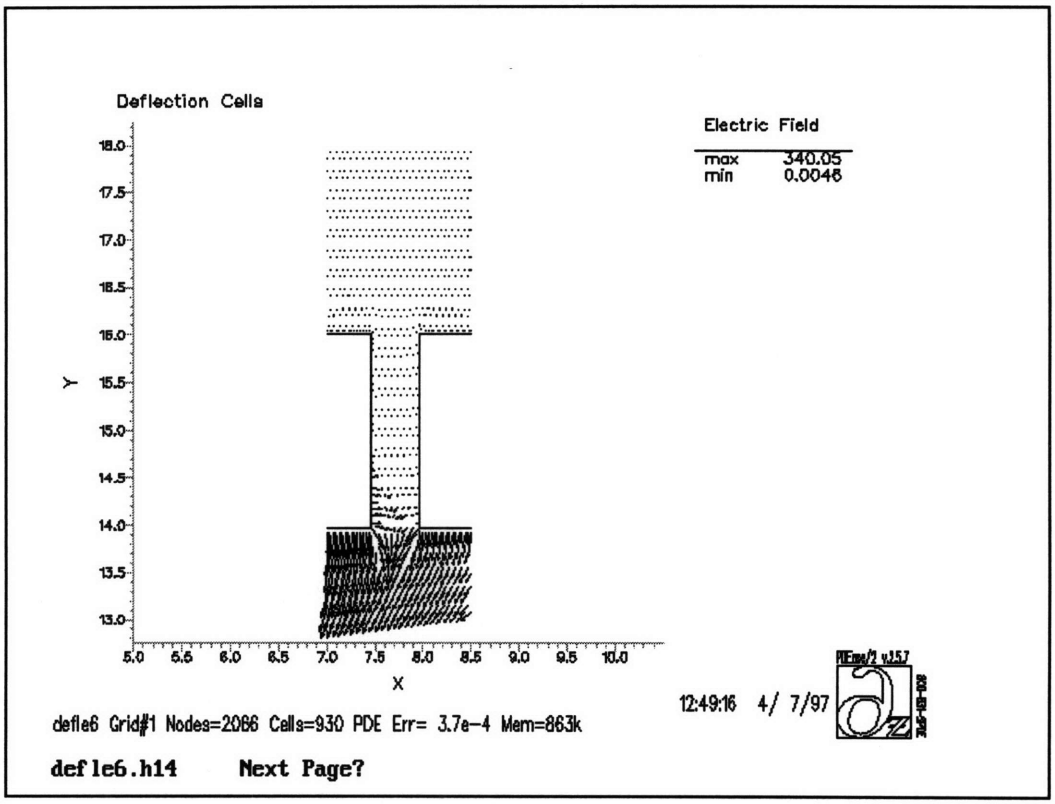


**Figure A-18 Electric Field. Charging Cell Voltage 100 V. Charging Cell gap 0.020 inch**

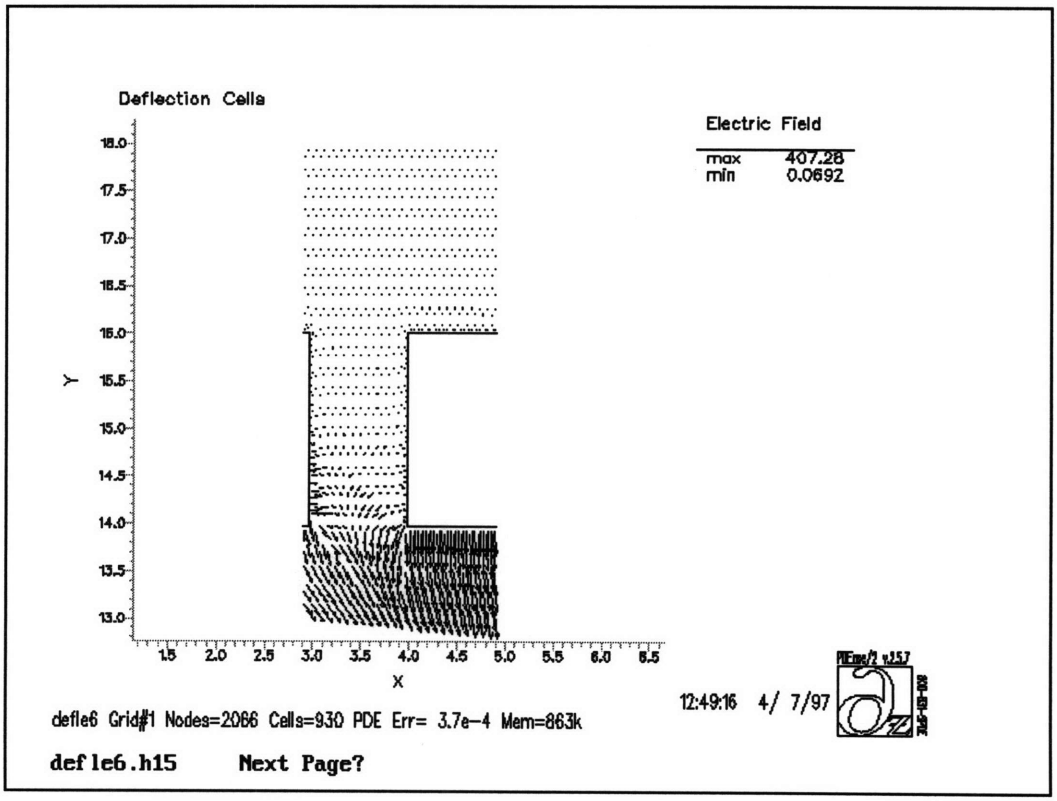


**Figure A-19 Electric Field. Charging Cell Voltage 100 V. Charging Cell gap 0.035 inch**

# Appendix B

# CAD Drawings

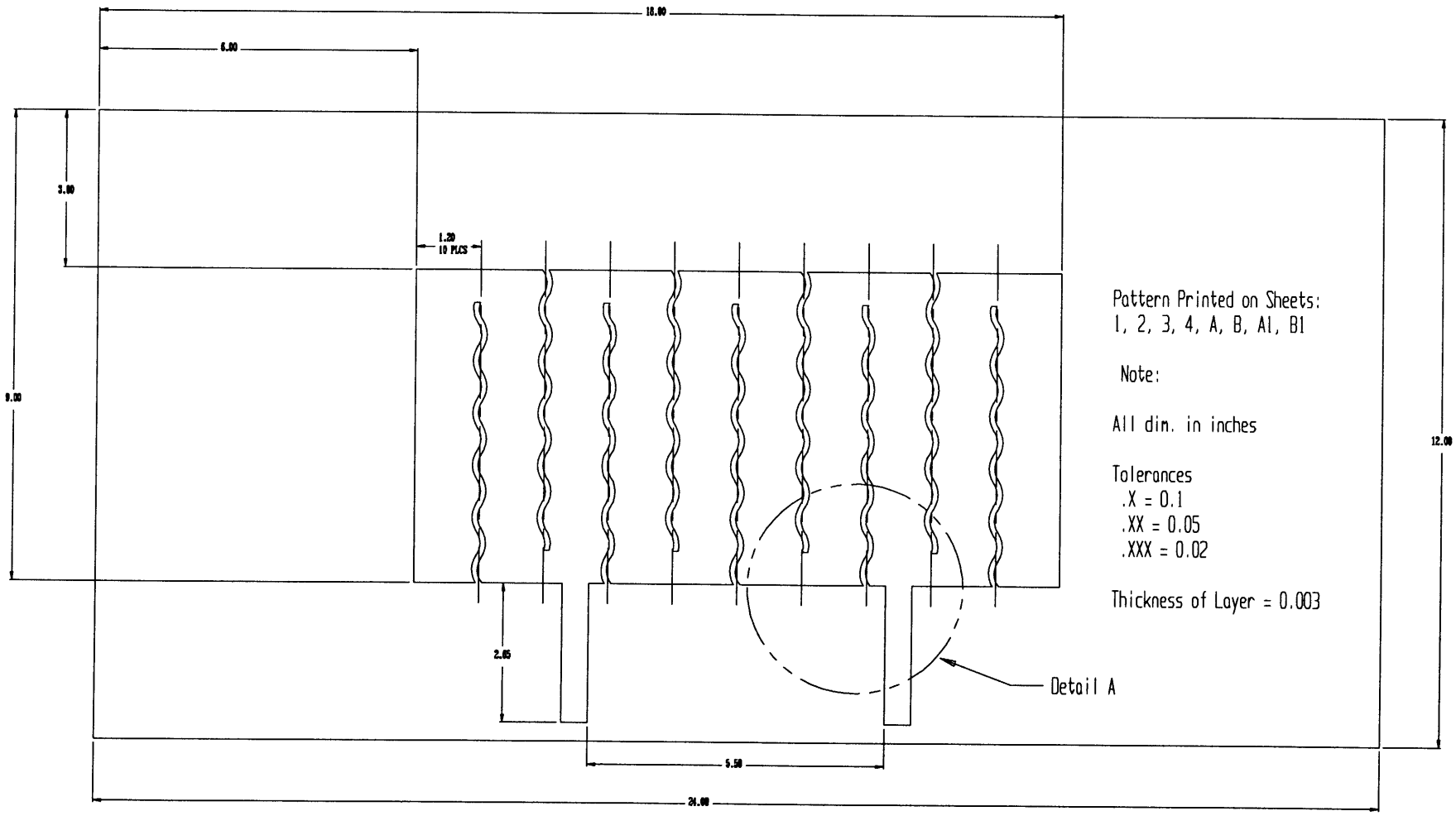
18.00
6.00
3.00
9.00
1.20
10 PLCS
2.05
5.50
26.00
12.00
Pattern Printed on Sheets:
1, 2, 3, 4, A, B, A1, B1
Note:
All din. in inches
Tolerances
.X = 0.1
.XX = 0.05
.XXX = 0.02
Thickness of Layer = 0.003
Detail A

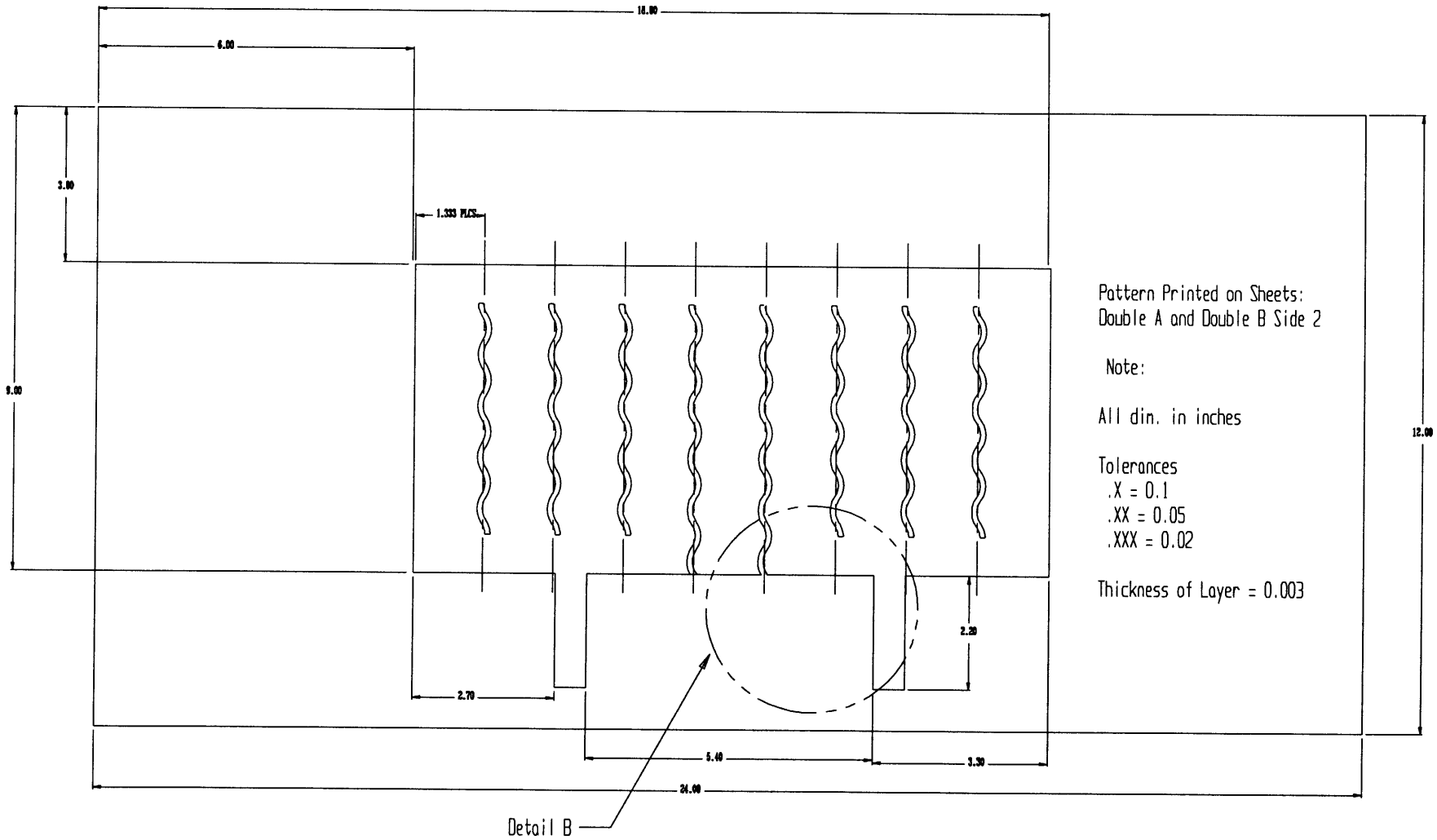
18.00
6.00
3.00
1.333 PLCS.
9.00
12.00
2.70
2.20
5.40
3.30
24.00
Detail B
Pattern Printed on Sheets:
Double A and Double B Side 2
Note:
All din. in inches
Tolerances
.X = 0.1
.XX = 0.05
.XXX = 0.02
Thickness of Layer = 0.003

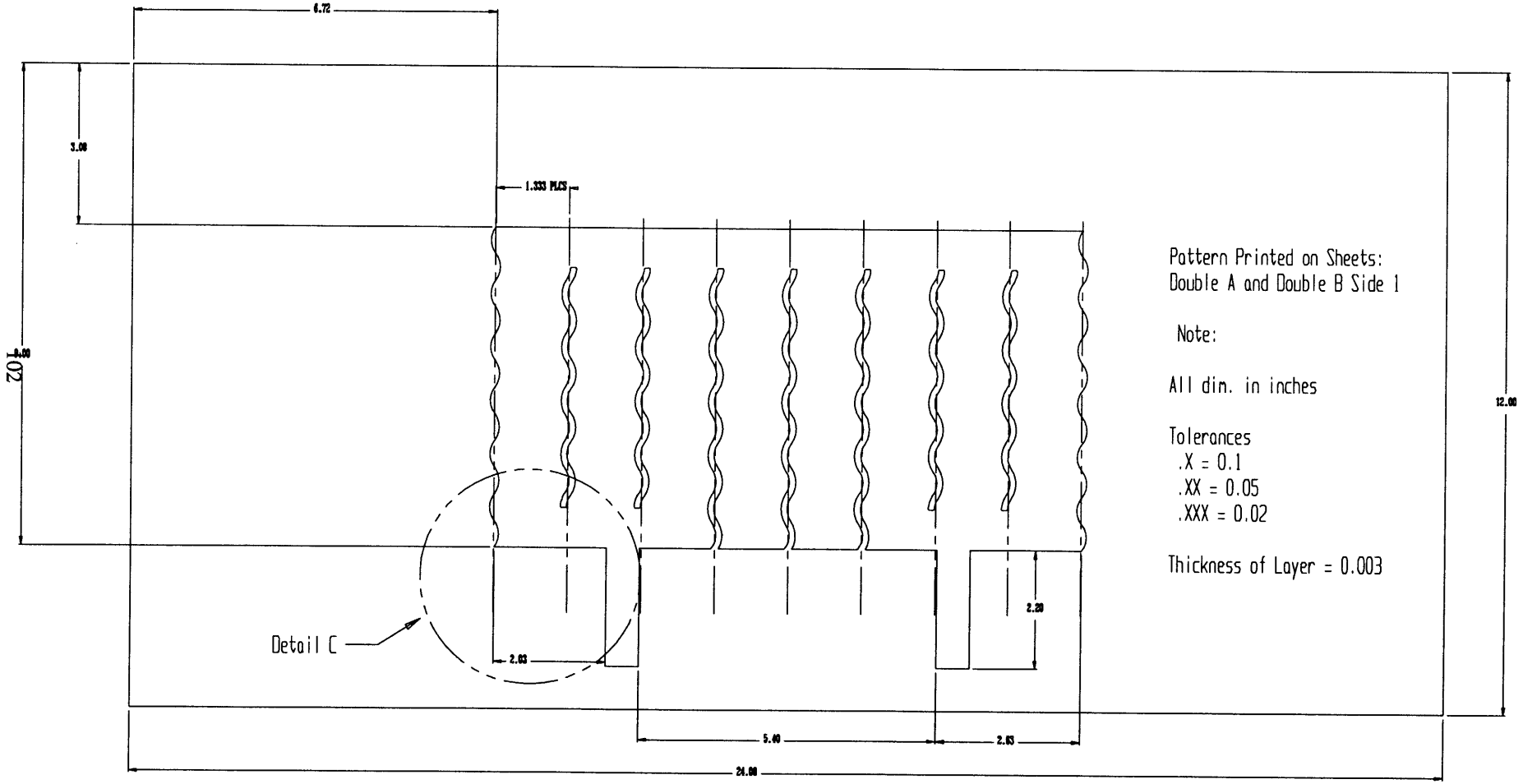
6.72
3.00
1.333 PLCS
102
Detail C
2.83
2.20
5.40
2.83
24.00
12.00
Pattern Printed on Sheets:
Double A and Double B Side 1
Note:
All din. in inches
Tolerances
.X = 0.1
.XX = 0.05
.XXX = 0.02
Thickness of Layer = 0.003

Detail A

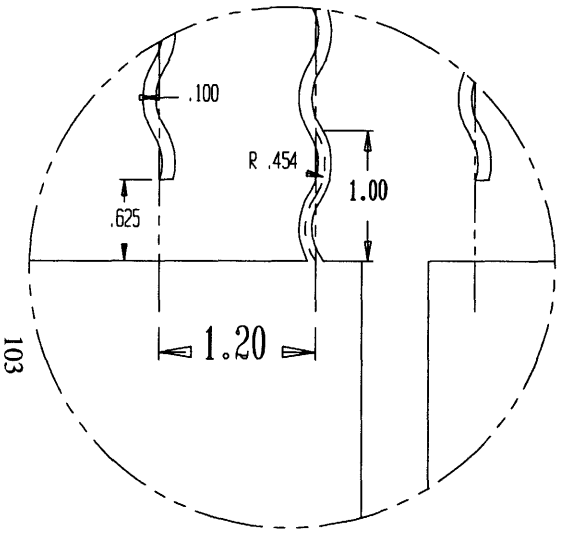


Detail B

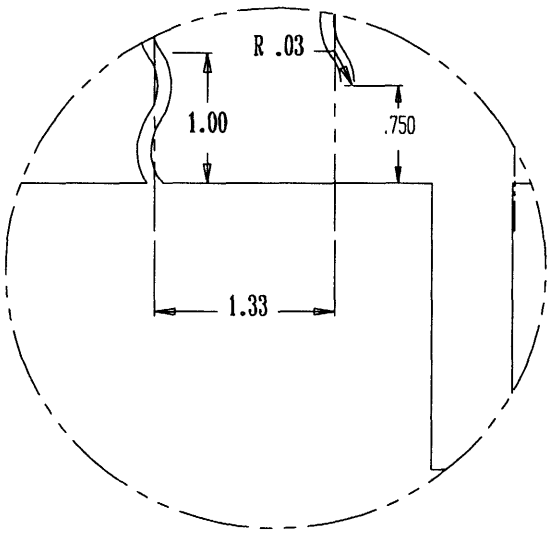


Detail C

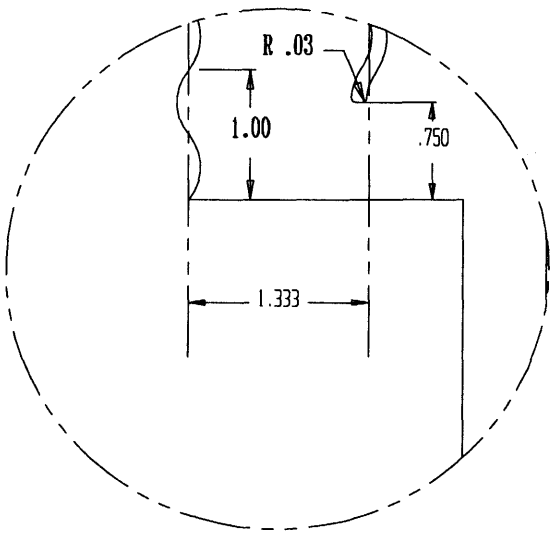


For all the DetailsSines Waves in Phase
Wavelenght=1.000
Half Amplitude=0.750
Bare strip=0.100
Dimensions in inches

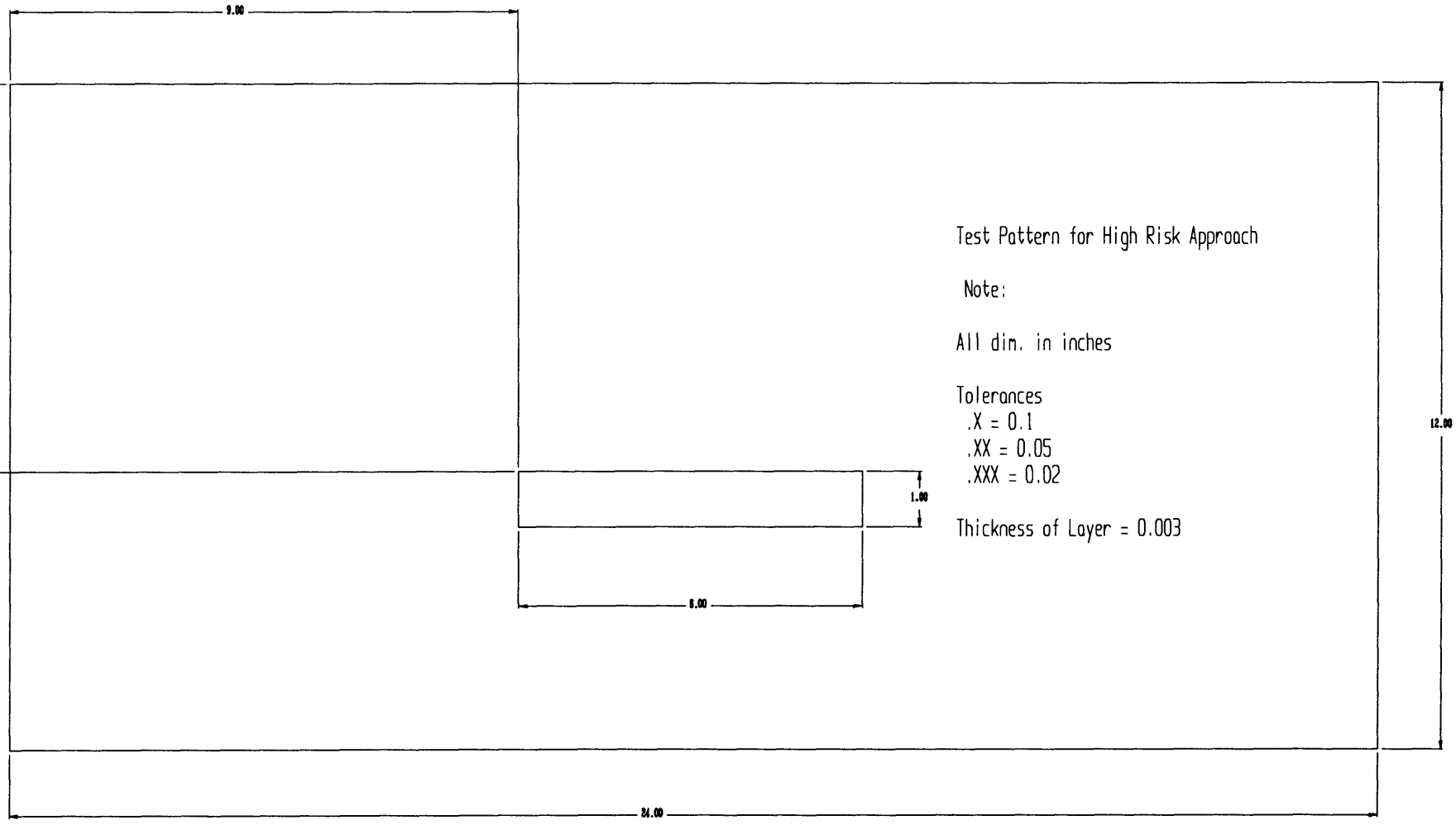


Test Pattern for High Risk Approach

Note:

All din. in inches

Tolerances
.X = 0.1
.XX = 0.05
.XXX = 0.02

Thickness of Layer = 0.003

# Appendix C

# Development of a Weight Switch for the Alpha Machine

# Appendix C

## Calculations for the Cantilever Weight Switch for the Alpha Machine

### Introduction

In order to be able to print parts for hours without stopping for a binder refill, the 3Dprinting Alpha Machine has a fluid system that allows the user to add binder while the machine is in normal operation. This system relies completely on a mechanical switch that is in charge of an automatic refill cycle. The switch senses changes in weight to then activate a series of pneumatic valves. These valves pressurize and depressurize a series of tanks to finally refill the main injection tank. In conclusion, the switch has to be completely reliable to avoid any problems with the binder. This appendix deals with the design of the switch.

Design

A cantilever beam type switch was constructed and tested in order to determine the best parameters for a reliable and robust operation. A steel bar is used as a flexible element that will respond to force changes. These force changes will produce position changes that will activate or deactivate and electrical switch. The diagram below depicts the arrangement.

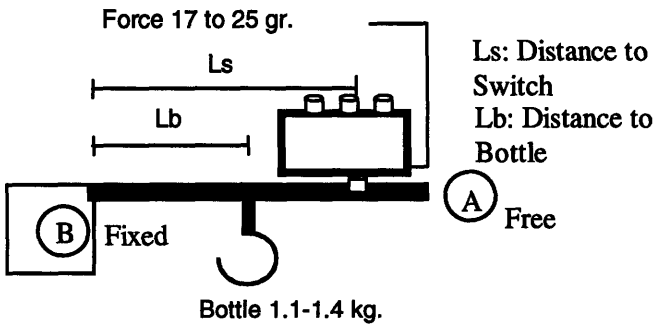


Figure C-1. Diagram of the switch setup.

Free Body Diagram:

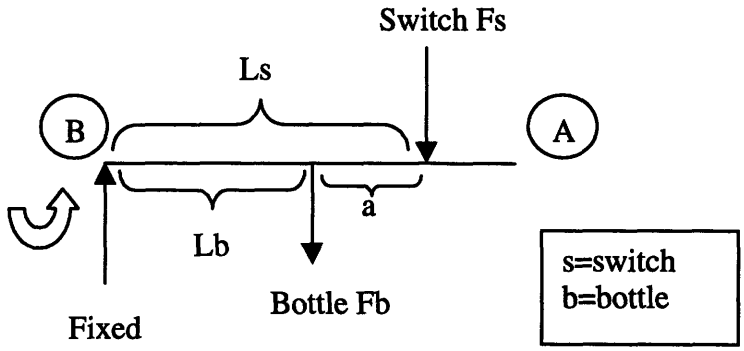


Figure C-2. Free Body Diagram of the switch setup.

The boundary conditions for the system are:

A: Free end, Ma=Ra=0

B: Fixed end, Yb=ø=0

The bottle actuates on the beam producing a deflection. This defection gets smaller as the binder leaves the bottle. After an amount of 250 ml has left, the beam should be able to trigger the electric switch and start the refill cycle. It is important to notice that the switch also produces a force when the bottle gets lighter. This force has to be taken into account in the equations of the system. The hysterisis in both electrical elements were very similar and about 0.14 mm. The moment of inertia of the beam is the following:

$$I_{Beam} = \frac{1}{12} w * h^3 \text{ where } \frac{w = 9.5\ mm}{h = 0.7\ mm} \text{ therefore } I_{Beam=3.34e\text{-}13}$$

Also the steel has an Elastic modulus of 2.06e5 MPa.

Because we have a fixed beam, one of the end points does not present any reacting force and we can say that the reaction in side B is RB=Fs+Fb, where Fs and Fb are the forces actuating in the beam.

The design of this system allows adjustability, in other words the switch can move horizontally on top of the beam making it possible to vary the hysterisis. On the other side the point where the force of the bottle is present is always the same. Lb never changes while Ls can vary almost half an inch. The value of Lb is 35 mm. while Ls can go from 38 to 50 mm. The deflection of the beam has to be approximately 0.2 mm in order to activate and deactivate the electric switch. In the next page we can see the equations derived to analyze the system and confirm its effectiveness.

Moment Equation :

$M_b = M_a - F_s * L_s - F_b * L_b$ *with the boundary conditions* $M_a$=0

*Integrating:*

$$\theta = \theta_s - \frac{F_s * x^2}{2EI} - \frac{F_b(x-a)^2}{2EI} \text{ with } \theta_b = 0 \text{ therefore}$$

$$\theta_s = \frac{F_s * L_s^2}{2EI} + \frac{F_b(L_b)^2}{2EI}$$

*Integrating again the deflection:*

$$Y = Y_s + \theta_s * x - \frac{F_s * x^3}{6EI} - \frac{F_b(L_b)^3}{6EI}$$

*Finally the deflection at the switch:*

$$Y_s = \left[ \frac{-F_s * L_s^3}{3EI} + \frac{F_b(L_b)^2}{2EI}\left(\frac{L_b}{3} - L_s\right) \right]$$

**Results and Experimentation:**

Results are presented in the next pages. An excel sheet was made using several different configurations for the same setup. First an ideal switch with no force was considered. Then just the force of the switch when the bottle was empty was taken into account. Finally the complete model was used using the average forces in the *on* position of the switch and the *off* position.

Experimentation was done to see if the physical switch followed the model. A set of different weights was used to simulate different parts of the cycle. Also, the placement of the switch on the beam was modified. The model followed very well the predictions.

It is widely adjustable for different densities of binders, setup points and hysterisis. The results can be seen in figures C-3 through C-7.

**The final configuration chosen is:**

**Ls can go from 38 to 50 mm**

**Lb is fixed at 35 mm**

Table C-1 and figure C-3 show the deflection versus weight for a setup with the switch placed at 40 mm from the fixed end. The force applied by the switch to the beam was not present in the experimental setup

| Force | Deflection (in) | Force (kg) | Experimental Deflection | Theoretical Deflection |
|---|---|---|---|---|
| 1.1 | 0.11 | 1.1 | 2.79 | 2.72 |
| 1.15 | 0.117 | 1.15 | 2.97 | 2.85 |
| 1.2 | 0.122 | 1.2 | 3.10 | 2.97 |
| 1.25 | 0.128 | 1.25 | 3.25 | 3.09 |
| 1.3 | 0.134 | 1.3 | 3.40 | 3.22 |
| 1.35 | 0.14 | 1.35 | 3.56 | 3.34 |

Table C-1

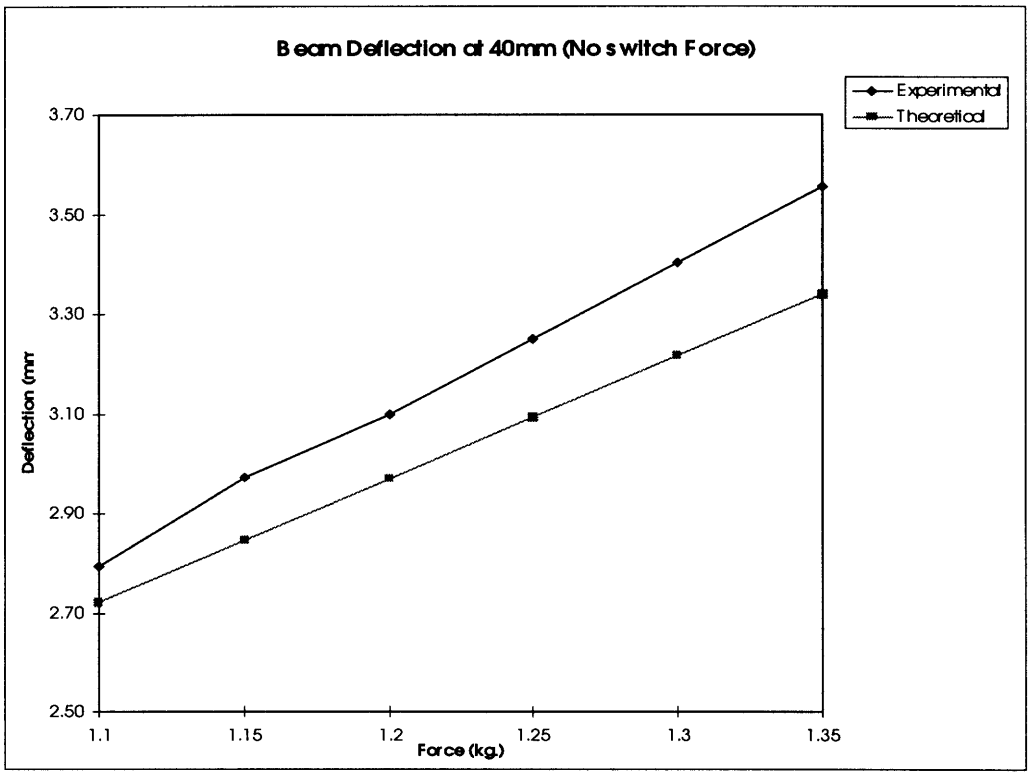


Figure C-3 Defection versus force

Table C-2 and figure C-4 show the deflection versus weight for a setup with the switch placed at 42 mm from the fixed end. The force applied by the switch to the beam was not present in the experimental setup.

| Force | Deflection (in) | Force (kg) | Experimental Deflection | Theoretical Deflection |
|---|---|---|---|---|
| 1.1 | 0.116 | 1.1 | 2.95 | 2.91 |
| 1.15 | 0.121 | 1.15 | 3.07 | 3.05 |
| 1.2 | 0.126 | 1.2 | 3.20 | 3.18 |
| 1.25 | 0.131 | 1.25 | 3.33 | 3.31 |
| 1.3 | 0.139 | 1.3 | 3.53 | 3.44 |
| 1.35 | 0.148 | 1.35 | 3.76 | 3.58 |

Table C-2

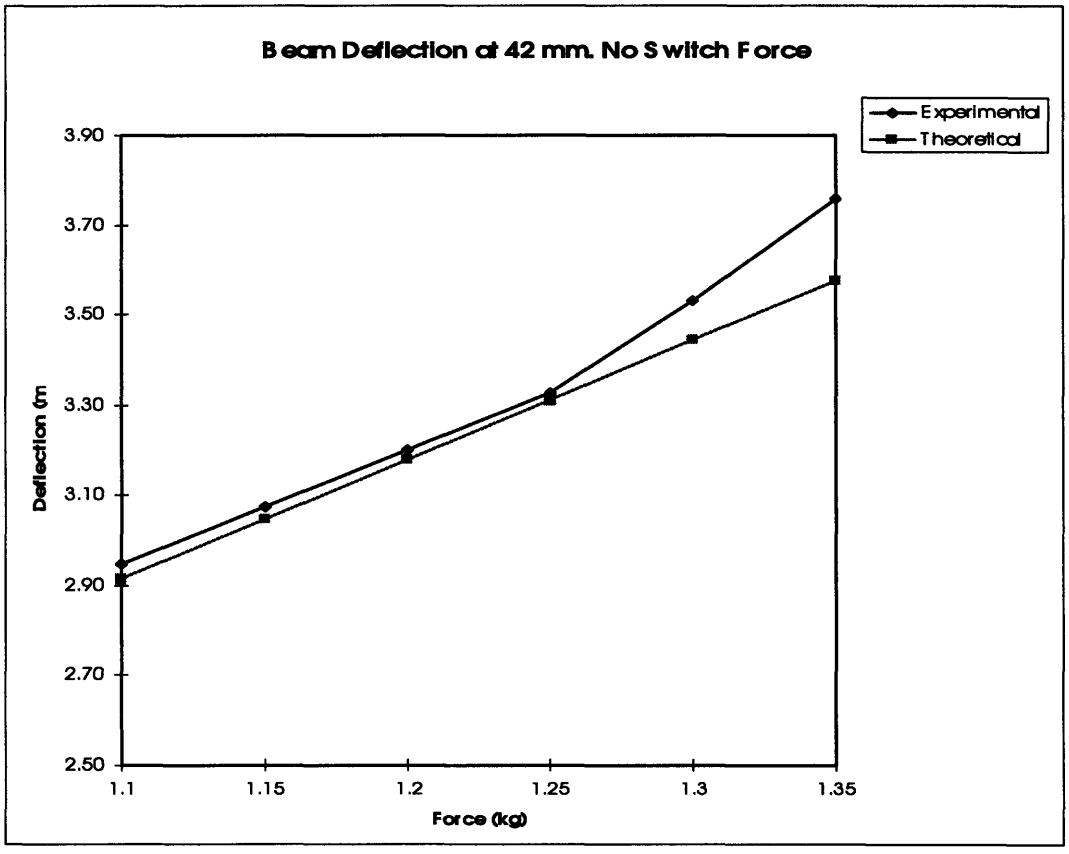


Figure C-4 Displacement versus force

Table C-3 and figure C-5 show the deflection versus weight for a setup with the switch placed at 45 mm from the fixed end. The force applied by the switch to the beam was not present in the experimental setup.

| Force | Deflection (in) | Force (kg) | Experimental Deflection | Theoretical Deflection |
|---|---|---|---|---|
| 1.1 | 0.13 | 1.1 | 3.30 | 3.20 |
| 1.15 | 0.139 | 1.15 | 3.53 | 3.35 |
| 1.2 | 0.144 | 1.2 | 3.66 | 3.49 |
| 1.25 | 0.149 | 1.25 | 3.78 | 3.64 |
| 1.3 | 0.154 | 1.3 | 3.91 | 3.78 |
| 1.35 | 0.16 | 1.35 | 4.06 | 3.93 |

Table C-3

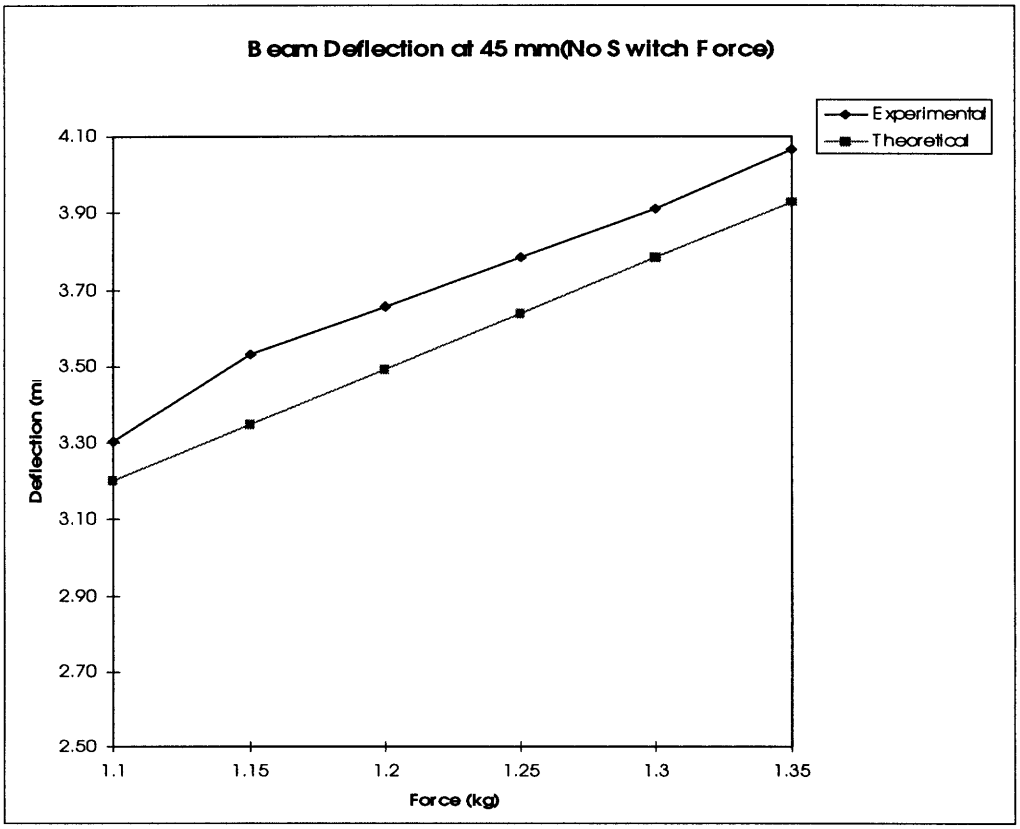


FigureC-5 Displacement versus force

Table C-4 and figure C-6 show the deflection versus weight for a setup with the switch placed at 40 mm from the fixed end. The force applied by the switch to the beam was 25 gr.

| Force | Deflection (in) | Force (kg) | Experimental Deflection | Theoretical Deflection |
|---|---|---|---|---|
| 1.1 | 0.113 | 1.1 | 2.87 | 2.81 |
| 1.15 | 0.1175 | 1.15 | 2.98 | 2.91 |
| 1.2 | 0.122 | 1.2 | 3.10 | 3.01 |
| 1.25 | 0.126 | 1.25 | 3.20 | 3.11 |
| 1.3 | 0.132 | 1.3 | 3.35 | 3.23 |
| 1.35 | 0.138 | 1.35 | 3.51 | 3.34 |

Table C-4

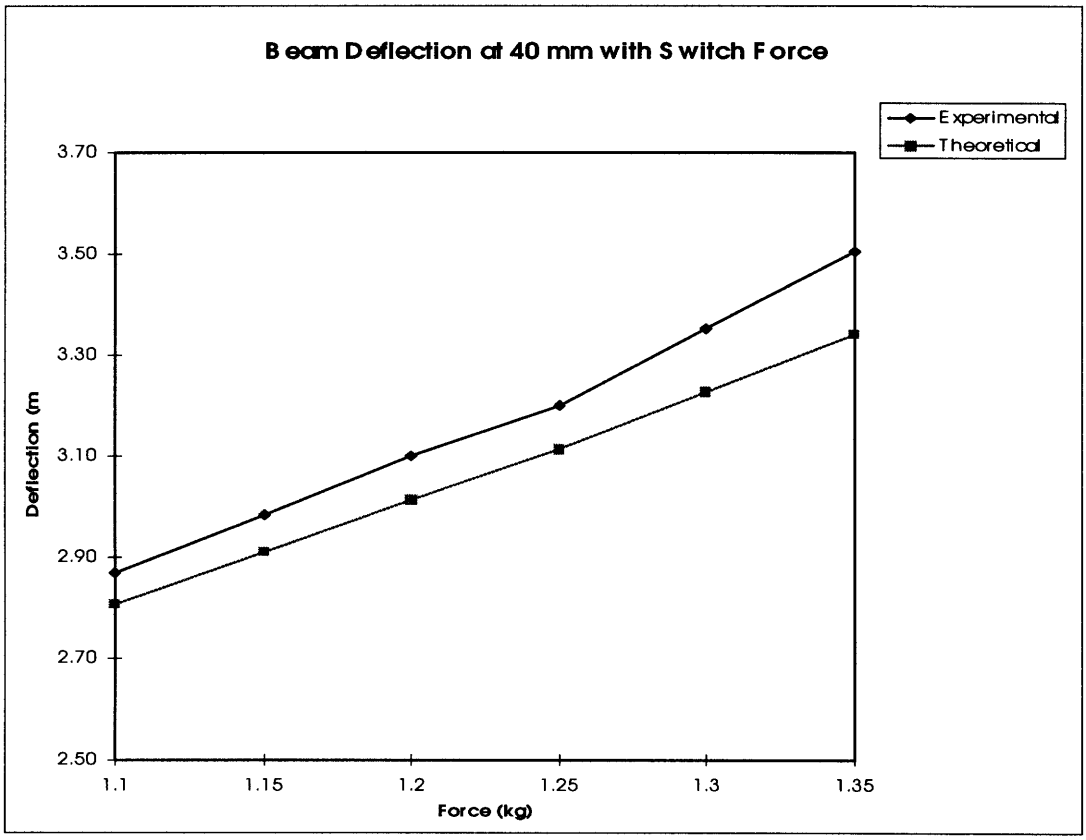


FigureC-6 Displacement versus force

Table C-5 and figure C-7 show the deflection versus weight for a setup with the switch placed at 45 mm from the fixed end. The force applied by the switch to the beam was 25 gr.

| Force | Deflection (in) | Force (kg) | Experimental Deflection | Theoretical Deflection |
|---|---|---|---|---|
| 1.1 | 0.14 | 1.1 | 3.56 | 3.32 |
| 1.15 | 0.144 | 1.15 | 3.66 | 3.44 |
| 1.2 | 0.149 | 1.2 | 3.78 | 3.55 |
| 1.25 | 0.152 | 1.25 | 3.86 | 3.67 |
| 1.3 | 0.154 | 1.3 | 3.91 | 3.80 |
| 1.35 | 0.158 | 1.35 | 4.01 | 3.93 |

Table C-5

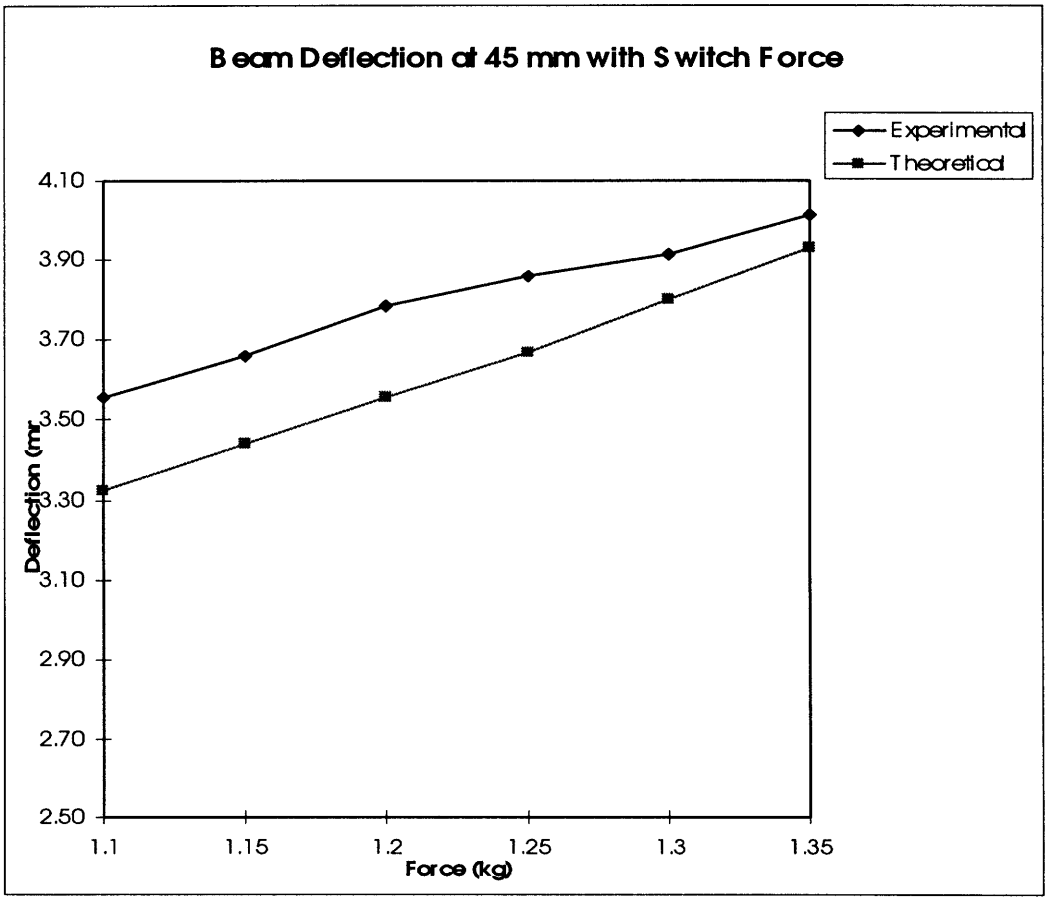


FigureC-7 Displacement versus force